



**UNIVERSITY of the
WESTERN CAPE**

**Photocatalytic degradation of organic pollutants
using Ag-Fe₃O₄/SiO₂/TiO₂ nanocomposite**

By
UNIVERSITY of the
WESTERN CAPE
Siyasanga Noganta

M.Sc. thesis submitted in partial fulfilment of the requirements for the
degree of Magister Scientiae Nanoscience

In the Department of Chemistry, Catalysis Research Group,
University of Western Cape

Supervisors

Prof. Salam Titinchi

Dr Hanna Abbo

DECLARATION

I declare that “Photocatalytic degradation of organic pollutants in wastewater using Ag-Fe₃O₄/SiO₂/TiO₂ nanocomposite” is my own work, that is has not been submitted for any degree or examination in any other university, and that all sources I have used or quoted have been indicated and acknowledged by complete references.

Full name: Siyasanga Noganta

Date

.....

Signature.....



ACKNOWLEDGEMENT

This thesis marks the end of my MSc degree. I would have not been able to do so without the support and assistance of a number of people and organisations. I take this opportunity to extend my utmost gratitude to my supervisor Prof. Titinchi for his support and guidance towards my project. I would also like to thank my co-supervisor Dr H. Abbo for her time, advice and assistance every step of the way. You have given me so much motivation to work hard towards my goals.

Thank you to all the members of the Catalysis Research Laboratory for all the assistance and support. To my mother, words cannot describe how grateful I am for all your sacrifices and patience. A special thanks to my family and friends. I would also like to thank the National Nanoscience platform and Department of Science and Technology for financial assistance.

This work has been the result of collaborations within different departments of the University of Western Cape and other research institutes, I would like to extend my appreciation to Mr T. Lesch, Chemistry department (UWC), for UV and GC, Mr A. Josephs, Physics department (UWC), for SEM, Dr R. Bucher, iThemba lab for XRD, Dr F. Cummings, Physics department (UWC), for HR- TEM and Dr W. Davids for BET and FTIR.

Dedicated to my mother, Belezwa Noganta

Contents

DECLARATION.....	2
ACKNOWLEDGEMENT	3
Contents.....	4
Glossary.....	8
List of figures	10
List of table.....	12
Abstract	13
Keywords.....	15
1 Introduction.....	16
1.1 Advanced Oxidation Processes.....	19
1.2 Catalysis	21
1.3 Photocatalysis.....	22
1.4 Nanotechnology	23
1.4.1 Iron oxide	24
1.4.2 Silica dioxide (SiO ₂).....	26
1.4.3 Titanium dioxide (TiO ₂).....	27
1.4.4 Silver-deposition	31
1.5 Problem statement.....	33
1.6 Aim and objectives	33



1.7 Thesis layout	34
2 Literature Review	35
2.1 Review of general methods and systems used to control contaminants in water.....	36
2.1.1 Coagulation and electrocoagulation.....	36
2.1.2 Ozonation	37
2.1.3 Filtration	37
2.1.4 Reverse Osmosis	38
2.1.5 Distillation.....	39
2.1.6 Biological Methods.....	39
2.2 Semiconductors.....	41
2.2.1 Properties of Titanium dioxide.....	42
2.3 Magnetism in materials.....	45
2.3.1 Iron oxide	47
2.4 Reviews on titanium dioxide based catalysts	49
2.4.1 Micro emulsion.....	52
2.5 Synthetic Techniques	52
2.5.1 Co-precipitation.....	53
2.5.2 Hydrothermal treatment	55
2.5.3 Sol-gel method	56
2.6 Factors affecting photocatalytic activity.....	58
2.6.2 Intrinsic parameters	63

3	Materials and Methodologies	65
3.1	Materials.....	65
3.2	Methodologies.....	66
3.2.1	Synthesis of iron oxide nanoparticles	66
3.2.2	Synthesis of silica coating (Fe ₃ O ₄ /SiO ₂) nanoparticles	67
3.2.3	Synthesis of titanium dioxide iron oxide (Fe ₃ O ₄ /SiO ₂ /TiO ₂) nanoparticles	67
3.2.4	Synthesis of silver doped magnetite titanium dioxide (Ag- Fe ₃ O ₄ /SiO ₂ /TiO ₂) nanoparticles	69
4	Characterization Techniques.....	70
4.1	Fourier- Transform Infrared Spectroscopy.....	70
4.1.1	Sample preparation.....	70
4.2	High Resolution Scanning Electron Microscopy	73
4.2.1	Sample Preparation for SEM.....	73
4.3	High Resolution Transmission Electron Microscopy	78
4.3.1	Sample Preparation	78
4.4	X-ray Diffraction.....	85
4.5	Braunauer Emmett Teller Analysis	88
4.5.1	Sample Preparation	89
4.5.2	N ₂ adsorption-desorption isotherms	90
4.6	Thermogravimetric Analysis and Differential Scanning Calorimetry.....	92

4.6.1	Thermogravimetric Analysis (TGA).....	92
4.6.2	Differential Scanning Calorimetry (DSC)	92
5	Results and Discussions	96
5.1	Photodegradation Studies	96
	99
5.2	Ultraviolet spectra.....	99
6	Conclusions, future work and recommendations	106
6.1	Conclusion.....	106
6.2	Future work and recommendations	107
7	References.....	108



Glossary

%T Percentage transmission

°C Degrees Celsius

Å Angstrom

Å Angstrom [10-10m]

Ag Silver

Ar Argon

EDX Energy dispersive x-ray spectroscopy

EG Ethylene Glycol

EtOH Ethanol

Fe₃O₄ Iron oxide

FT-IR Fourier- Transform infrared spectroscopy

g Gram

H Hours

H⁺ Hydrogen ion

H₂ Hydrogen

M Molar

ml Millilitres

nm Nanometre

SEM Scanning electron microscope

SiO₂ Silica dioxide



TEM Transmission electron microscope

TGA Thermogravimetric analysis

TiO₂ Titanium dioxide

UV/Vis Ultraviolet-visible spectroscopy

VSM Vibrating sample magnetometer

XRD X-ray diffraction



List of figures

Figure 1.1: Structure of Methylene Blue, (Umoren , et al., 2013).....	17
Figure 1.2: Schematic representation of photo catalysis process occurring on the semiconductor materials; where VB: Valence Band and CB: Conduction Band (Xu, et al., 2014).....	30
Figure 2.1: Bandgap energies of (a) insulators (b) semiconductors and (c) conductors	42
Figure 2.2: TiO ₆ polyhedral for TiO ₂ (a) rutile, (b) brookite and (c) anatase phases, (Landmann, <i>et al.</i> , 2012).	44
Figure 2.3: Illustration of various arrangements of individual atomic magnetic moments that constitute (a) paramagnetic, (b) ferromagnetic (c) ferrimagnetic and (d) antiferromagnetic materials (Poole, Jr. & Owens , 2003).	47
Figure 2.4: Crystal structures of (a) hematite and (b) magnetite, (Teja & Koh, 2009).	48
Figure 3.1: Synthesis of Fe ₃ O ₄	66
Figure 3.2: Synthesis of Fe ₃ O ₄ /SiO ₂	67
Figure 3.3: Synthesis of Fe ₃ O ₄ /SiO ₂ /TiO ₂	68
Figure 3.4: Synthesis of Ag-Fe ₃ O ₄ /SiO ₂ /TiO ₂	69
Figure 4.1: FT-IR spectra of Fe ₃ O ₄ and Fe ₃ O ₄ /SiO ₂	71
Figure 4.2: FT-IR spectra of Fe ₃ O ₄ /SiO ₂ /TiO ₂ and Ag-Fe ₃ O ₄ /SiO ₂ /TiO ₂	71
Figure 4.3: (a) Scanning electron micrograph and (b) EDX of Fe ₃ O ₄	74
Figure 4.4: (a) Scanning electron micrograph and (b) EDX of Fe ₃ O ₄ /SiO ₂	75
Figure 4.5: (a) Scanning electron micrograph and (b) EDX of calcined Fe ₃ O ₄ /SiO ₂ /TiO ₂	76
Figure 4.6: (a) Scanning Electron Micrograph and (b) EDX of calcined Fe ₃ O ₄ /SiO ₂ /TiO ₂	77
Figure 4.7: (a) Scanning Electron Micrograph and (b) EDX of Ag-Fe ₃ O ₄ /SiO ₂ /TiO ₂ .	77

Figure 4.8: TEM images, corresponding SAED and EDX of Fe ₃ O ₄	79
Figure 4.9: TEM images, corresponding SAED and EDX of Fe ₃ O ₄ /SiO ₂	80
Figure 4.10: TEM images, corresponding SAED and EDX of Fe ₃ O ₄ /SiO ₂ /TiO ₂	82
Figure 4.11: TEM images, corresponding SAED and EDX of Ag-Fe ₃ O ₄ /SiO ₂ /TiO ₂ ...	83
Figure 4.12: XRD patterns of (a) iron oxide, (b) Fe ₃ O ₄ /SiO ₂ , (c) Fe ₃ O ₄ /SiO ₂ /TiO ₂ and (d) Ag-Fe ₃ O ₄ /SiO ₂ /TiO ₂	85
Figure 4.13: Nitrogen adsorption-desorption isotherms and corresponding pore size distributions of (a) Fe ₃ O ₄ (b) Fe ₃ O ₄ /SiO ₂ (c) Fe ₃ O ₄ /SiO ₂ /TiO ₂ (d) Ag-Fe ₃ O ₄ /SiO ₂ /TiO ₂	90
Figure 4.14: TGA and DSC graphs of Fe ₃ O ₄	93
Figure 4.15: TGA and DSC graphs of Fe ₃ O ₄ /SiO ₂ /TiO ₂	94
Figure 4.16: TGA and DSC graphs of Ag-Fe ₃ O ₄ /SiO ₂ /TiO ₂	94
Figure 5.1: Photodegradation process of MB.....	97
Figure 5.2: Reaction setup.....	97
Figure 5.3: Separation method with external magnet.....	98
Figure 5.4: MB samples drawn after 5 min, 10 min, 15 min, 30 min, 60min and 120min from left to right respectively.	99
Figure 5.5: UV spectra of the photodegradation process over time using (a) blank, (b) Fe ₃ O ₄ , (c) Fe ₃ O ₄ /SiO ₂ /TiO ₂ , (d) Ag-Fe ₃ O ₄ /SiO ₂ /TiO ₂ (e), Commercial TiO ₂ , (f) Com TiO ₂ (no UV irradiation) and (g) Fe ₃ O ₄ /SiO ₂ /TiO ₂ (no UV irradiation)	101
Figure 5.6: UV spectra of the photodegradation process over time using	102
Figure 5.7: Degradation percentage of MB dye over time	104

List of table

Table 1.1: Conduction band potentials, valence band and bandgap energies of titanium dioxide (TiO_2), magnetite (Fe_3O_4), maghemite ($\gamma\text{-Fe}_2\text{O}_3$) and hematite($\alpha\text{-Fe}_3\text{O}_4$) (Beydoun , et al., 2002).	28
Table 2.1: Outlines the advantages and disadvantages of physical/chemical methods (Zille, <i>et al.</i> , 2005; Robinson, <i>et al.</i> , 2001).....	40
Table 2.2: Reviews different catalyst types, the organic pollutants and their degradation rates.....	50
Table 2.3: Outlines the properties of different synthetic methods (Lu, <i>et al.</i> , 2007). ...	57
Table 3.1: Chemicals used and respective suppliers	65
Table 4.1: XRD patterns of as-synthesized photocatalysts, indices and d- spacing values.....	87
Table 4.2: BET surface area of the as-synthesized photocatalysts.....	91



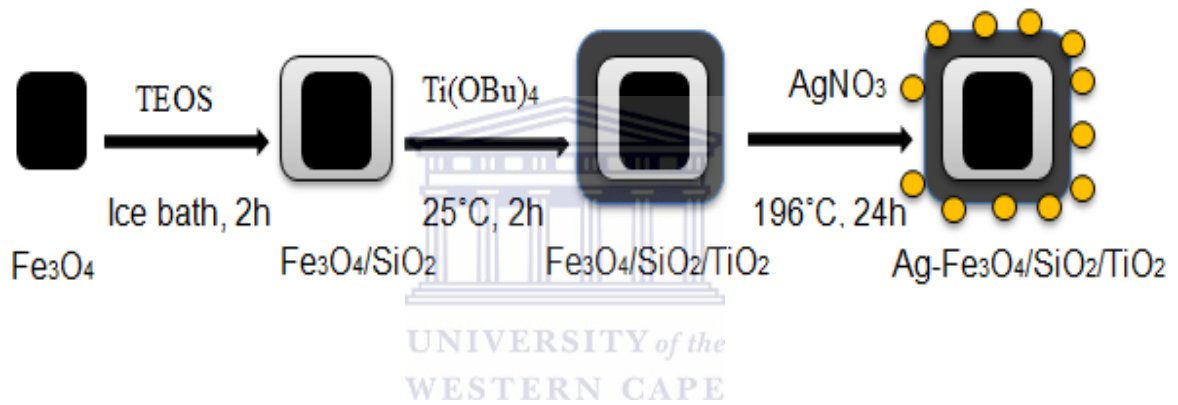
Abstract

The global lack of clean water for human sanitation and other purposes has become an emerging dilemma for human beings. The presence of organic pollutants in wastewater produced by textile industries, leather manufacturing and chemical industries is an alarming matter for a safe environment and human health. For the last decades, conventional methods have been applied for the purification of water but due to industrialization these methods fall short. Advanced oxidation processes and their reliable application in degradation of many contaminants have been reported as a potential method to reduce and/or alleviate this problem. Lately, it has been assumed that incorporation of some metal nanoparticles such as magnetite nanoparticles as photocatalyst for Fenton reaction could improve the degradation efficiency of contaminants. Core/shell nanoparticles, are extensively studied because of their wide applications in the biomedical, drug delivery, electronics fields and water treatment.

The current study is centred on the synthesis of silver-doped $\text{Fe}_3\text{O}_4/\text{SiO}_2/\text{TiO}_2$ photocatalyst. Magnetically separable $\text{Fe}_3\text{O}_4/\text{SiO}_2/\text{TiO}_2$ composite with core-shell structure were synthesized by the deposition of uniform anatase TiO_2 NPs on $\text{Fe}_3\text{O}_4/\text{SiO}_2$ by using titanium butoxide (TBOT) as titanium source. Then, the silver is doped on TiO_2 layer by hydrothermal method. Integration of magnetic nanoparticles was suggested to avoid the post separation difficulties associated with the powder form of the TiO_2 catalyst, increase of the surface area and adsorption properties. Lastly and most importantly magnetic nanoparticles upsurge the production of hydroxyl groups or reduced charge recombination.

The as synthesized catalysts were characterized using Transmission Electron Microscopy, X-ray Diffraction; Infra-red Spectroscopy, Scanning Electron Microscope

and Energy Dispersive Spectroscopy. Other characterization techniques include Vibrating Sample Magnetometry, Brunauer Emmett Teller analysis and Thermogravimetric analysis. The average size of the particles size is 72 nm. Furthermore the photocatalytic performances of the magnetic catalysts were assessed in comparison with that commercial titanium dioxide for the degradation of methylene blue using photochemical reactor under ultra violet light. The results showed that the photocatalytic activity was enhanced using $\text{Fe}_3\text{O}_4/\text{SiO}_2/\text{TiO}_2$ and $\text{Ag-Fe}_3\text{O}_4/\text{SiO}_2/\text{TiO}_2$ compared with that for Fe_3O_4 , commercial titanium dioxide powder.



Keywords

Magnetite nanoparticles

Titanium dioxide

Photocatalyst

Organic pollutants

Silver nanoparticles



Chapter 1: Introduction

Water is a basic need, as stipulated in 27(1) b of the South African constitution; where it states that everyone has the right to sufficient water, yet some people are still deprived of this need. South Africa is a water scarce country and various strategies are being formulated to try and preserve the water still available. According to the World Bank, South Africa has an annual average rainfall of 495 mm in depth. According to UN statistics, of the 51 million people in South Africa, about 60% live in urban areas and the remaining 40% constitutes people in rural areas. The country depends on 77% surface water, 9% groundwater and 14% recycled water. However, the population's dependence on water is not evenly distributed.

Numerous industries use pigments and dyes for the colouring of their products such as paper, rubber, plastics, leather, cosmetics, pharmaceuticals, textiles and food to name a few (Nandhini, et al., 2012). Research has shown that over 15% of the total production of dyes is lost untreated in effluents posing a threat to the health and general well-being of man and animals (Houas , et al., 2001).

These dyes form part of the undesirable substances found in wastewater effluents from the textile, printing and food and cosmetics industries. Due to the low biodegradability of dyes, conventional biological treatment processes do not effectively treat dye wastewater (Akpan & Hameed, 2009). The same dyes, pharmaceuticals and hormones designed to stimulate a physiological response in humans, plants, and animals pose a significant threat to the aquatic environment due to their intrinsic lipophilic nature, tendency to interact with living tissues, and continued comprehensive use (Dalrymple, et al., 2007). When these compounds are present in liquid effluents, they can be

disastrous because their presence may pose a threat to the immediate recipients (Akpan & Hameed, 2009).

Dyes may be defined as substances that produce colour when applied to a substrate by temporarily changing the crystal structure of the coloured substances (Chequer, et al., 2013). They adhere to compatible surfaces by solution, by forming covalent bond or complexes with salts or metals, by physical adsorption or by mechanical retention, (Bafana, et al., 2011). Dyes are categorized according to their chemical structures, application and the groups of atoms (chromophores) present. The chromophores are diverse functional groups determining the colour and the behaviour of the dyes, such as arilmethane, azo, methane, nitro, and anthraquinone amongst others (Chequer, et al., 2013).

The current study focuses on methylene blue; an azo dye as a model compound to evaluate the effectiveness of the synthesized magnetite titanium dioxide catalyst for the degradation of methylene blue. Methylene blue forms a large fraction of dyes used in textile industries and has shown the possibility of endocrine disruption in aquatic life (Soriano , et al., 2014).

Methylene blue is cationic dye used in industries such as the textile industry for a variety of purposes. It is a heterocyclic aromatic chemical compound with a molecular formula $C_{16}H_{18}N_3SCl$.



Figure 1.1: Structure of Methylene Blue, (Umoren , et al., 2013)

This dye gives a blue solution when mixed with water, and has been reported to be toxic or induce endocrine disruption in aquatic organisms when persistent in water (Soriano , et al., 2014). Throughout a chemical or biological reaction pathway, these dye compounds not only deplete the dissolved oxygen in water bodies, they also release toxic compounds that threaten aquatic life (Umoren , et al., 2013). It can also cause eye burns which may be responsible for permanent injury to the eyes of both human and animals. Upon inhalation, it can give rise to short periods of rapid or difficult breathing whereas ingestion through the mouth causes gastrointestinal tract irritation, producing a burning sensation and may cause nausea, vomiting, profuse sweating, mental confusion and methemoglobinemia (Rafatullah, et al., 2010). It is thus crucial to control the amount of methylene blue used and thereby eventually eliminate the presence of such dyes in water and which are subsequently released into the environment.

The need for novel processes, economical, easily available and highly effective processes for the degradation of dye deposits in water is crucial and various methods have been investigated for the application on industrial effluents in the future (Garg , et al., 2003). Several methods have been investigated which include, ultrasonic decomposition (Shimizu, et al., 2007; Wu & Chern, 2006), electrocoagulation (Golder, et al., 2005; Ma, et al., 2009); advanced chemical oxidation (Height, et al., 2006; Tayade, et al., 2007; Sannino, et al., 2013) and chemical coagulation (Lee, et al., 1999; Chakrabarti & Dutta, 2004) however the current study focuses on advanced oxidation processes.

Advanced Oxidation Processes

Advanced Oxidation Processes (AOP) has been reported to have been effectively applied to purify refractory pollutants found in industrial wastewater, (Saggiaro, et al., 2011). According to Ollis, (1993), AOPs aqueous phase oxidation processes which are based primarily on the intermediacy of the hydroxyl radical in the mechanism(s) resulting in the destruction of the target pollutant or xenobiotic or contaminant compound. AOPs have been reported to degrade high loading of organic compounds in high saline conditions over the years (Neyens & Baeyens, 2003; Bacardit, et al., 2007).

AOPs not only convert chemical pollutants but offer complete mineralization of some compounds, improve organoleptic properties of the treated water and ensure the low consumption of energy more so than other methods (Herney-Ramirez, et al., 2010). AOPs work under ambient conditions to generate hydroxyl radicals and have different reacting systems such as electrochemical oxidation, chemical oxidation processes using hydrogen peroxide, ozone, combined ozone and hydrogen peroxide, hypochlorite, Fenton's reagent, and ultra-violet enhanced oxidation (Pignatello, et al., 2006; Hussein, 2011). A number of AOPs use hydrogen peroxide as the main oxidizing agent, which is a reagent more efficient than gaseous oxygen concerning the contaminants' mineralization, allowing also the diminution of the residence time in the oxidation process, especially when focusing on dangerous polluting compounds.

Hydrogen peroxide (H_2O_2) is said to be environmental friendly, because it produces water and oxygen when decomposed (Herney-Ramirez, et al., 2010). Amidst the processes mentioned above using H_2O_2 as an oxidant, the photo-Fenton has received vast attention (Khataee, et al., 2009; Klavarioti, et al., 2009). However conventional homogeneous Fenton processes have a number of disadvantages limiting their extensive

application - these include the generation of huge amounts of iron sludge, narrow pH range (pH 2–3), difficulty in recycling catalysts and deactivation by the iron complexation reagents (Liu, et al., 2014; Zhou, et al., 2015). These drawbacks have led to the development of heterogeneous catalysts for the Fenton processes.

To address these issues, heterogeneous Fenton oxidation based on various iron catalysts has been developed over the past few years (Soon & Hameed 2011; Sun *et al.* 2012). These disadvantages led to several attempts which have been made to develop solid supports for the active iron species. Scientists have turned to heterogeneous catalysts because they offer complete mineralization of the organic pollutants. The use of solid supports also allows for easy separation of the catalysts from the treated wastewater, while preventing secondary metal ion pollution (Colmenares & Luque, 2014).

The current study directs its focus on Fenton's reagent and ultraviolet enhanced oxidation using iron oxide and titanium dioxide. According to Barbusiński (2009) Fenton's reagent is a reaction in which organic substrates are oxidized by iron (II) and hydrogen peroxide. This reaction may be enhanced using ultra-violet light and may be used in the combination of semiconductors such as in photocatalytic systems (Lodha, et al., 2011).

The major advantages of the photocatalytic oxidation process are as follows:

- Firstly, it offers a good route for the use of broadly available renewable and pollution-free solar energy.
- Secondly, this process does not have waste disposal problems.
- Thirdly, the photocatalytic process is a non-selective oxidation process for most organic pollutants; therefore, it can destroy a variety of hazardous organic compounds in different influents.

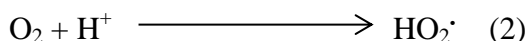
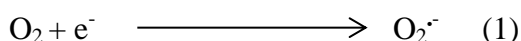
- Fourthly, it can transform organic pollutants into innocuous products by redox reactions and complete the mineralization of the organic pollutants, (Liu, 2012)
- Fifthly, it is inexpensive, (Xie & Li, 2006). Thus, the photocatalytic degradation of environmental pollutants is an interesting topic for study.

Catalysis

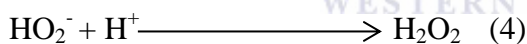
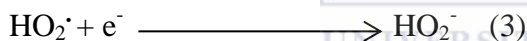
Catalysis defines the acceleration of a chemical reaction with the aid of a catalyst and can be classified into two types; homogeneous and heterogeneous catalysts. Homogeneous catalysts are present in the same phase as reactants and products, usually liquid, while heterogeneous catalysts are present in a different phase, usually the solid and liquid or gaseous phase. Homogeneous catalysts are effective with high yields, however they are time consuming and expensive because catalysts cannot be recovered. Heterogenizing catalyst is one of the efficient ways to overcome the post separation challenge associated with homogeneous catalysts. This is done by entrapment or embedding molecules on solid supports such as alumina, silica or ceria (Polshettiwar, et al., 2011). This makes catalysts and reaction mixture in heterogeneous systems can be easily separated by simple filtration and can be reused thus saving costs, making heterogeneous catalysts more applicable in industry (Xia, et al., 2005). This study focuses on use of magnetic titanium dioxide catalyst easily recovered using an external magnet.

Photocatalysis

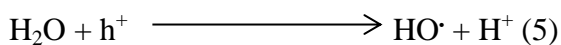
Photocatalysis is the speeding up of a photoreaction in the presence of a catalyst. Recently the photocatalysis technique has been widely applied due to the increase of persistent dyes and other organics in water which conventional methods cannot degrade (Kulkarni & Thakur, 2014). Photocatalysis employs semiconductors to increase its effectiveness and activity. The process of operation of the semiconductor of the photo-excitation of the semiconductor is illustrated below;



In this way, electron/hole recombination can be successfully prevented and prolong the lifetime of the holes. HO_2^{\cdot} can lead to the formation of H_2O_2 .



Photogenerated holes can react with adsorbed water molecules (or hydroxide anions) to give hydroxyl radicals:



Upon photo-excitation of the semiconductor, electron/hole pairs are created, through the excitation of an electron from the valence band to the conduction band. At this point in the process both oxidative and reductive processes can occur at/or near the surface of the photo- excited semiconductor particle. In aerated aqueous suspensions, oxygen is able to obtain electrons from the conduction band forming superoxide ions ($\text{O}_2^{\cdot -}$) and its protonated form, the hydroperoxyl radical (Kulkarni & Thakur, 2014).

The combination of Fenton processes and photocatalysis can not only increase the total efficiency of the degradation but also has the advantage of treating large quantities of wastewater, especially with electro-catalysis, biodegradation, and wetland technology (Zheng, et al., 2013). Chemistry and other fields have turned to nanotechnology to further increase the effectiveness and efficiency of existing conventional and new systems.

Nanotechnology

Nanotechnology was introduced by Nobel laureate, Richard P. Feynman, during his now famous 1959 lecture “*There’s Plenty of Room at the Bottom*,” (Feynman, 1960). Since the talk there have been many revolutionary developments in physics, chemistry, and biology that have demonstrated Feynman’s ideas of manipulating matter on an extremely small scale, the level of molecules and atoms. Nanotechnology refers to matter observed on a nanometer scale which offers novelty to materials compared to those observed on a bulk scale (Allhoff, et al., 2010). It holds out the promise of immense improvements in manufacturing technologies, electronics, telecommunications, health and even environmental remediation (Kim, et al., 2003). It involves the production and utilization of a diverse array of nanomaterials, which include structures and devices ranging in size from 1 to 100 nm and displays unique properties not found in bulk-sized materials (Dutta, et al., 2008; Wang, et al., 2010). Nanotechnology offers materials great tunable properties varying from electrical, magnetic, conductive catalytic, mechanical and chemical properties, allowing materials to be applied in a variety of fields.

This study employs silver doped magnetite titanium oxide nanoparticles for the degradation of methylene blue at laboratory scale. This method offers the advantages of simplicity, low cost, and low reaction temperatures; in addition, it is environment-friendly as it produces no by-product effluents. The as-synthesized catalyst would not completely replace existing conventional systems for now, however it can be a supplementary method. The catalyst is a core-shell structure with iron oxide as the core, silica comprising the insulator, a linker between the magnetic core and the titanium dioxide and silver forming the outermost shell.

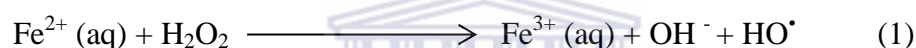
Iron oxide

Iron is amongst the most used transition metals for incorporation in wastewater treatment catalysts (Chen, et al., 2009). Iron oxide has found great attention in the catalysis and adsorbent chemistry due to its unique properties, such as extremely small size, surface modifiability, high surface-area-to-volume ratio, great biocompatibility and excellent magnetic properties (Xu, et al., 2012). For these unique properties it has found applications in gene therapy, targeted drug delivery (Kronick, et al., 1986), biochemical sensing, ultra-sensitive disease detection, high throughput genetic screening, and rapid toxicity cleansing (Cheng, et al., 2005; Gu, et al., 2006).

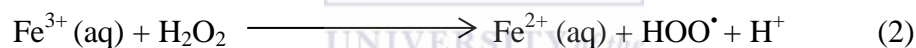
Iron oxide has been incorporated in composites either as a core or a shell (Wang, et al., 2009) and in other cases as alloys (Harraz, et al., 2014). Extensive literature suggests that the use of iron for water purification offers several advantages both in the presence of ultra violet, visible light and in the absence of either (Andreozzi, et al., 1999; Legube & Leitner, 1999). The iron oxide nanoparticles show remarkable new phenomena such as superparamagnetism, high saturation field, high field irreversibility, extra anisotropy contributions or shifted loops after field cooling.

The superparamagnetism of iron oxide is also advantageous for the post separation step after the degradation process is complete, is easily functionalized and is biocompatible (Tartaj , et al., 2003). Nanometer-size iron oxide particles offer increased surface to volume atoms ratio causing the surface properties to dominate the nanostructure. Secondly, sufficiently small magnetic nanoparticles show superparamagnetic behaviour and require reduced temperatures to activate reaction hence lowering energy consumption, (Chin & Yaacob, 2007).

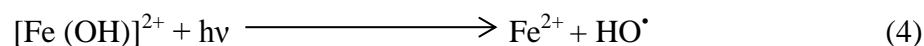
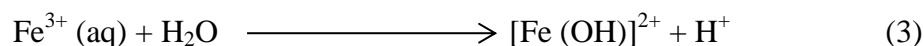
When water is treated in the absence of light, ferrous salt is reacted with hydrogen peroxide (H₂O₂) in the aqueous phase, resulting in the formation of hydroxyl radicals, (Chong , et al., 2010) as shown below: (reaction 1)



The Fe²⁺ can be reverted back to Fe³⁺ via (reaction 2) and yield more radicals:



By using UV-visible radiation during the process, degradation rates are increased significantly. This process is called photo-Fenton, the ion Fe (II) oxidized to Fe (III) in the Fenton reaction and is reduced back to Fe (II) by the radiation. This occurs by the following steps (reaction 3) and (reaction 4) (Hernández-Rodríguez, et al., 2014)



The use of iron oxide is said to avoid the post separation difficulties associated with the powder catalysts, it upsurges the production of hydroxyl groups or reduced charge recombination and increases the surface area and adsorption properties of the catalyst (Song & Gao, 2007).

Silica dioxide (SiO₂)

Silica has received increased attention due to its abundance, easy availability and low cost (Rafatullaha, et al., 2010). The silica coating is applied between the iron oxide core and the titanium shell to link the two layers of the catalyst. Moreover silica was chosen as a spacer to separate the magnetic core and TiO₂ shell due to its undeviating surface and deposition chemistry compatible with both of these oxide materials (Linley, et al., 2013). It also prevents the oxidation of the iron oxide core by the titanium dioxide shell which would reduce its magnetism.

The passive shell over the magnetic core does not merely prevent charge exchange between the magnetic support and the photocatalytic shell but also impedes the undesirable doping of titanium dioxide during strengthening of the catalyst or during calcination. Furthermore silica does not only act as a linker but also increases the surface area, improves the photocatalytic activity and facilitates the separation and recovery of the catalyst (Harraz, et al., 2014).

The shell can also modify the charge, stability and dispersibility of the magnetic core and improve its thermal stability and the acid resistance of magnetic core in a corrosive solution (Cheng, et al., 2012). Additionally the presence of a silica (SiO₂) layer between TiO₂ shell and Fe₃O₄ nanoparticles increases the lifetime of photogenerated holes which in turn, increases the photoreactivity of the magnetic core (Gad-Allah, et al., 2007; Pang, et al., 2012)

Titanium dioxide (TiO₂)

Among the photocatalysts, titanium dioxide (TiO₂) is a semiconductor material which is extensively used due to its superior photoreactivity, long-term stability, non-toxicity, low operating cost, and radically low level of energy consumption (Beydoun, et al., 2002; Valencia, et al., 2010; Huang, et al., 2011). The photocatalytic activity of TiO₂ depends on various parameters, including surface area, crystallinity, impurities and density of the surface hydroxyl groups. Generally, TiO₂ could be used as a photocatalyst in anatase and rutile crystal structures, the anatase phase displaying much higher activity than the rutile structure (Harraz, et al., 2014). Titanium shows a novel photoinduced superhydrophilic phenomenon and hence the interest in its application in water treatment and purification systems (Fujishima, et al., 2000).

Photo-Fenton processes have been studied for many years and the technology has improved and advanced since its introduction, (Pouran, et al., 2015). Titanium dioxide (TiO₂) bandgap energy (E_g) = 3.2 eV, means that it absorbs radiation below 390 nm, for photoexcitation (Kumar & Bansal, 2013). According to Chong et al. (2010) it is the most active photocatalyst under the photon energy of $300 \text{ nm} < \lambda < 390 \text{ nm}$ and remains stable after repeated catalytic cycles. The table below summarizes the bandgaps of iron oxide and titanium dioxide.

The narrower bandgap of the iron oxides is thought to lead to an increase in the incidence of electron-hole recombination, lowering photoactivity, hence the incorporation of titanium to reduce this phenomenon. When this catalyst is directly used for organic matter degradation it causes slurry (Ehrampoush, et al., 2011). The present work incorporates silica coated iron oxide nanoparticles to avoid post separation difficulty while also increasing the catalyst's lifespan.

Table 1.1: Conduction band potentials, valence band and bandgap energies of titanium dioxide (TiO₂), magnetite (Fe₃O₄), maghemite (γ -Fe₂O₃) and hematite(α -Fe₃O₄) (Beydoun , et al., 2002).

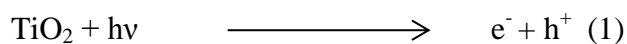
Material	TiO₂	Fe₃O₄	γ-Fe₂O₃	α-Fe₃O₄
Conduction band potential (V)	-0.04	0.17	0.29	0.21
Valence band potential (V)	3.16	0.27	2.59	2.42
Band gap energy (eV)	3.20	0.10	2.30	2.20

The TiO₂ catalyst in nano-dimensions allows a large surface area-to-volume ratio, increased surface energy due to quantum confinement and can therefore further promote the efficient charge separation and trapping at the physical surface (Nagaveni, et al., 2004). In 2008 Siddiquey et al. (2008) reported that the light opaqueness of nanoscale TiO₂ catalysts also enhanced oxidation capability compared to the bulk TiO₂ catalysts, thus increasing the interest in nanosized titania.

During the photocatalytic process, TiO₂ absorbs photons which promote electrons from the valence band to the conduction band, generating electron-hole pairs. The electron in the conduction band reacts with oxygen dissolved in water, and the hole in the valence reacts with OH⁻ or H₂O species, which are absorbed on the surface of TiO₂, yielding a hydroxyl radical (Kumar & Bansal, 2013). Moreover when the catalyst is in contact with the azo dye, the dye adsorbs on the surface of TiO₂ shell and undergoes successive oxidation steps, leading to decolorization and formation of intermediates, such as aliphatic and aromatic acids. The intermediates are further oxidized to lower molar mass molecules and ultimately, to CO₂ and inorganic ions, such as ammonium, nitrate and sulphate. (Stylidi, et al., 2003).

Oxidation-reduction reactions that occur during photocatalytic process are below (Chong , et al., 2010):

1. Photoexcitation



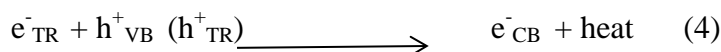
2. Charge-carrier trapping of electrons



3. Charge-carrier trapping of h^+



4. Electron- hole recombination



5. Photoexcited e^- scavenging



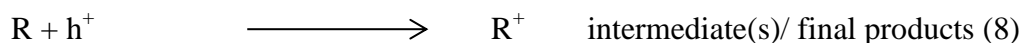
6. Oxidation of hydroxyls



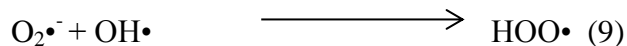
7. Photodegradation by OH^{\bullet}



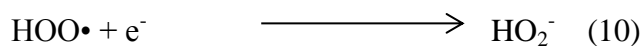
8. Direct photoholes



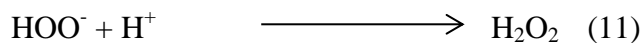
9. Protonation of superoxides



10. Co-scavenging of e^-



11. Formation of H_2O_2



The reactions that occur during the oxidation process of TiO₂ can also be summarized with the diagram below.

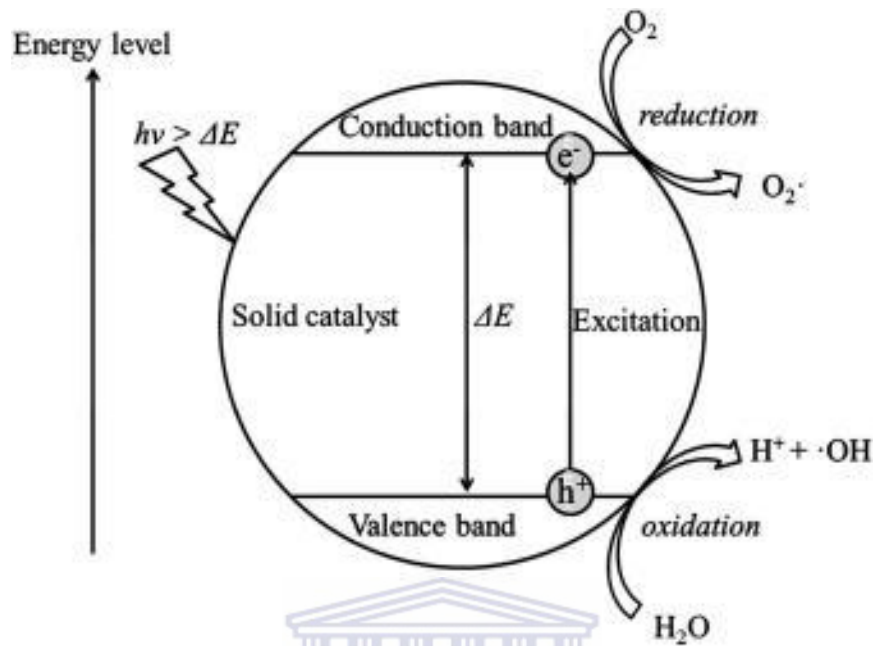


Figure 1.2: Schematic representation of photo catalysis process occurring on the semiconductor materials; where VB: Valence Band and CB: Conduction Band (Xu, et al., 2014).

Silver-deposition

The surface doping effect is synergetic to the charge separation process and the photocatalytic results are explained on the basis of a mechanism involving efficient separation of electron-hole pairs induced by silver-ions (Ag^+). TiO_2 has a high bandgap ($E_g > 3.2$ eV) and is excited only by UV light ($\lambda < 390$ nm) to inject electrons into the conduction band and to leave holes in the valence band (Sobana, et al., 2006). According to Arabatzis et al. (2003) silver particles can act as an electron trap, assisting with electron-hole separation, thereby enhancing quantum efficiency and favouring the oxidation of dye substrates.

In noble metals, the decrease in size below the electron mean free path (the distance which the electron travels between scattering collisions with the lattice centres) gives rise to intense absorption in the visible-near-UV region (Tartaj, et al., 2003) and modifies the surface properties of photocatalysts, (Sobana, et al., 2006). Silver particles also facilitate electron excitation by creating a local electrical field and increasing the total surface of the titanium dioxide shell (Sclafania & Herrmann, 1998). Silver nanoparticles deposited on the TiO_2 surface acts as sites where electrons accumulate. Silver deposits also improve the separation of electrons and holes on the modified TiO_2 surface, therefore allowing increased efficient channelling of the charge carriers into useful reduction and oxidation reactions rather than recombination reactions (Vamathevan, et al., 2002).

Amongst other noble metals; silver is predominantly suitable for industrial applications because of its relatively low price and the ease of the synthesis of Ag/TiO_2 (Wodka, et al., 2010). The modified surface properties of the TiO_2 photocatalyst, improves the attraction affinity of cationic dye towards the TiO_2/Ag surface due to the increased

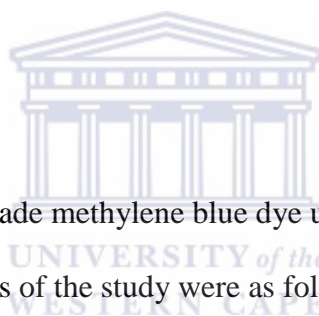
number of electron traps (Carp, et al., 2004). Additionally, silver nanoparticles further shorten the diffusion distance, increase the specific surface area, and improve quantum size effect as the particles are <10 nm in diameter. On the other hand, as dosage levels of silver exceed optimum loading, silver can act as electron-hole recombination centres which are detrimental to the photocatalytic activity (Chen, et al., 2009) thus careful doping has to be employed for optimum results to be attained.



Problem statement

Water scarcity is an increasing crisis and more people are deprived of clean water each day. Water sources are tainted with industrial effluents and other industrial activities become part of water supplies. Methylene blue forms part of the contaminants found in textile industry effluents. Commercial titanium dioxide powder has been used for the degradation of methylene however it causes slurries making it difficult to separate it from the reaction mixture. The need for an easily separated, efficient, cost-effective, speedy, environmentally and user friendly catalysts is essential.

Aim and objectives



The aim of this study is to degrade methylene blue dye using Ag-Fe₃O₄/SiO₂/TiO₂ under ultra-violet light. The objectives of the study were as follows:

- Synthesize Ag-Fe₃O₄/SiO₂/TiO₂ nanocomposite
- Evaluate the catalytic performance of the as-synthesized nanocomposites for the photodegradation of methylene blue
- Compare as-synthesized nanocomposites to commercial titanium dioxide powder
- Optimize the reaction conditions to determine the best conditions for the degradation of MB.

Thesis layout

Chapter 1, summarizes the problem identification, research approach and an outline of the catalytic process studied

Chapter 2 provides a clear state of the art and focuses on the contribution silver doped magnetite titanium dioxide nanocomposite has made in catalytic degradation of organic pollutants.

Chapter 3 gives descriptive experimental methods followed to obtain the nanocomposite.

Chapter 4 shows the characterization of the as-synthesized nanocomposites. It represents the results obtained from the characterization techniques and discusses the observations.

Chapter 5 demonstrates the evaluation of the as-synthesized nanocomposites' catalytic performance for the degradation of methylene blue. It also represents and discusses the results obtained.

Chapter 6 is the conclusion of the current study and also outlines the future prospective of the study.

Chapter 7 presents the references used to write the current study.

Chapter 2: Literature Review

This chapter highlights the methods that have been applied for water purification and specifically evaluates the methods used for the degradation of methylene blue. It gives information about homogeneous catalysts and their shortcomings. It also highlights and elaborates on the use of the heterogeneous catalyst used in the current paper. This chapter provides details on synthetic techniques that are used to develop heterogeneous catalysts and factors that affect photocatalytic activities of synthesized catalysts.

The quality and abundance of water is an indication of the way of life within the community through which it flows. Adequate supply of fresh drinking water is a human basic need, yet some people are deprived of this (Swaminathan, *et al.*, 2013). The change in population growth, climate patterns, microbial growth and rapid development of industrialization have become a critical issue worldwide and key sources that we tap for drinking water are being tainted with pollution (Cundy, *et al.*, 2008).

With the changes in the environment and increased pollution rates, global natural resources are slowly becoming limited and as such the use and reuse of water is becoming an accelerating issue. There is a need for effective, less costly and clean methods for treating a wide range of textile wastewater pollutants in order to conserve the climate, environment and save lives for future generations (Deb & Majumdar, 2013).

Review of general methods and systems used to control contaminants in water

Currently there are various conventional methods used for the decolouration and degradation of dyes from wastewater, however each of them have their limitations and hence multiple studies have been reported to improve these methods. The technologies can be divided into three categories: biological, chemical and physical (Robinson, *et al.*, 2001). These technologies include primary (adsorption, flocculation), secondary (biological methods) and chemical processes i.e. chlorination, ozonation (Mohabansi, *et al.*, 2011). Other methods include reverse osmosis, distillation, filtration and advanced oxidation processes.

Coagulation and electrocoagulation

According to Mollah, *et al.*, (2001) coagulation is a process in which the charged particles in colloidal suspension are neutralized by mutual collision with counter ions and are agglomerated, followed by sedimentation. In contrast electrocoagulation is a process by which coagulants are produced in situ by the electro-oxidation of sacrificing anodes followed by the formation of aluminium or iron hydroxide flocculation which destabilizes and aggregates the suspended particles or precipitates and adsorbs dissolved contaminants (Deb & Majumdar, 2013). Electrocoagulation (EC) consists of electrodes (anodes and cathodes).

EC employs a direct current source between the metal electrodes submerged in electrolytes. The electric current causes the suspension of the metal plates into the wastewater thereby degrading the contaminants. This technology uses aluminium and iron as common electrode material because they are effective and cheap (de Carvalho,

et al., 2015). Numerous researchers have been used this technology (Koby, *et al.*, 2003), (Inan, *et al.*, 2004).

Ozonation

Ozone is a very strong oxidant and virucide. According to the United States Environmental Protection Agency, ozone is formed when oxygen (O₂) molecules are dissociated by an energy source into oxygen atoms and subsequently collide with an oxygen molecule to form an unstable gas, ozone (O₃). Ozone decomposes rapidly producing several free radicals including OH• (hydroxyl), HO₃•, HO₄• and O₂⁻ (superoxide). These radicals have great oxidizing capacity; which reacts instantly with any organic compounds present in water, like dyes and bacteria (García-Morales, *et al.*, 2013). In particular, it is an effective decolourizing technique which acts by attacking the double bond usually allied with colour in wastewater. It has a stronger oxidation potential than that of chlorine and hydrogen peroxide (Su, *et al.*, 2013). A number of studies have been conducted on the use of ozone as a degradation agent; the decolourization and degradation of azo dyes (Peralta-Zamora, *et al.*, 1999; Turhan & Ozturkcan, 2013). Furthermore the disinfection by-products resulting from the ozone treatment of polluted surface water have been conducted (Huang, *et al.*, 2005).

Filtration

The process of filtration involves the flow of water through a porous, fibrous or granular medium that captures the solids in its matrix or retains them on its surface (Madaeni, 1999). During this process the media selectively restrict the passage pollutants such as

organics, turbidity, nutrients, microorganisms, and oxygen depleting pollutants, inorganics, and metal ions, permitting relatively clear water through (Mulder, 1997). Filtration has the ability to remove larger matter and small hazardous chemicals the same as it is able to rid water of the larger compound materials, like salt, while selectively removing much smaller and dangerous chemicals, like chlorine and pesticides. This process also uses less energy than reverse osmosis and distillation however it is not appealing to industries due to its low selectivity of dyes (Al- Bastaki & Banat, 2004).

Reverse Osmosis

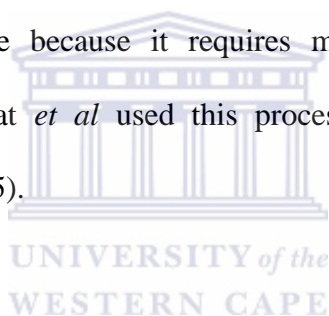
Reverse osmosis refers to a process of water purification that has been used primarily for the desalination of seawater. It adopts the principle of osmosis where two solutions of different concentrations are separated by a semi-permeable membrane. The water migrates from the low concentration to the higher concentration until both sides have the same concentration. However in reverse osmosis pressure is applied to the system to overthrow the natural flow of water to move from higher to lower concentration in so doing retaining bulkier salt molecules (Binnie, *et al.*, 2002).

This process usually uses membranes of polyamide-based materials to resist biological degradation; however they are prone to chemical degradation. Therefore with an ideal membrane that resists both biological and chemical degradation on applying desalination, pre-treatment is required to prevent water hardening chemicals from making a hard mineral on the membrane as this would reduce the membrane effectiveness (Vigneswaran, *et al.*, 1991).

Distillation

Distillation is a process that uses the principle of chemicals that vaporize at different temperatures. During this process wastewater is heated until its boiling point and the temperature is kept at a constant to vaporize the water, while barring other undesirable elements from vaporizing (Kiss, 2014). In this way all the chemicals with higher boiling points cannot escape the container, therefore forming sediment. The vaporized water is directed using tubes into a different container where it is cold and condenses to water.

This process has been used for several decades because it takes advantage of solar energy; which is an infinite source making this method of water purification cheaper (Sampathkumar, *et al.*, 2010). However solar energy is efficient for smaller amounts of water and takes a long time because it requires multiple distillations to ensure significant water purity. Banat *et al* used this process for the removal of MB in wastewater (Banat , *et al.*, 2005).



Biological Methods

Bio-treatment is cheaper and environmentally friendlier (Sudha, *et al.*, 2014). A number of researchers developed enzyme systems for the decolourization and mineralization of azo dyes under certain environmental conditions. These enzymes (which include azo reductases, hydrogenase, laccase and peroxidase), reduce dyes and further mineralize them into simpler compounds (Stolz, 2001).

Bacteria, yeasts and fungi are amongst the microorganisms used for this purpose (Fu & Viraraghavan, 2001; Forgacs, *et al.*, 2004). These treatment technologies require microorganisms to be resistant to the toxic effects of dyes and other contaminants present in wastewater and to have the ability for organisms to excrete active enzymes that aid the decolourization process. Bacteria have been used for the degradation of

synthetic dyes in wastewater. Jafari, *et al.*, (2012) used *Candida tropicalis* JKS2 coupled with photocatalytic (UV/TiO₂) for the treatment of Reactive Black 5 (RB5).

Table 2.2: Outlines the advantages and disadvantages of physical/chemical methods (Zille, *et al.*, 2005; Robinson, *et al.*, 2001)

Treatment methods	Advantages	Disadvantages
Electrocoagulation/ coagulation	Cost-effective	Sludge production
Ozonation	Used in a gaseous state and therefore has no volume limitations	Has a short half-life - approximately 20 minutes
Filtration	Can be used universally for all dyes	Produces slurries
Biological methods	Environmentally friendly and cost-effective	May form by-products, require secondary treatment
Irradiation	Can be successfully applied at lab scale	Requires a large amount of dissolved oxygen
Ion-exchange	Stable adsorbent and has the ability to redevelop	Cannot effectively remove all dyes
Fenton's reagent	Effective decolourisation of all dyes	Sludge production
Activated Carbon	Applicable to a wide variety of dyes	Expensive
Silica gel	Removes basic dyes	Cannot be used for commercial use, due to side reaction
Photochemical	No sludge formation	Produces by-products

Semiconductors

Semiconductors can be described as materials with electrical conductivity halfway between that of insulators and metals. Semiconductor-supported photocatalysis has received significant interest amongst advanced oxidation processes (AOP) for application on a large scale as a wastewater purification method (Comparelli, *et al.*, 2005). This type of photocatalytic procedure has been extensively studied, mainly due to its ability to degrade a high number of refractory chemicals in gaseous or aqueous systems, through rather inexpensive procedures. When semiconductors are photo-excited, charge separation takes place initiating the oxidation of organic compounds (Curri, *et al.*, 2003).

This process takes advantage of the strong reactivity of hydroxyl radicals in driving oxidation processes, ultimately leading to the extensive mineralization of a variety of environmental pollutants. To enhance the oxidation process the semiconductor materials are nano-sized, thus increasing potential for gaining charge-separation, which elevates performances even with immobilized photocatalysts (Banerjee, *et al.*, 2012). This is due to increased surface-to-volume ratio as compared to the bulk materials (Comparelli, *et al.*, 2005). Titanium dioxide is one of the most studied semiconductors due to its superior photoreactivity, long-term stability, non-toxicity, low operating cost, and radically low level of energy consumption when using this method (Beydoun, *et al.*, 2002; Valencia, *et al.*, 2010). Other semiconductors include zinc oxide (ZnO), cadmium sulphide (CdS) (Soltani, *et al.*, 2013), and tin oxide (SnO₂) (Naje, *et al.*, 2013). The diagram below summarizes the difference in the bandgap energies of insulators, semiconductors and conductors.

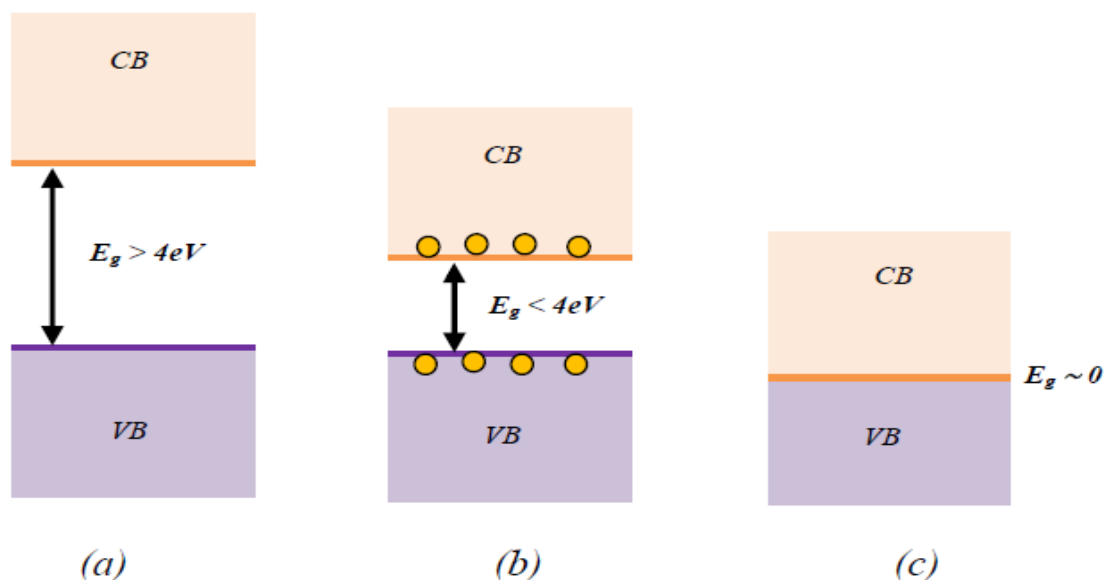


Figure 2.3: Bandgap energies of (a) insulators (b) semiconductors and (c) conductors

Properties of Titanium dioxide

Titanium dioxide, also known as titania, has received increasing attention due to its proven ability to function as a photocatalyst and facilitate important environmentally beneficial reactions, such as water splitting to generate hydrogen and treatment of polluted air and water (Hanaor & Sorrell, 2011). It has increased interest because of its non-toxicity, low cost, relatively high chemical stability and the possibility of using sunlight as a source of irradiation (Zhang & Gao, 2009). Daneshvar, *et al.*, 2004), regarded TiO_2 as an efficient photocatalyst for the degradation of various pollutants because of its fast electron transfer to molecular oxygen.

The oxygen vacancies act as electron donors, thus TiO_2 is an n-type semiconductor, in contrast with p-type semiconductors which contain electron acceptors and where the charge carriers are holes rather than electrons (Kim, *et al.*, 1996). Substoichiometric TiO_2 is regarded as both a poor insulator and a modest semiconductor; the electrical

properties of TiO_2 can be controlled by oxygen vacancies (Tang, *et al.*, 2009). According to Lu, *et al.*, (2007), the electrical conductivity can be improved by increasing the number of oxygen vacancies in the crystal thereby obtaining a non-stoichiometric titanium dioxide, TiO_2 , depending on its application. Titanium dioxide has three known structures under ambient conditions: anatase, rutile and brookite.

Anatase

Anatase is one of the tetragonal structures with a distortion of the TiO_6 octahedron larger than that of the rutile phase (Gupta & Tripathi, 2011) resulting in a less orthorhombic symmetry (Thompson & Yates, Jr, 2006). It is considered a metastable structure of titanium and exhibits exceptional photocatalytic activities. Anatase TiO_2 has a larger bandgap than rutile TiO_2 and can raise the valence band maximum to higher energy levels relative to the redox potential of adsorbed molecules (Luttrell, *et al.*, 2014). According to Muscat, *et al.*, (2002) the anatase phase is more stable than the rutile at 0 K, the energy difference between these two phases is small (~2- 10 kJ/mol). At high temperatures anatase may be transformed to the rutile phase (Hanaor & Sorrell, 2011). The heat treatment increases the crystallinity of anatase titanium. Since the activity of amorphous titania is insignificant, an anatase powder with a high degree of crystallinity and high surface area is important to increase the photocatalytic activity, (Ohtani, *et al.*, 1997).

Rutile

Rutile TiO_2 has a tetragonal structure and contains six atoms per unit cell (Gupta & Tripathi, 2011). A slight distortion from the orthorhombic structure occurs, and the unit

cell is where the unit cell is stretched past a cubic shape (Thompson & Yates, Jr, 2006). The rutile structure is the most stable and also the most studied. TiO_2 can be synthesized as single crystals, powders, ceramics and thin films. It can be formed from anatase and brookite structures after reaching a particular particle size, with the rutile phase being more stable than anatase at particle sizes. In general, it is found that the rutile form of TiO_2 is less photoactive than anatase, (Henderson, 2011). Sclafani, *et al.*, (1990), concluded that the rutile phase can be active or inactive, depending on its preparation conditions.

Brookite

According to Bokhimi, *et al.*, (1999) the brookite phase of TiO_2 is an orthorhombic crystal system. It has a cell unit made of eight formula units of titanium dioxide and is formed by edge-sharing TiO_6 octahedra. The brookite phase is the least dense of the three forms, has a larger cell volume. It is more complicated and seldom used for experimental investigations, (Thompson & Yates, Jr, 2006).

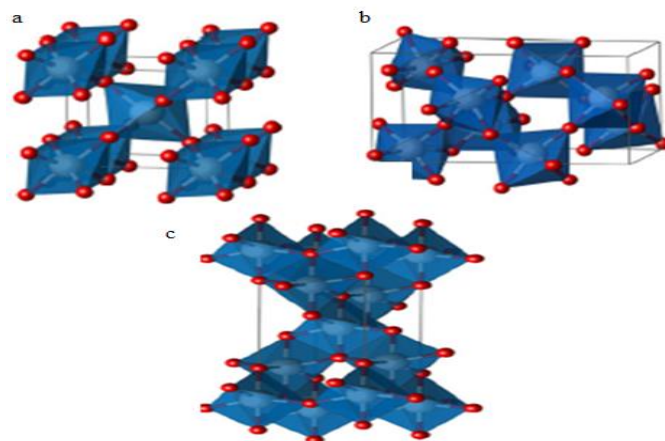


Figure 2.4: TiO_6 polyhedral for TiO_2 (a) rutile, (b) brookite and (c) anatase phases, (Landmann, *et al.*, 2012).

Magnetism in materials

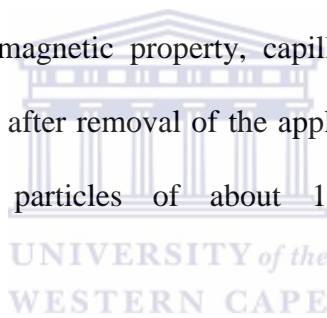
Materials are categorized according to their response to an externally applied magnetic field. Different forms of magnetism can be identified by the orientation of the magnetic moments. There are five basic types of magnetism; ferromagnetism, antiferromagnetism, ferrimagnetism, diamagnetism and paramagnetism (Poole, Jr. & Owens, 2003). When a magnetic field is applied to the material, the atomic current loops created by the orbital motion of electrons counter the applied field (Stefanita, 2008). This type of repulsion is diamagnetism and very weak, therefore the effects of the current loops can be suppressed by any magnetic behaviour which a material may display. Materials with filled electronic subshells, show diamagnetism and have negative susceptibility ($\chi < 0$) and weakly repel an applied magnetic field. In materials with a net magnetic moment or a long-range ordering of magnetic moments, the effects of atomic current loops are overcome (Jana, et al., 2004).

All other types of magnetic behaviour observed in materials show paramagnetism due to unpaired electrons in the 3d or 4f shells of each atom. These materials' magnetic moments have no long-range order and have positive magnetic susceptibility ($\chi \approx 0$) (Jana, et al., 2004). Different magnetic states can arise from iron atoms; iron as an element possesses a strong magnetic moment due to four unpaired electrons in its 3d orbital. In the paramagnetic state, the individual atomic magnetic moments are randomly aligned with respect to each other resulting in a zero net magnetic moment. In the presence of an external magnetic field, some of these moments will align, and the crystal gains a small net magnetic moment.

In a ferromagnetic crystal, all the individual moments are aligned even without an external field. Ferromagnetic materials are known as hard magnets (Kahn, et al., 1988). Ferrimagnetic crystals have an antiparallel arrangement of two types of atoms with

different strengths. When these antiparallel magnetic moments are of the same magnitude, then the crystal is antiferromagnetic with no net magnetic moment below a certain characteristic temperature, known as the Neel temperature (e.g., Fe_3O_4 and Fe_3S_4). Above the Neel temperature (T_N) thermal energy is adequate to cause the equal and oppositely aligned atomic moments to randomly alter, leading to a loss of their long range order, exhibiting paramagnetic behaviour.

In nanotechnology the particle size reduction leads to the formation of single-domain particles resulting in the phenomenon of superparamagnetism. Xuan, *et al.*, (2009), described superparamagnetism as the responsiveness of material to an applied magnetic field without retaining any magnetism after the applied magnetic field has been removed. With the superparamagnetic property, capillary blockage by aggregations formed by residual magnetism after removal of the applied field will be avoided. With synthesis of nanoparticles, particles of about 10nm are likely to display superparamagnetic behaviour.



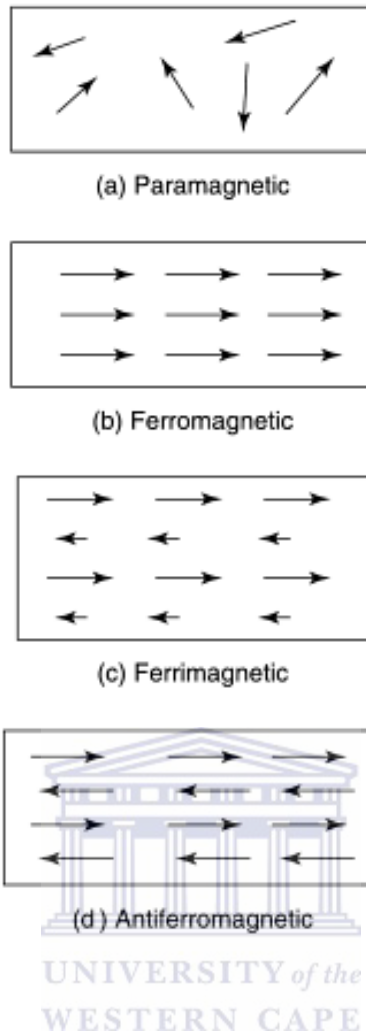


Figure 2.5: Illustration of various arrangements of individual atomic magnetic moments that constitute (a) paramagnetic, (b) ferromagnetic (c) ferrimagnetic and (d) antiferromagnetic materials (Poole, Jr. & Owens , 2003).

Iron oxide

Iron oxides exist in many forms in nature, with maghemite ($\gamma\text{-Fe}_2\text{O}_3$), magnetite (Fe_3O_4), and hematite ($\alpha\text{-Fe}_2\text{O}_3$) being probably the most common (Islam, et al., 2012). The iron atom has a strong magnetic moment due to four unpaired electrons in its 3d orbitals (Teja & Koh, 2009). Hematite polymorph has a rhombohedral-hexagonal,

prototype corundum structures and maghemite cubic spinel structure (Chirita & Grozescu , 2009). Hematite is paramagnetic at temperatures above its Curie temperature of 956 K, weakly ferromagnetic at room temperature and at 260 K (the Morin temperature, T_M) undergoes phase transition to an antiferromagnetic state (Dronskowski, 2001). The magnetic behaviour of hematite depends on particle size, crystallinity and on the extent of cation substitution (Raming, et al., 2002).

Maghemite is ferrimagnetic at room temperature, unstable at high temperatures, and loses its susceptibility with time, (Dronskowski, 2001). In time, at room-temperature, maghemite turns into a hematite crystalline structure. It differs from the inverse spinel structure of magnetite (which is ferromagnetic at room temperature) through vacancies on the cation sublattice (Chirita & Grozescu , 2009). Magnetite nanoparticles are superparamagnetic at room temperature however their magnetic properties depend strongly on the synthesis methods used (Chapline & Wang, 2005). The magnetic properties depend on crystal morphology because it affects coercivity in the order: spheres<cubes<octahedra in line with an increase in the number of magnetic axes along this series of shapes (Margulies, et al., 1997).

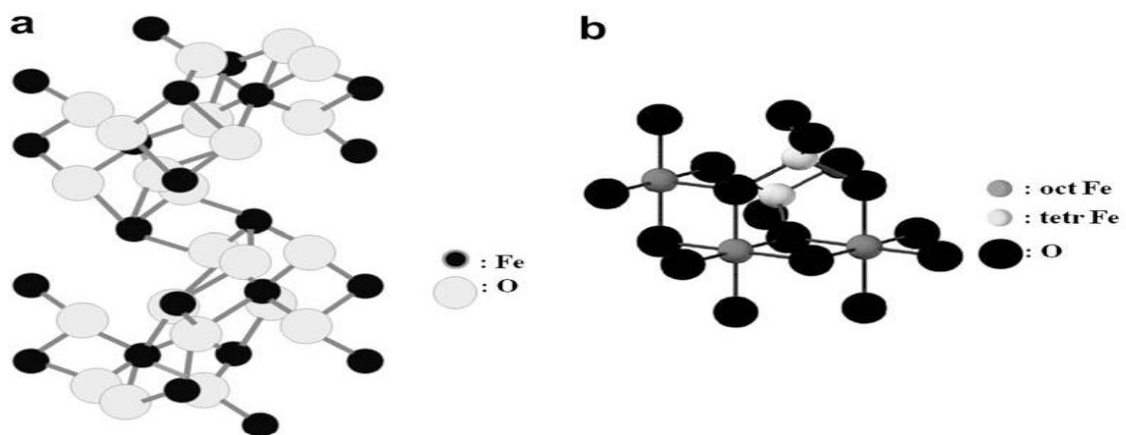


Figure 2.6: Crystal structures of (a) hematite and (b) magnetite, (Teja & Koh, 2009).

In the current study the incorporation assists with the catalyst separation from treated water. This approach is suitable because it may prevent the agglomeration of the catalyst particles during recovery and increase the durability of the catalysts, (Xuan, et al., 2009).

Reviews on titanium dioxide based catalysts

The current paper investigates degradation of methylene blue (azo dye) using silver doped magnetite titanium dioxide nanoparticles for the degradation of methylene blue. In the 1960s Honda and Fujishima were the first to discover the electrochemical photolysis of water using TiO_2 as an electrode (Fujishima & Honda, 1972). For the past 20 years titania has been used by several researchers for water treatment application with different modifications (Sclafani & Herrmann , 1998), with the aim of enhancing its photoactivity.

Table 2.3: Reviews different catalyst types, the organic pollutants and their degradation rates

Catalyst type	Organic pollutant	Degradation rate/ percentage	Reference
TiO₂/SiO₂/Fe₃O₄	Remazole golden yellow G., remazole brilliant blue R, and reactive orange 16	Complete decolourization and degradation in 45min	Gad-Allah, <i>et al.</i> , 2009
nanoTiO₂/Fe₃O₄ composite particles	Methyl blue	Efficient	Li , <i>et al.</i> , 2009
Commercial catalyst TiO₂/halloysite nanotube composite	Methylene blue	Commercial photocatalyst showed lower photocatalytic activity	Chin, <i>et al.</i> , 2010
TiO₂/SiO₂/Fe₃O₄	Methylene blue	95.3% in 45minutes	Hu, <i>et al.</i> , 2011
Fe₃O₄/SiO₂/TiO₂ nanoparticles	organic compounds of olive mill wastewater	~50% in 120min	Ruzmanova, <i>et al.</i> , 2013
Fe₃O₄/SiO₂/TiO₂ nanoparticles	Fluorsein, orange II and red under visible and UV irradiation	-	Chen, <i>et al.</i> , 2001
TiO₂/UV	Alizarin, crocein orange G, methyle red, congo red and methylene blue	Complete mineralization into harmless ions	Lachheb, <i>et al.</i> , 2002
Fe₃O₄/SiO₂ /TiO₂	Methylene blue, red basic dye, blue basic dye, nonylphenol, and octylphenol, under UV	Good adsorption and photolytic decomposition	Kurinobu, <i>et al.</i> , 2007
γ-Fe₂O₃@SiO₂)n@TiO₂	Methylene blue	80% in 80min	Wang, <i>et al.</i> , 2009
Fe₃O₄@TiO₂ Hollow Spheres	Rhodamine B	89.6% in 120min	Xuan, <i>et al.</i> , 2009
TiO₂/SiO₂@Fe₃O₄	Rhodamine B	98.1% in 60 minutes	Liu, <i>et al.</i> , 2011

Titanium dioxide nanoparticles	2-chlorophenol, 2,4-dichlorophenol and 2,4,6-trichlorophenol	99% 98% 92% after 90min	Ba-Abbad, <i>et al.</i> , 2012
Fe₃O₄/SiO₂/TiO₂ core-shell structure	Rhodamine B	80% in 120 minutes	Cheng, <i>et al.</i> , 2012
Fe₃O₄/SiO₂/TiO₂	2-chlorophenol	97.2% after 3hours	Rashid, <i>et al.</i> , 2015
TiO₂/SiO₂/CoFe₂O₄ nanoparticles	Methylene blue	98.3% in 40min	Harraz, <i>et al.</i> , 2014
CdS-TiO₂/Fe₃O₄	Reactive Brilliant Red X-3B dye	78.9%	Dong, <i>et al.</i> , 2013
GO-NiFe₂O₄	Methylene blue	Stable for 8 cycles	Liu, <i>et al.</i> , 2013
G-TiO₂	Methylene blue	100% in 90min	Liu, <i>et al.</i> , 2013
ZnO-GRs	Methylene blue	60%	Fan, <i>et al.</i> , 2012
ZnO-C	Methylene blue	20%	Shen, <i>et al.</i> , 2008
ZnO-SiO₂	Methylene blue	90%	
ZnO particles	Methylene blue Eosin Y. under UV radiation	76% 74%	Chakrabarti, <i>et al.</i> , 2004
Ag-TiO₂ particles	Sucrose Salicylic acid	Enhanced activity	Vamathevan, <i>et al.</i> , 2002
Ag-TiO₂ thin films	Methyl orange	effective	Arabatzis, <i>et al.</i> , 2003
Ag-TiO₂	Rhodamine B	effective	Sung-Suh, <i>et al.</i> , 2004
Pure TiO₂	Humic acid, oxalic acid and formic acid	6%	Seery, <i>et al.</i> , 2007
Ag-TiO₂		50%	
Ag-Fe₃O₄/SiO₂/TiO₂	Direct diazo dyes, direct red 23 and direct blue 53	Good activity	degradation Sobana, <i>et al.</i> , 2006
1wt%- Pt, Au and Pd deposited TiO₂	Leather dye, acid green 16	High efficiency	photonic Sakthivel, <i>et al.</i> , 2004
Ag or Pd/-TiO₂/CNTs	Methylene blue	92% in 4hours, silver showing best activity	Hintsho, <i>et al.</i> , 2014

Titanium dioxide photocatalyst has been applied for the degradation of a number of dyes as indicated in the table above. The catalyst has proven to be a good and effective catalyst. To overcome the post separation difficulty incurred from powder TiO₂, solid supports, metals or silica has been incorporated in the photocatalyst. The results have shown to maintain good activity under ultra-violet and/ or visible light and even without irradiation; however UV irradiation has presented the best results. The doping of the silver nanoparticles on the TiO₂ layer extends the region of the light spectrum the catalyst can absorb in. This makes it possible to use it under visible light. Zinc oxide is one of the photocatalysts used, however TiO₂ has reported most due to its superior photoreactivity, long-term stability, non-toxicity, low operating cost, and radically low level of energy consumption (Valencia, et al., 2010).

Synthetic Techniques

Micro emulsion



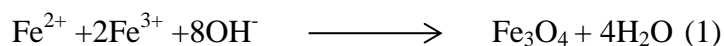
The micro emulsion is described as an isotropic and thermo-dynamically stable single-phase system made up of three components; water, oil, and an amphiphilic molecule (surfactant) (Santra, *et al.*, 2001). The surfactant molecule lowers the interfacial tension between water and oil resulting in the formation of a transparent solution. The nanodroplets (either water or oil) present in the bulk oil or water phase serve as a nanoreactor for the synthesis of nanoparticles. The size and shape of the microemulsion droplets are determined by the water to surfactant ratio, and are governed by factors such as concentration of reactants (especially surfactant) and flexibility of the surfactant film (Teja & Koh, 2009). The water in the microemulsions may be substituted with other polar solvents; moreover microemulsions offer convenient templates for

nanoparticle synthesis and a low cost synthetic process, (Margulis-Goshen & Magdassi, 2012). With this binary system, different structures can be formed ranging from (inverted) spherical and cylindrical micelles to lamellar phases and continuous microemulsions, which may coexist with predominantly oil or aqueous phases, (Wu, *et al.*, 2008). This method has also been used for the synthesis of bimetallic nanoparticles, (Zhang & Chan, 2003), and quantum dots (Darbandi, *et al.*, 2005). Chin & Yaacob, (2007), reported the synthesis of magnetic iron oxide nanoparticles using the w/o microemulsion method and Massart's procedure. The particles produced by the microemulsion method showed smaller particle sizes (less than 10 nm), higher in saturation magnetization.

Recently Wongwailikhit *et al.*, used the W/O microemulsion for the synthesis of Iron (III) oxide, Fe_2O_3 using a standard solution of n-heptane as oil phase, and water and sodium bis (2-ethylhexyl) sulfosuccinate as the surfactant. Iron (III) chloride was used as a starting material and ammonium hydroxide as a precipitating agent. Particle sizes were dependent on the water content, and increased with water content resulting in an average particle size smaller than 100nm, (Wongwailikhit & Horwongsakul, 2011).

Co-precipitation

The co-precipitation technique can be considered the most efficient and simple chemical route for the synthesis of magnetic particles. Metal oxide particles (either Fe_3O_4 or $\gamma\text{Fe}_2\text{O}_3$) can also be prepared by an aging stoichiometric mixture of the two metal ions in an aqueous medium, (Laurent, *et al.*, 2008). The chemical reaction of the preparation of magnetite may be summarized as (McBain, *et al.*, 2008)



Controlling the pH, ionic strength and particle size can be tunable to less than 15 nm (Tartaj, *et al.*, 2005), which is governed by kinetic factors, moreover complete precipitation of Fe_3O_4 is expected at a pH between 8 and 14. Magnetic oxides oxidize when exposed to oxygen and hence should be avoided.



The size and shape of the iron oxide NPs depends on the type of salt used (such as chlorides, sulfates, nitrates, perchlorates, etc.), the ferric and ferrous ions ratio, the reaction temperature, the PH value, ionic strength of the media, and the other reaction parameters (e.g. stirring rate, dropping speed of basic solution). Co-precipitation was often employed, but this method presents low control of the particle shape, broad distribution of sizes and particles tend to aggregate due to large surface to volume ratio to reduce their surface energy (Kim, *et al.*, 2001; Tartaj, *et al.*, 2005; Wu, *et al.*, 2008). The suspension of nanoparticles can be stabilized by adding anionic surfactants as dispersing agents (Lin, *et al.*, 2005). Co-precipitation methods are commonly inexpensive, have high product yields and particle surfaces are easily treated (Majewski & Thierry, 2007).

The co-precipitation method was applied for the synthesis of iron oxide nanoparticles for the removal of procion dye, yielding Fe_3O_4 with a mean diameter of 5-20 nm and capable of removing 24.40% of the dye in 30 minutes (Hariani, *et al.*, 2013). Sequentially this method has been used for magnetic oxide preparations by Mascolo, *et al.*, (2013) resulting in supermagnetic nanoparticles and lower saturation magnetization depending on the particle size (Kandpal, *et al.*, 2014), obtaining 20-22nm particle sizes respectively.

Hydrothermal treatment

Hydrothermal synthesis is a process that is performed in aqueous media in reactors or an autoclave, where the temperatures and pressure are elevated higher than 200 °C and 2000 psi respectively (Suchanek & Riman, 2006; Laurent, *et al.*, 2008). The temperature and pressure limits can spread beyond 1000°C and 500 MPa, (Roy, 1994). The ionic product (K_w) has a maximum value of about 250–300 °C and hydrothermal synthesis is generally carried out below 300 °C. Since water is the most used solvent for this synthesis, its critical temperature and pressure of water are 374 °C and 22.1 MPa, respectively. Under supercritical conditions solvent properties for many compounds, such as dielectric constant and solubility, change intensely (Hayashi & Hakuta, 2010). The technique requires that starting materials should be as pure, fine and homogeneous as possible and have an accurately known composition (Somiya & Roy, 2000).

Hydrothermal synthesis performed at supercritical water gives a favourable reaction field for particle formation, due to the enhancement of the reaction rate and large supersaturation based on the nucleation theory, owing to the lowering of the solubility. The reaction rate is improved more than 103 times than conventional hydrothermal conditions because the dielectric constant is lowered to (<10) yielding high crystalline products (Hakuta, *et al.*, 2003).

A surfactant free, one-step hydrothermal process was used by Wang, *et al.*, (2003) synthesizing highly crystalline Fe₃O₄ nanopowders. The resultant nanoscale Fe₃O₄ powder (40 nm) obtained at 140 °C for 6 h possessed a saturation magnetization of 85.8 emug⁻¹, a little lower than that of the correspondent bulk Fe₃O₄ (92 emug⁻¹). Zheng, *et al.*, (2006), reported the preparation of 27nm Fe₃O₄ nanoparticles via a hydrothermal route in the presence of a surfactant, sodium bis (2-ethylhexyl) sulfosuccinate and

exhibited superparamagnetic behaviour at room temperature. A hydrothermal synthetic route seems to be the optimal method for controlling the particle sizes and morphology of iron oxide nanoparticles (Wu , *et al.*, 2008).

Sol-gel method

The sol-gel method can be described as the hydrolysis and condensation of metal alkoxide precursors or alkoxides, leading to oxides dispersed in a sol (Teja & Koh, 2009). The sol is then dried or gelled. The particles agglomerate to clusters and eventually form interconnected chains (Lam, *et al.*, 2008). According to Hench & West, (1990) three tactics can be used to make sol-gel monoliths: method 1; hydrolysis and polycondensation of alkoxide or nitrate precursors followed by hypercritical drying of gels; method 2; hydrolysis and polycondensation of alkoxide precursors followed by aging and drying under ambient atmospheres; method 3; gelation of a solution of colloidal powders.

The reaction usually takes place at room temperature, in water or organic solvents, acidic and basic; with acidic and basic solutions forming a polymeric gel and colloidal gel respectively (Coradin, *et al.*, 2006; Lam, *et al.*, 2008). The sol-gel process is generally useful for the production of silica, glass, and ceramic materials because of its ability to produce pure and homogenous products at mild conditions (Rahman & Padavettan, 2012). Aerogels have been limited for use as insulating materials or wide gap materials due to the chemical systems used for gel formation (Nahar & Arachchige, 2013). This method has been applied for the synthesis of metal oxides and nanosized metals, heteroelement and fused bimetallic particles (Gubin, *et al.*, 2005).

The sol-gel method offers the possibility for obtaining pure amorphous phases, monodispersity, and good control of the particle size. By tailoring experimental conditions, materials with predetermined structures can be attained. Additionally the microstructure and the homogeneity of the reaction products can be controlled, and there is a possibility of embedding molecules, which maintain their stability and properties within the sol-gel matrix (Raileanu, *et al.*, 2005). This technique has been used by several researchers. Li, *et al.*, (2009) used the sol-gel technique for the synthesis of superparamagnetic TiO₂/Fe₃O₄ composite whose photocatalytic activity increased with increased TiO₂ content while decreasing the magnetization saturation. It has also been used for the synthesis of graphene–titania composites (Liu, *et al.*, 2013), and novel magnetic photocatalyst by direct deposition of nanosized TiO₂ crystals onto a magnetic core (Watson, *et al.*, 2002; Gad-Allah, *et al.*, 2008).

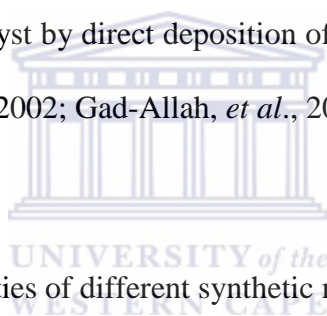


Table 2.4: Outlines the properties of different synthetic methods (Lu, *et al.*, 2007).

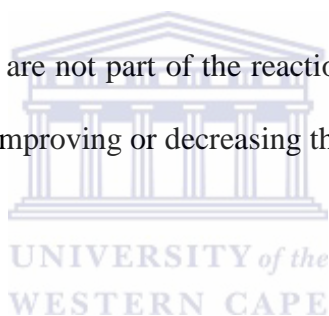
Synthetic Method	Synthesis	Reaction temp (°C)	Reaction period	Size distribution	Shape control	Yield	Solvent
Micro-emulsion	complicated, ambient conditions	20- 50	hours	relatively narrow	good	Low	organic compound
Co-precipitation	simple, ambient conditions	20- 90	minutes	relatively narrow	not good	High	water
Hydrothermal synthesis	simple, high pressure	220	hours ca. days	very narrow	very good	Medium	water-ethanol
Sol-gel method	simple ambient	T < 100		narrow	Good	High	water acids and bases

Factors affecting photocatalytic activity

The photocatalytic performance of the catalyst is influenced by several factors; extrinsic and intrinsic. The intrinsic factors include crystal structure, crystallinity and the morphology (Xia, *et al.*, 2008) particle size, surface hydroxyls, and surface area (Tia, *et al.*, 2011; Behnajady, *et al.*, 2008). The extrinsic parameters are temperature, light intensity, pH, reaction time, catalyst loading and initial concentration of pollutant.

Extrinsic parameters

Extrinsic factors are those that are not part of the reaction but are an external influence towards the reaction by either improving or decreasing the end result.



Temperature

To enhance the photocatalytic activity of TiO₂ catalyst, usually heat treatment is a useful method (Yu, *et al.*, 2006). Yu, *et al.*, (2000) revealed that photocatalytic activity increased after thermal treatment due to the increase in oxygen adsorbed on the catalyst surface. Additionally Sato, *et al.*, (1984) made a similar observation suggesting that improved photocatalytic activity was obtained after calcination due to release of lattice oxygen from TiO₂. Heat treatment of TiO₂ catalyst facilitates the transformation of amorphous TiO₂ into a more photoactive crystalline phase.

However caution needs to be taken as very high temperatures and prolonged heat treatment times may lead to a decrease in the catalyst's surface area (due to sintering

and crystal growth) and loss of hydroxyl groups; consequently leading to a decrease in photocatalytic activity. Moreover the decrease in the activity may also be ascribed to the interaction of the magnetic core and titanium dioxide coating, leading to a decrease in the magnetic properties of the prepared photocatalyst (Beydoun & Amal, 2002; Watson, *et al.*, 2002).

Reaction temperature is also an important process parameter, usually photocatalytic systems are operated at room temperature (Gogate & Pandit, 2004). In the range of 20–80°C, usually weak dependence of the degradation rates on temperature has been observed (Herney-Ramirez, *et al.*, 2010; Andreozzi, *et al.*, 1999). According to Casbeer, *et al.*, (2012) temperature alters the crystal structure of the photocatalyst, therefore the surface defects are changed, which decreases the reaction of the recombination of electron/hole pairs, eventually improving photocatalytic activity. However, heating above 80°C requires cooling as this may reduce the rate of reaction leading to the decrease in the adsorption of pollutant on the catalyst surface, (Herrmann, 1999). The degradation of azo-dye acid black 1 between a temperature range 30-75°C was investigated by Sum, *et al.*, (2005). Their findings showed enhanced total organic carbon removal in the first 30 minutes of the reaction was attributed to the increase of the collision frequency of molecules on the surface of the catalyst under the range of the studied temperature.

Initial concentration

The most critical factor governing photodegradation of organic pollutants is the formation of hydroxyl radicals on the catalyst's surface and their interaction with the dye. High initial concentration of dyes show low degradation efficiency and hence

dilutions are necessary (Gogate & Pandit, 2004). In highly concentrated effluents an increased number of dye molecules are adsorbed on the catalyst surface, covering most active sites. Additionally, concentrated dye solution decreases the path length of photon entering the pollutant solution (Mills, *et al.*, 1993). The light is absorbed by the pollutant, shielding it from reaching the catalyst and reducing the formation of hydroxyl radicals leading to decreased photocatalytic activity (Harraz, *et al.*, 2014).

The solar photocatalytic degradation of acid brown 14 using ZnO and TiO₂ was reported by Sakthivel, *et al.*, (2003). The degradation reaction was carried out varying initial concentration (2×10^{-4} to 6×10^{-4} mol l⁻¹). The rate of degradation increases with the increase in the concentration. However increase in concentration exceeding the optimum concentration (5×10^{-4} mol l⁻¹) led to a noticeable decrease in the rate of dye.

Similarly (Harraz, *et al.*, 2014), examined the effect of initial concentration of MB from 100 to 250 ppm with a constant catalyst loading 0.165 g/L at pH 9 for 40 min irradiation time. With increasing initial concentration more dye molecules were adsorbed on the catalyst surface covering all active sites thus a further increase lead to a decrease in the photodegradation. Rashid, *et al.*, (2015), conveyed complete mineralization of 25 mg/L 2-chlorophenol (2-CP) within 130 min while 97.2 % degradation of 50 mg/L 2-CP could be achieved after three hours (Rashid, *et al.*, 2015).

The concentration of dye molecules is affected by the available catalyst active sites and thus the concentration of dye should increase with increasing catalyst loading for optimal results.

Catalyst Loading

Catalyst loading plays a major role in photocatalytic degradation as it is the absorbent of the dye molecules. The increase in catalyst loading increases the surface area, thus increasing active sites and formation of hydroxyl radicals responsible for the degradation (Harraz, *et al.*, 2014). However when catalyst loading exceeds the optimal value it becomes detrimental to the photodegradation reaction. The catalyst particles tend to aggregate, decreasing the surface area, and increasing light scattering (Toor, *et al.*, 2005) causing difficulty in light penetration through the solution. Increased catalyst concentration decreases photo absorption which sequentially reduces the dye adsorption onto the catalyst surface thus reducing the reaction rates (Epling & Lin, 2002).

The photocatalytic degradation of methylene blue using titanium oxide (TiO₂) was reported by Madhu, *et al.*, (2009). The effect of photocatalyst loading was investigated between 0.025 to 0.15wt. % at pH 7 and 27°C under atmospheric pressure conditions. The degradation rate increased from 0.025% to 0.1wt. % catalyst loading, and decreased when the catalyst was increased thereafter, showing that loading above optimal loading negatively affects the photodegradation performance.

Light source

The light source used for the degradation of the organic pollutants is essential as it determines performance of the catalyst used. The threshold wavelength corresponds to the band gap energy for the semiconductor catalyst; e.g. for the TiO₂ catalyst having a band gap energy of 3.02 eV, thus the ideal wavelength is at 400 nm (Gogate & Pandit,

2004) i.e. UV light region. Sunlight and visible light has also been used as an effective light source as reported by, Muruganandham, *et al.*, (2006); Epling & Lin, (2002).

The degradation of sulforhodamine-B in aqueous TiO₂ dispersions was investigated under three lighting regimes: UV light, visible and sunlight. The results revealed that UV and sunlight showed better degradation efficiency compared to visible light (Fang , *et al.*, 2007).

pH

The pH of the dye solution also has an important effect on the photocatalytic performance and the stability of the catalyst during the degradation process. pH effect is typically dependent on the point charge of the semiconductor used in the degradation reaction (electrostatic interaction of the catalyst with the pollutant) and on the type of pollutant used in the study (Gogate & Pandit, 2004). According to Saien, *et al.*, (2010) titanium dioxide has an amphoteric character with a zero point charge pH of 6.25; its surface is positively charged under acidic conditions and negatively charged under alkaline conditions. The maximum oxidizing capacity of the titania is at lower pH however the reaction rate is known to decrease at low pH due to excess H⁺. The adsorption of the pollutant and photocatalytic performance is enhanced near the zPc of the catalyst (Subramanian, *et al.*, 2000).

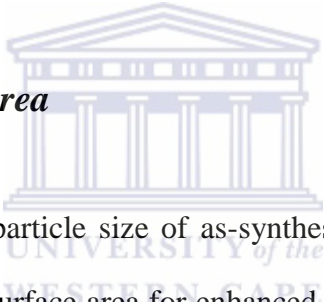
The effect of pH is not only dependent on surface charge, but also on the generation of hydroxyl free radicals. Piscopo, *et al.*, (2001), studied the degradation of benzamide (BA) and para-hydroxybenzoic acid (4-HBZ) using TiO₂ in a pH range of 3–11 and chloride anions (range 0–0.8 mol /l). The degradation rate of 4-HBZ increased with

decreasing pH, but BA was affected by the chloride anions concentration. It is evident that different dyes have different activity in a photocatalytic reaction. Some can be degraded at a high and others at a low pH. This phenomenon is dependent on the nature of the pollutant being investigated (Akpan & Hameed, 2009).

Intrinsic parameters

Intrinsic factors are those that are not part of the reaction but are an internal influence on the reaction by either improving or decreasing the end result.

Particle size and surface area



Various effects influence the particle size of as-synthesized catalyst. Nanotechnology has been used to improve the surface area for enhanced photodegradation performance. It has been thus assumed and proven that the smaller the particle size, the more the surface area increases and thus more surface hydroxyls are available to degrade organic pollutants. Xu , *et al.*, (1999) conducted a study of the effect which particle size has on photocatalytic performance during a degradation reaction. The results showed an increased adsorption rate and adsorbability of methylene blue in a suspended aqueous solution with decreased TiO₂ particle sizes, especially when the particle size is less than 30 nm. Multiple researchers have proven similar results (Gribb & Banfield, 1997, Shi, *et al.*, 2000).

Surface morphology

Surface morphology also has a great influence on catalyst effectiveness. Crystalline morphology has been reported to have enhanced photodegradation performance compared to amorphous morphologies. Heat treatment has been used to transform amorphous titania to crystalline titania, (Xuan, *et al.*, 2009).



Chapter 3: Materials and Methodologies

This chapter presents the materials, methods and schematic diagrams used of the synthesis of Ag-Fe₃O₄/SiO₂/TiO₂ nanocomposite.

Materials

The chemicals were used as received without any further purification.

Table 3.5: Chemicals used and respective suppliers

Chemical	Supplier	Purity
Ethanol	Sigma- Aldrich	99.9%
Ethylene glycol	Sigma- Aldrich	99.8%, anhydrous
Titanium Isopropoxide	Aldrich Chemical company	99.99%
Potassium nitrate	Kimix	99%
Potassium hydroxide	Sigma- Aldrich	99.9%
Iron (II) sulphate heptahydrate	Saarchem-Holpro Analytic	99.9%
Ammonia	Sigma-Aldrich	99%
Tetraethyl orthosilicate	Sigma Adrich	99.9%
Oleyalamine	Aldrich Chemistry	70%
Silver nitrate	Sigma- Aldrich	99%

Methodologies

The synthetic methods used in the current study are presented below.

Synthesis of iron oxide nanoparticles

Iron oxide nanoparticles were synthesized using a method previously reported by (Girginova, et al., 2010). An Fe(II) solution was prepared by using 5g of $\text{FeSO}_4 \cdot 7\text{H}_2\text{O}$ and dissolved in 35ml of distilled water in a 50ml round bottom flask under nitrogen. In a separate flask 0.4053g of KNO_3 and 2.8075g of KOH were dissolved in 15ml water(solution b) at 90°C in an oil bath . Solution b was added dropwise for 5 minutes into the Fe(II) under nitrogen yielding a black solution. The solution was maintained in the bath at 90°C for an hour to ensure homogeneity of the solution, and was left overnight at the same temperature.

After 15 hours the nanoparticles were separated magnetically and washed with 30ml water six times

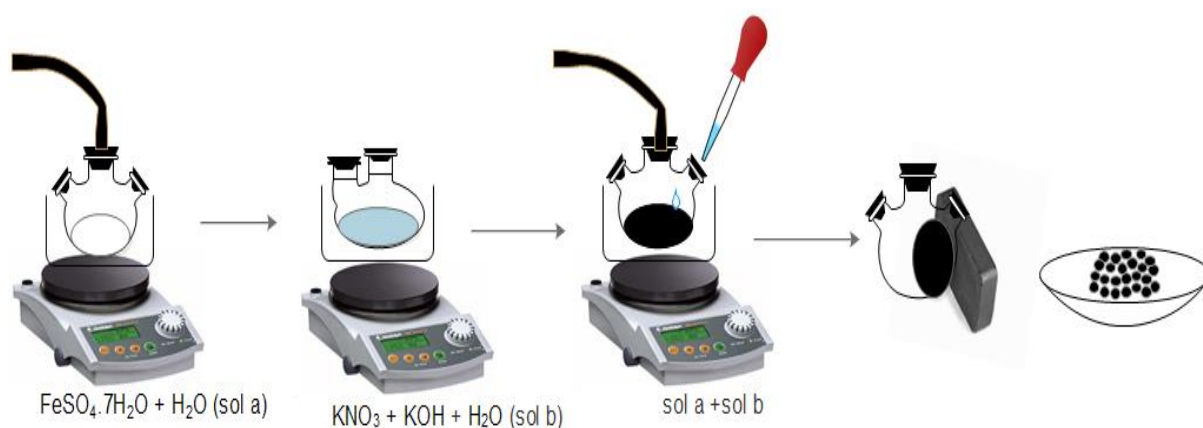


Figure 3.7: Synthesis of Fe_3O_4

Synthesis of silica coating ($\text{Fe}_3\text{O}_4/\text{SiO}_2$) nanoparticles

Iron oxide nanoparticles were coated with silica to create an insulating layer on the surface in a similar fashion like that reported by (Girginova, et al., 2010).

Around 0.6g of the asynthesized particles were dispersed in 450ml ethanol and sonicated in an icebath for 15 minutes. To the mixture 36ml ammonia and 1.2ml of TEOS were added and the suspension allowed to sonicated for further 2 hours in an ice bath. The particles were collected, washed and dried.

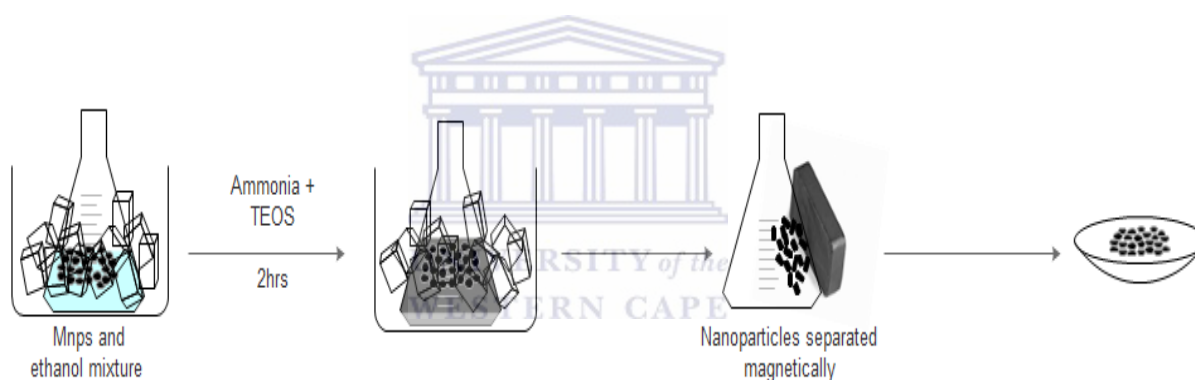


Figure 3.8: Synthesis of $\text{Fe}_3\text{O}_4/\text{SiO}_2$

Synthesis of titanium dioxide iron oxide ($\text{Fe}_3\text{O}_4/\text{SiO}_2/\text{TiO}_2$) nanoparticles

The silica coated iron oxide nanoparticles were coated with titanium dioxide which acts as the photo-catalytic layer of the catalyst to aid the degradation of methylene blue.

These particles were synthesized using a sol-gel technique. About 0.3g of silica coated iron oxide nanoparticles were disseminated in a solution 3ml of titanium (IV) butoxide and 105ml ethanol and sonicated for 10 minutes. The mixture was stirred and to this 6ml of water and ethanol solution (1:5 v/v) was added dropwise. The suspension was allowed to stir for 2 hours at room temperature. The particles were collected and washed several times with water and ethanol. The resulting particles were dried and calcined at 450°C at a rate of 8°C/min for 2 hours under nitrogen in order to change the amorphous titanium dioxide into a photoactive crystalline phase.

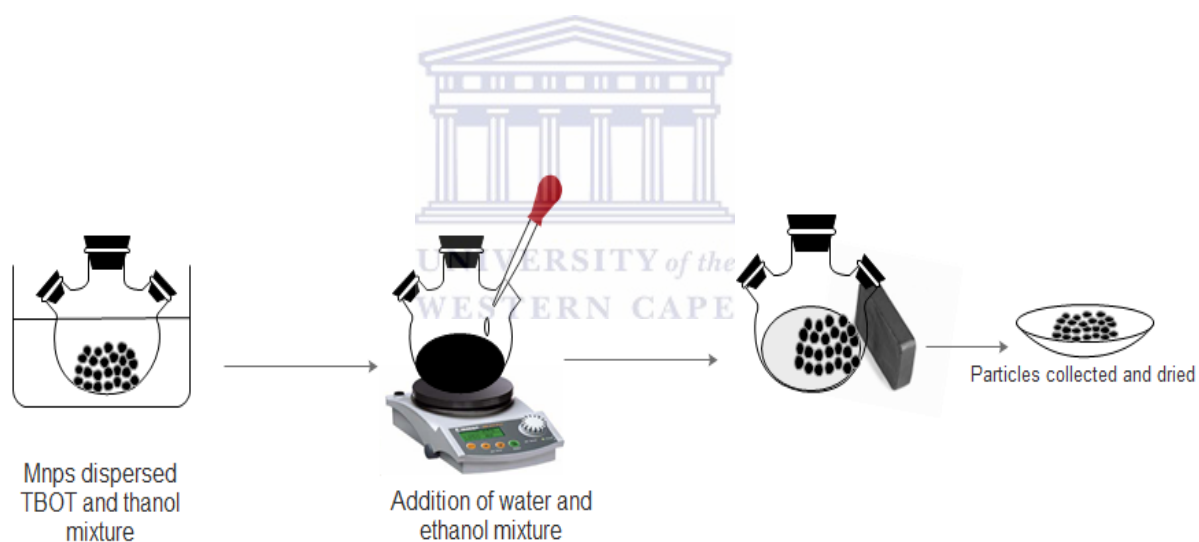


Figure 3.9: Synthesis of $\text{Fe}_3\text{O}_4/\text{SiO}_2/\text{TiO}_2$

Synthesis of silver doped magnetite titanium dioxide (Ag- $\text{Fe}_3\text{O}_4/\text{SiO}_2/\text{TiO}_2$) nanoparticles

The $\text{Fe}_3\text{O}_4/\text{SiO}_2/\text{TiO}_2$ nanoparticles were doped with silver to increase the catalyst's photocatalytic activity.

In a round bottom flask, 0.2g of asynthesized nanoparticles were dispersed in 0.4ml oylamine and 17ml of ethylene glycol and sonicated for half an hour. The suspension was transferred into an autoclave, stirred and heated at 196°C for 24 hours. The resulting particles were collected and washed with water and ethanol several times. The particles were dried and calcined at 450°C for 2 hours.

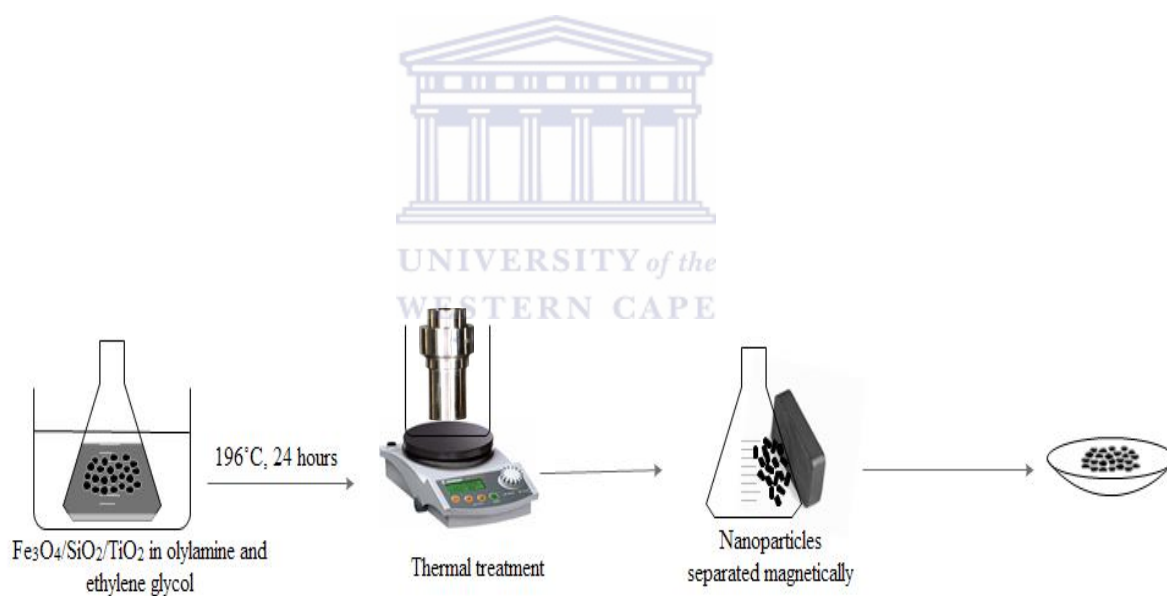


Figure 3.10: Synthesis of Ag- $\text{Fe}_3\text{O}_4/\text{SiO}_2/\text{TiO}_2$

Chapter 4: Characterization Techniques

This chapter shows the characterization of the as-synthesized nanocomposites. It represents the results obtained from the following characterization techniques; Fourier- Transform infrared spectroscopy, High- resolution transmission microscopy, scanning electron microscopy, X-ray diffraction, Brauneur Emmett Teller analysis, thermogravimetric analysis and differential scanning calorimetry and discusses the observations.

Fourier- Transform Infrared Spectroscopy

FT- IR is a technique used to analyse and identify unknown materials; it gives information about the quality or consistency of a sample and the amount of components in a mixture/ sample. This is done by passing infra-red radiation through a sample. The sample absorbs some of the infrared radiation and some of it is transmitted.

The resulting spectrum represents the molecular absorption and transmission, creating a molecular fingerprint characteristic of the sample of interest. This technique holds great reliability because no two samples can have the same fingerprint.

Sample preparation

The samples were in powder form and did not require preparation. The samples were dried completely and were ready to be run. The catalysts were characterized using the Perkin Elmer Spectrum Two, at a scanning range of 400 -4000 cm^{-1} .

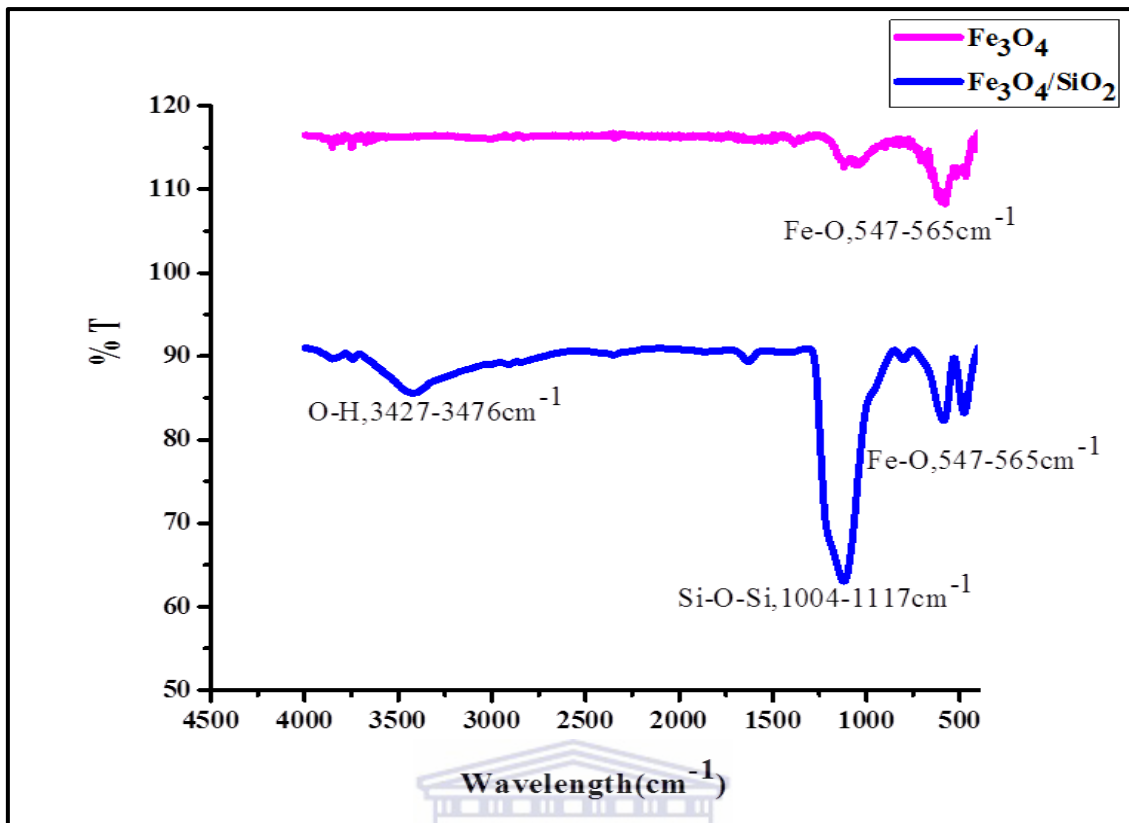


Figure 4.11: FT-IR spectra of Fe_3O_4 and $\text{Fe}_3\text{O}_4/\text{SiO}_2$

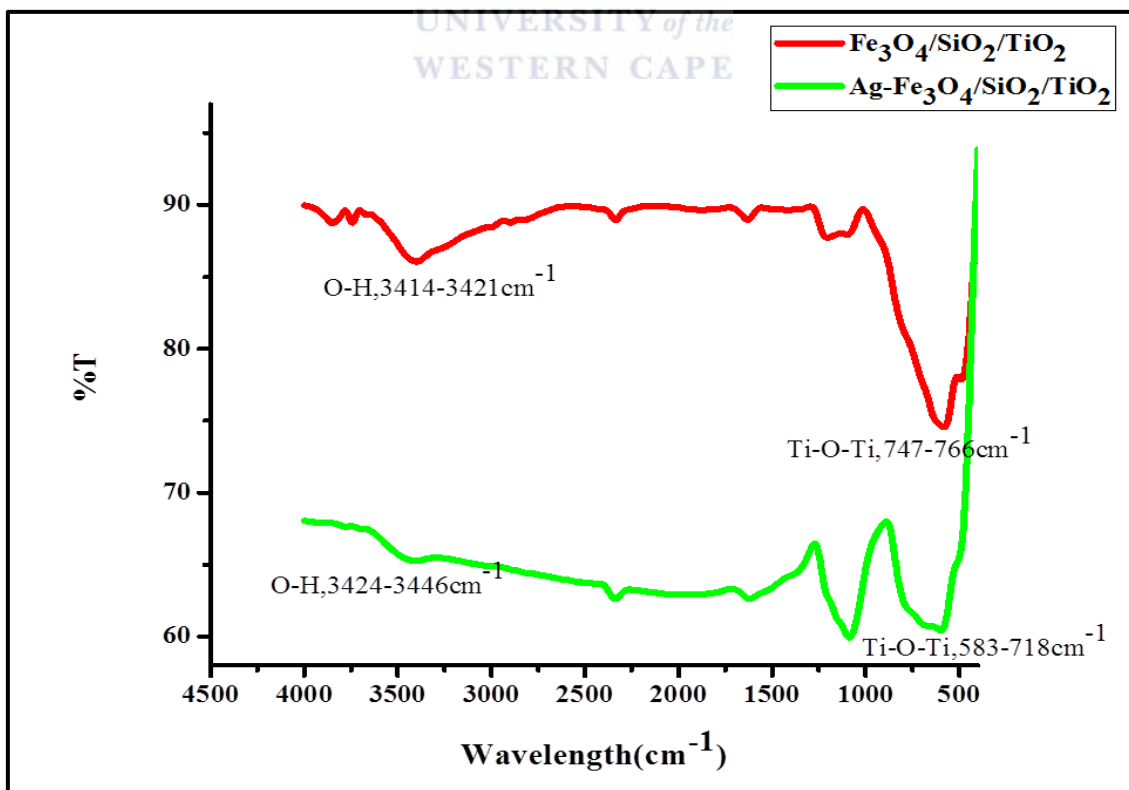


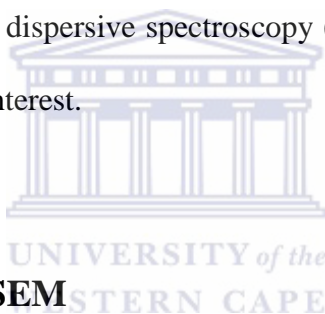
Figure 4.12: FT-IR spectra of $\text{Fe}_3\text{O}_4/\text{SiO}_2/\text{TiO}_2$ and $\text{Ag-Fe}_3\text{O}_4/\text{SiO}_2/\text{TiO}_2$

The FT-IR spectra (fig 4.1) show the functional groups present in the as-synthesized Fe_3O_4 and $\text{Fe}_3\text{O}_4/\text{SiO}_2$ core-shell structure. In all curves in figure 4.1, the bands at around 1620 and 3430 cm^{-1} can be assigned to the H-O-H stretching modes and bending vibration of the free or adsorbed water, respectively. The band at 547 cm^{-1} the Fe-O, is related to bending vibration, while it shifted towards 565 cm^{-1} after the iron oxide particles were coated with silica. After the iron oxide nanoparticles were coated with silica, a band of Si-O-Si is observed at about 1004-1033 cm^{-1} which is associated with the motion of oxygen in the Si-O-Si antisymmetric stretch, due to the asymmetric stretching bonds of Si-O-Si in SiO_2 . The band at 790 cm^{-1} is assigned to the Si-O-Si symmetric stretch, while the band at 451 cm^{-1} corresponds to the Si-O-Si or O-Si-O bending modes. The band at 578 cm^{-1} is for Si-O-Fe.

At 964 cm^{-1} there is a Si-O symmetric stretch. This peak disappeared after immobilization of titanium dioxide on $\text{Fe}_3\text{O}_4/\text{SiO}_2$. Figure 4.2 shows Fe-O shifted towards higher wavenumbers after the titanium dioxide coating appearing at around 584 cm^{-1} and a Ti-O-Ti stretching vibrations at about 747- 766 cm^{-1} . The wide peak around 3342- 3500 cm^{-1} may be attributed to Ti-OH and Ti-O bonds, similar to that reported by (Luntraru, et al., 2011). These results show that the surface modification of $\text{Fe}_3\text{O}_4/\text{SiO}_2$ with TiO_2 was successful. The silver doped sample showed a stretching vibrations of Ti-O-Ti around 583-718 cm^{-1} . This alteration of bands shows the presence of the magnetite titanium dioxide core-shell support on which the silver nanoparticles are doped.

High Resolution Scanning Electron Microscopy

The specimen is bombarded by a convergent electron beam to an energy range 0.1-30 keV (Radetic, 2011), which is scanned across the surface. This electron beam produces several types of signals, which are emitted from the area of the specimen where the electron beam is impinging. These signals are detected and the intensity of the signals (one at a time) is amplified and used as the intensity of a pixel on an image when presented as an image. The scanning electron microscope gives information about the chemical composition, surface topography, crystal structure and properties on a local scale of the sample being analysed (Börjesson, 2006). A scanning electron microscope is usually coupled with energy dispersive spectroscopy (EDX) to analyse the elemental composition of the sample of interest.



Sample Preparation for SEM

The sample was prepared as follows; because oxides are not conductive and have to be prepared well to increase their conductivity. A carbon grid was pasted on a sample stand; the samples were mounted on the grid, paying special attention to ensuring a uniform layer. The samples were spin coated using gold/ palladium to reduce thermal damage, prevent charge build-up on electrical insulating samples, and increase the secondary electron signal necessary for topographic examination (Gruber, 2013)

According to De Gree (2015), the gold/ palladium coating is attained through the use of an electric field and argon gas. The electric field removes an electron from the argon, giving off charged ions, which are attracted to negatively charged gold/palladium foil. As they settle onto the gold/palladium, the argon ions expel gold/ palladium atoms,

which fall onto the specimen, forming a thin conductive coating. Furthermore the preparation also removes water from the species which would give unclear images when present during the imaging. The analysis was done using a Zeiss Auriga field emission gun (FEG) SEM, operated at 5 keV. The EDX spectra were collected at 20keV using a silicon solid-state drift detector.

The results obtained from SEM are presented from figure 4.3- 4.7 and are shown below.

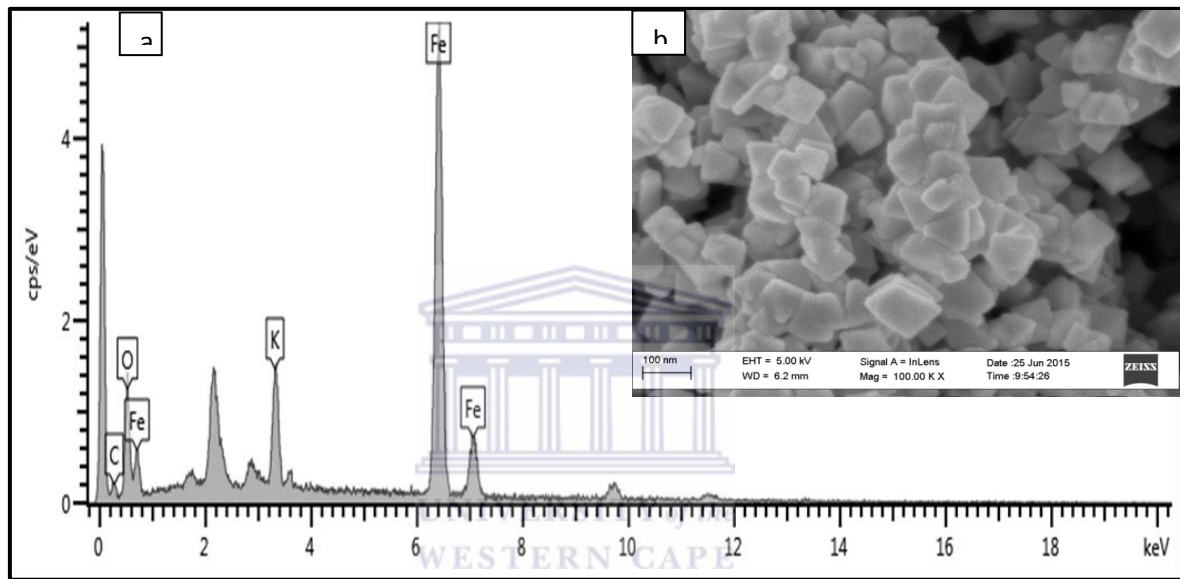


Figure 4.13: (a) Scanning electron micrograph and (b) EDX of Fe_3O_4

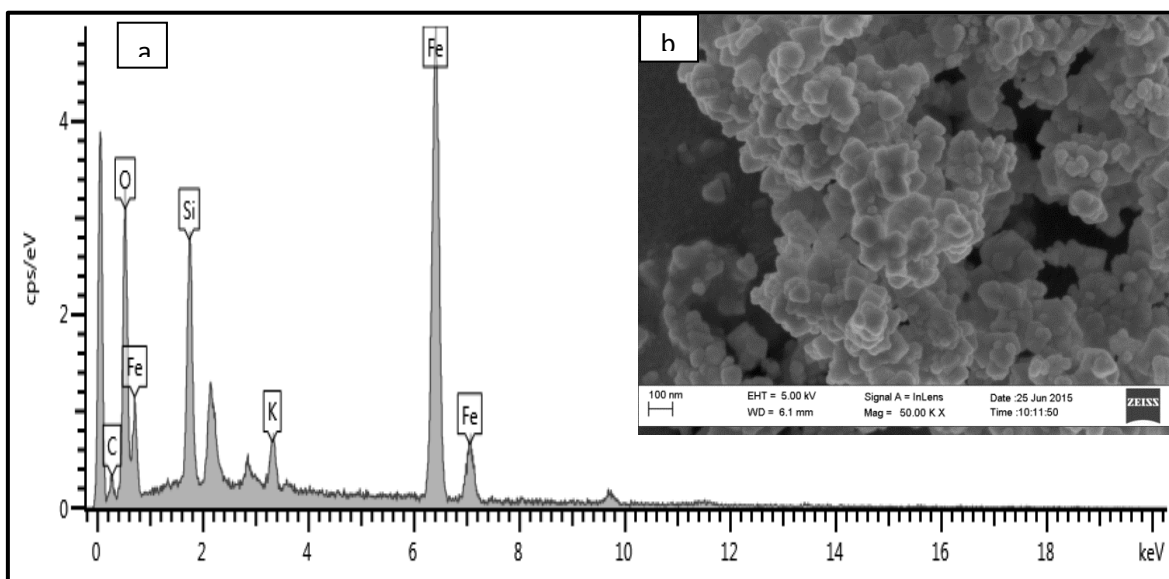


Figure 4.14: (a) Scanning electron micrograph and (b) EDX of $\text{Fe}_3\text{O}_4/\text{SiO}_2$

The micrographs shows cubic agglomerated iron oxide nanoparticles and this may be due to the superparamagnetism of the nanoparticles. EDX analysis was performed to determine the composition of the nanoparticles. The EDX spectrum shown in figure 4.3(a) represents the as-synthesized iron oxide particles consisting of Fe and O elements, the carbon is from the carbon grid on which the sample is mounted and the potassium was used in the starting chemicals.

Figure 4.4 presents the micrographs of Fe_3O_4 after the coating process with silica (Gad-Allah, *et al.*, 2007). Figure 4.4 shows the nanoparticles were agglomerated even after coating with silica, to preserve their magnetism. The roughness of the silica layer indicates that the silica shell was successfully coated with the core iron oxide nanoparticles. It is clear from the images that there is a clear difference between the iron oxide core and the silica shell which appears as a halo lining on the interface of the shell

which confirms the presence of the silica layer. This is also confirmed by the EDX presented in figure 4.4(a).

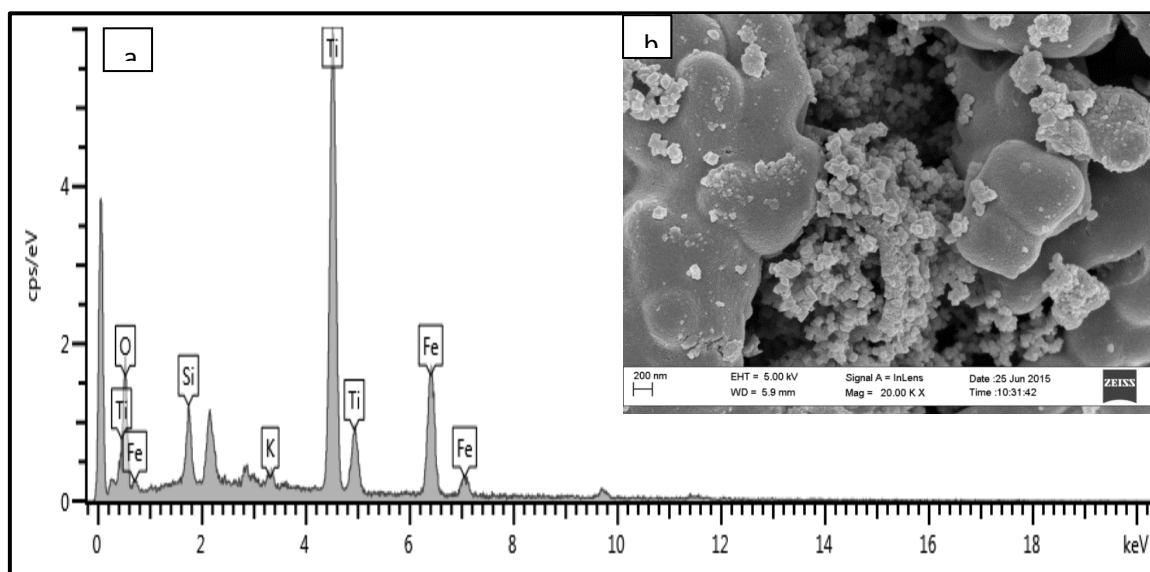


Figure 4.15: (a) Scanning electron micrograph and (b) EDX of calcined



UNIVERSITY of the
WESTERN CAPE

Figure 4.5 shows the SEM image and EDX of $\text{Fe}_3\text{O}_4/\text{SiO}_2/\text{TiO}_2$ core and shell nanostructures. The calcined nanoparticles show less agglomeration than the uncalcined samples. This can be explained as follows: during the heat treatment, the iron oxide core may be partially oxidized by the titanium shell, hence decreasing the magnetic properties of the core and hence the dispersion was observed (Watson, *et al.*, 2002). The particle size is increased slightly due to the multilayers on the magnetic core. Figure 4.5(a) confirms the successful coating with TiO_2 .

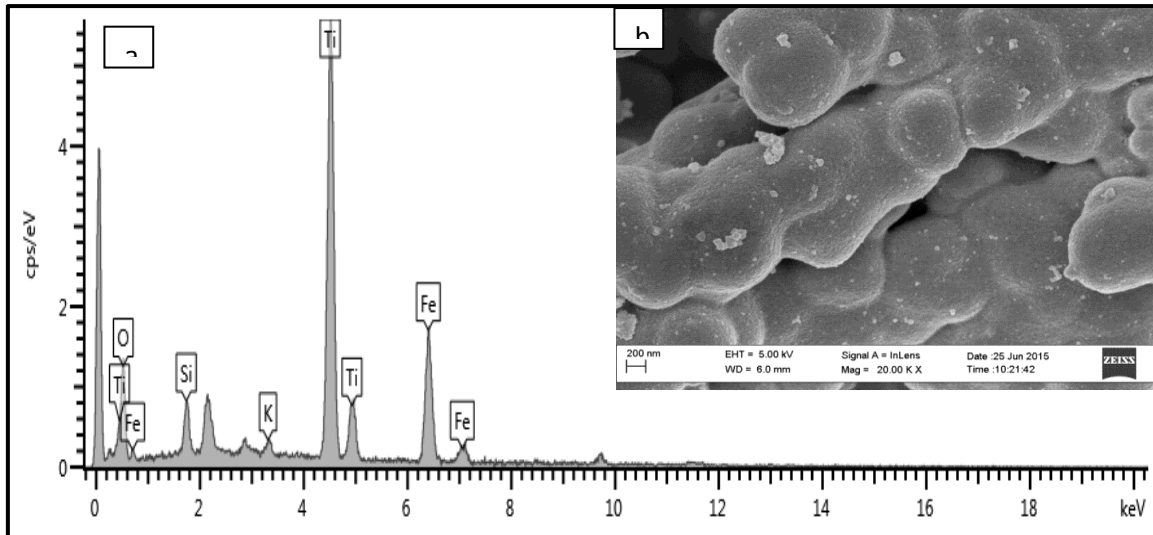


Figure 4.16: (a) Scanning Electron Micrograph and (b) EDX of calcined $\text{Fe}_3\text{O}_4/\text{SiO}_2/\text{TiO}_2$

Figure 4.6 shows the micrograph of uncalcined titanium dioxide coated iron oxide nanoparticles. The particles are agglomerated which confirm that the core was successively coated with SiO_2 and TiO_2

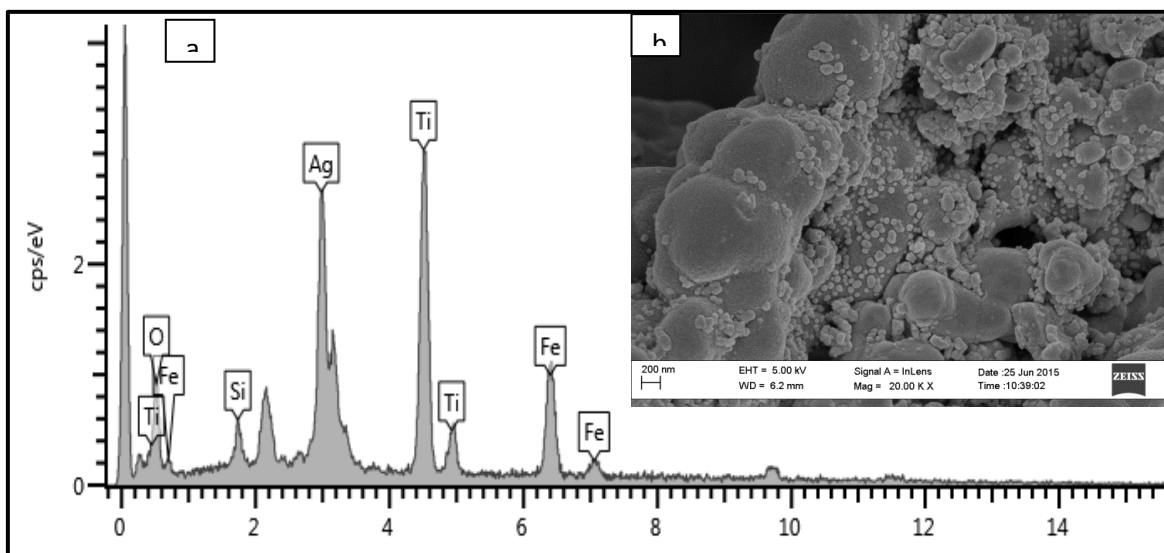


Figure 4.17: (a) Scanning Electron Micrograph and (b) EDX of $\text{Ag-Fe}_3\text{O}_4/\text{SiO}_2/\text{TiO}_2$

Figure 4.7 presented the SEM image of Ag-Fe₃O₄/SiO₂/TiO₂ particles; it is clear that Ag nanoparticles were formed on the surfaces of TiO₂/SiO₂/Fe₃O₄ and have spherical morphologies. The particles also show coarse surfaces which could be attributed to the silver coating. The EDX spectrum in figure 4.7a shows that the composition of the obtained core-shell structure consisted of Fe, Si, Ti and Ag elements.

High Resolution Transmission Electron Microscopy

Transmission Electron Microscopy (TEM) is a microscope used to directly image nanomaterials to obtain their quantitative measures of particle and/or grain size, size distribution, and morphology. TEM operates using a focused beam of electrons through the sample of interest, producing an image of the transmission of these electrons. TEM imaging has a significantly higher resolution (by a factor of about 1000) than light-based imaging techniques; hence it is preferred for nano-sized structures.

Sample Preparation

All the samples were prepared in ethanol. An adequate volume of ethanol was used to disperse the samples by sonicating them for five minutes or more to ensure the dispersion of the nanoparticles in ethanol. Then drops of samples were drawn on a carbon coated copper grid. The grids were put under a white light to evaporate the ethanol from the sample, the samples were placed on a sample holder and analysed. This analysis was done using FEI Technai G²20 Field Emission Gun (FEG)-TEM operated at 200kV, coupled with Electron dispersive X-ray spectroscopy (EDAX SiLi detector) for elemental analysis.

The TEM images of the asynthesized nanocomposites are shown below

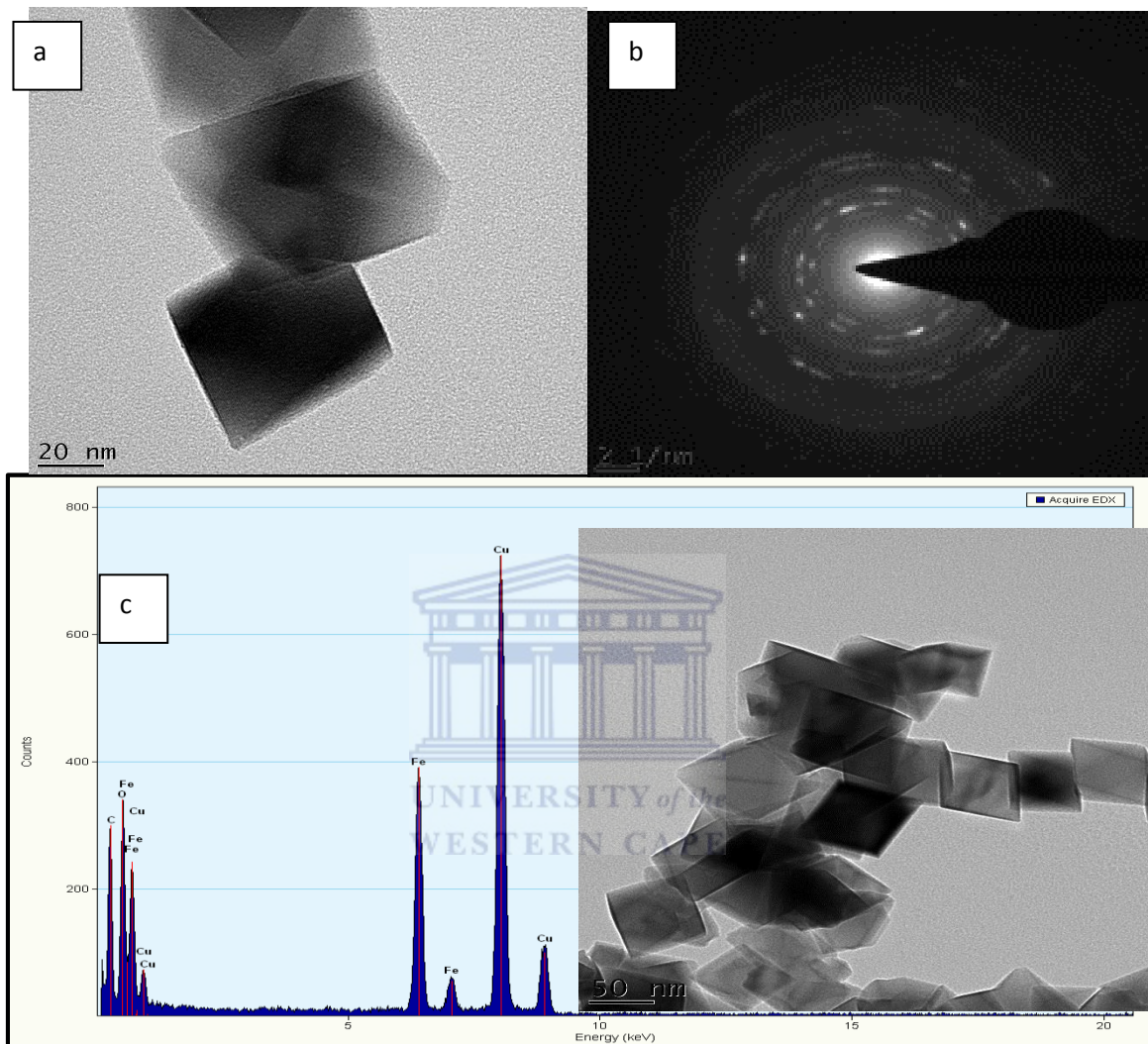


Figure 4.18: TEM images, corresponding SAED and EDX of Fe_3O_4

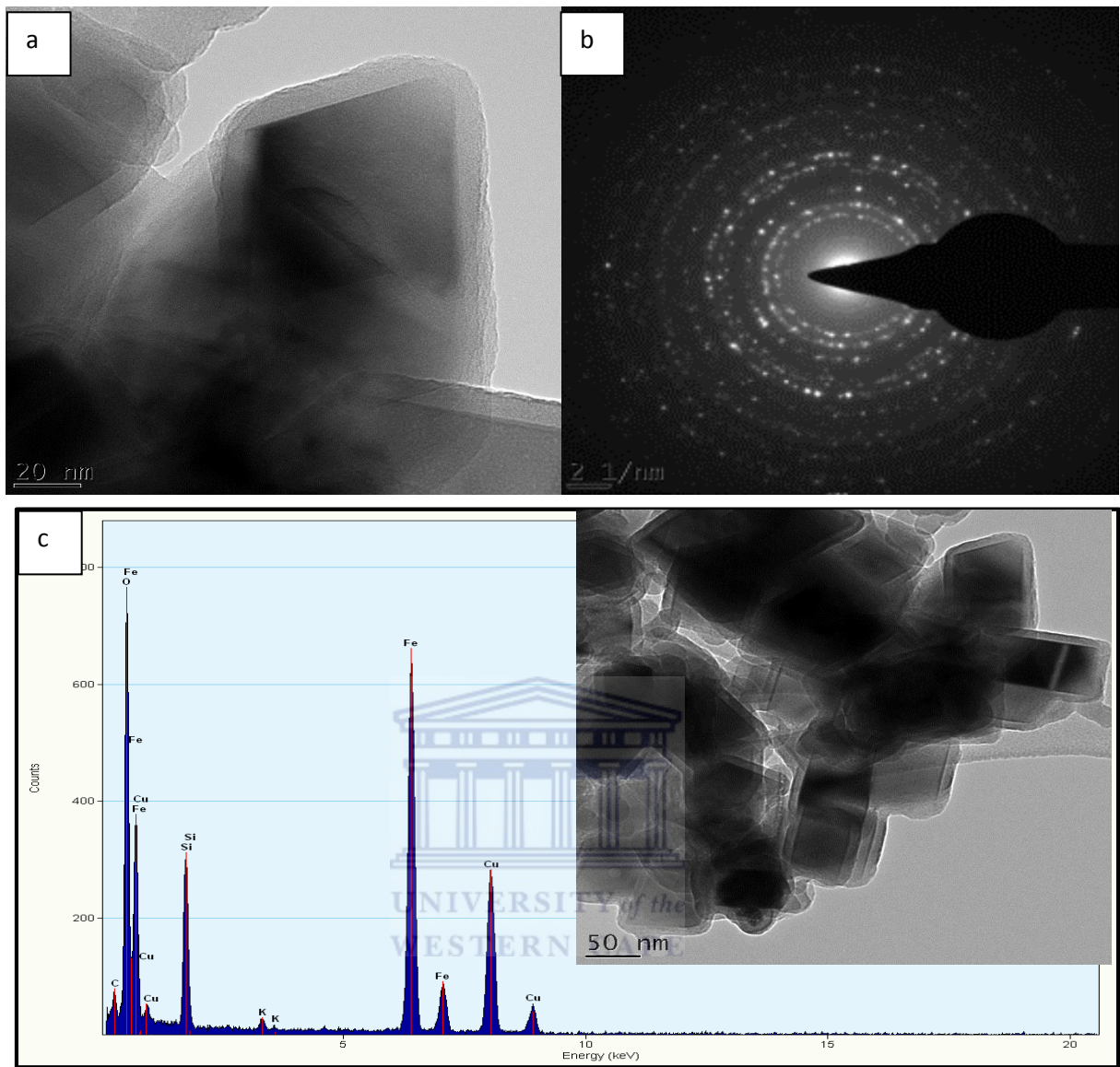


Figure 19: TEM images, corresponding SAED and EDX of Fe₃O₄/SiO₂

The HRTEM images of Fe₃O₄ magnetic nanoparticles (Fig.4.8) were cubic shaped with a size of about 56nm. The Fe₃O₄ nanoparticles appear to be aggregated to minimize the total surface energy (Wu, *et al.*, 2008). The magnetite nanoparticles have two advantages for the final composite particle product. The total magnetic force exerted by the particles in a magnetic field is strong due to the simultaneous magnetization of the

many smaller particles. This phenomenon allows for substantial magnetic moment, resulting in quick separation even after loading with SiO₂ and TiO₂. The EDX shows that both iron and oxygen are present in the nanoparticles confirming that the magnetite nanoparticles were successfully obtained. The copper is from the grid used to hold the sample.

The TEM image of silica-coated iron oxide nanoparticles (Fig. 4.9) shows that the iron oxide core appears clearly darker than the silica shell which may be attributed to the fact that the iron oxide core has a much higher density than the silica shell. The images show that the Fe₃O₄ nanoparticles were fully encapsulated within the SiO₂ shell. The mean size of Fe₃O₄/SiO₂ core-shell nanoparticles were roughly 66nm. The silica shell is 11nm thick. The Fe₃O₄/SiO₂ core-shell nanoparticles were cubic in shape. This could be owing to the dispersing status of magnetic nanoparticles related to their surface charge density which led to the formation of Fe₃O₄/SiO₂ core-shell nanoparticles of a number of morphologies and structures (Rao, *et al.*, 2005). The EDX also shows the presence of silica in the as-synthesized nanoparticles which confirmed the Fe₃O₄/SiO₂ core-shell structure.

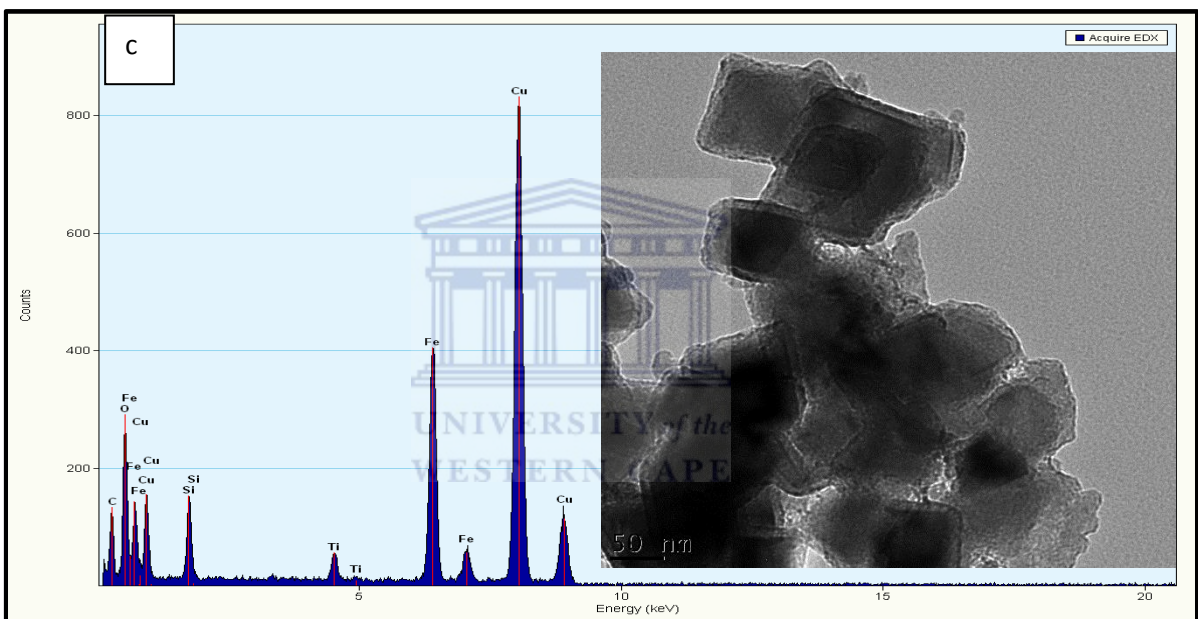
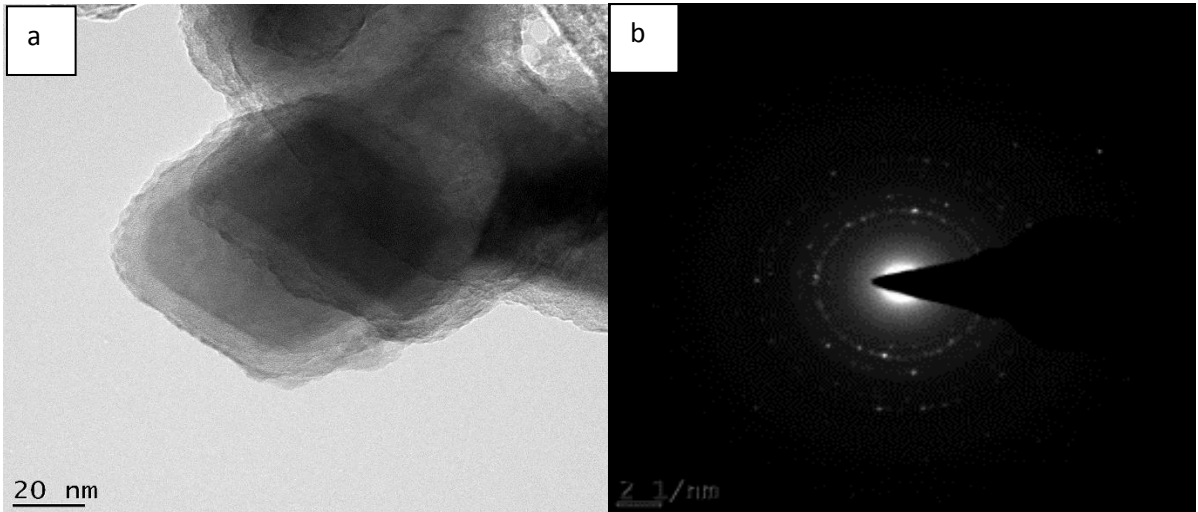


Figure 4.20: TEM images, corresponding SAED and EDX of $\text{Fe}_3\text{O}_4/\text{SiO}_2/\text{TiO}_2$

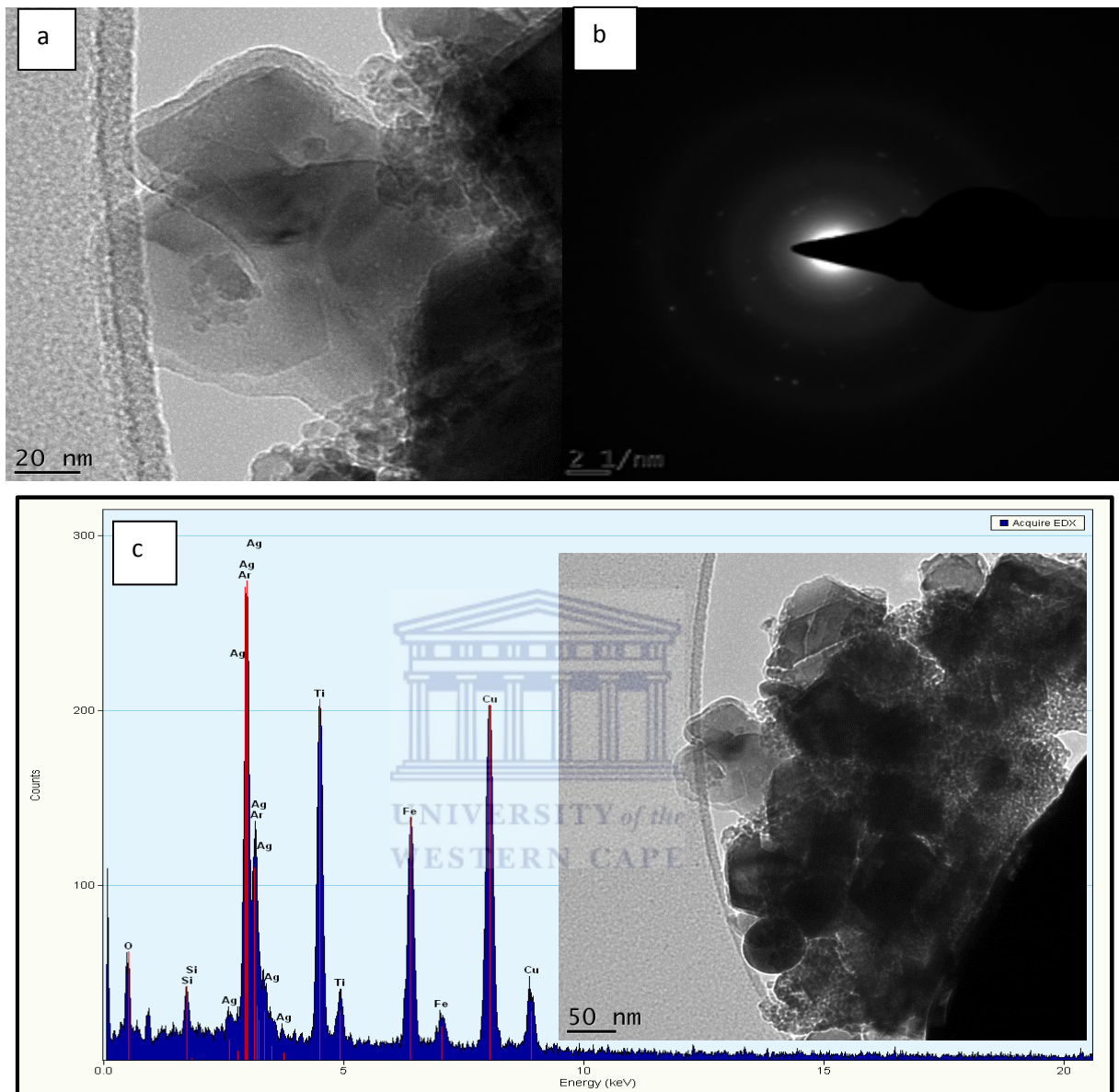


Figure 4.21: TEM images, corresponding SAED and EDX of Ag-Fe₃O₄/SiO₂/TiO₂

The Fe₃O₄/ SiO₂ /TiO₂ (fig.4.10) were calcined at 450°C for two hours. It is obvious that the TiO₂ shell possesses a rough consistency after heat treatment due to the crystallization of the amorphous TiO₂ shell and the coalescence of small particles to big particles (Song & Gao, 2007). It is also evident from the HRTEM images that the core-

shell structure was obtained. The particles had a size of around 74nm, almost the same size as that obtained by (Pang, *et al.*, 2012) which could mean the titanium dioxide layer was approximately 17nm.

Figure 4.11 shows inhomogeneity of the core- shell morphology of Ag-Fe₃O₄/ SiO₂ /TiO₂ and varying size distribution of the silver particles on the surface of the magnetite titanium dioxide core-shell structure. There are a large number of silver particles with an average diameter of approximately 61nm which are doped on the crystalline titanium dioxide shell. The as-synthesized silver nanoparticles have similar particle size as reported by Pastoriza-Santos, *et al.*, (2000) and smaller particle size than that reported by (Vamathevan , *et al.*, 2002; Hermann, *et al.*, 1988) 125nm and 400nm respectively.

The selected area electron diffraction (SAED) patterns of Fe₃O₄ NPs displayed in figure 4.8(c) confirm a typical magnetite crystalline structure (Ge, et al., 2009). Figure 4.10(c) clearly shows a ring diffraction pattern characteristic of anatase TiO₂. The first four rings of the diffraction pattern of figure 4.10 correspond to (101), (004), (200), and (105) indices, starting from the centre ring (Linley, et al., 2013). These indices are discussed further in XRD.

X-ray Diffraction

X-ray diffraction was used to determine the phase structure of the samples such as the crystallinity of the catalyst, measure their size and their average spacing layers/ rows of atoms. The diffractogram was recorded in the low-angle incident mode to increase sensitivity to the surface. The analysis was performed using a BRUKER AXS (Germany), D8 Advance diffractometer. The measuring parameters were set to 40kV, 30mA with a rate of 2°/ min and ran at the 2θ range (10- 80°).

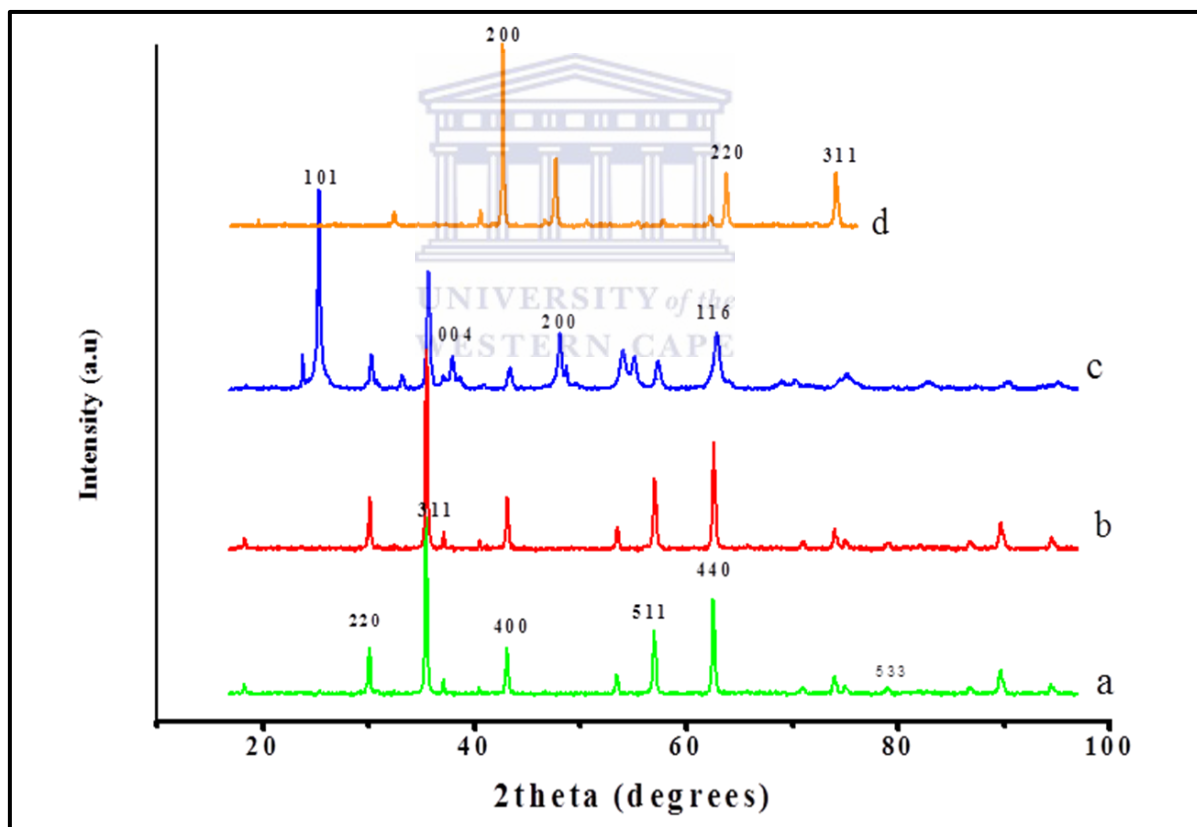


Figure 4.22: XRD patterns of (a) iron oxide, (b) Fe₃O₄/SiO₂, (c) Fe₃O₄/SiO₂/TiO₂ and (d) Ag-Fe₃O₄/SiO₂/TiO₂

The iron oxide and silica coated nanoparticles show diffraction peaks at 30.1° , 35.5° , 43.14° , 53.35° , 57.03° , 62.63° and 78.9° . The results show the main phases of magnetic core are pure magnetite with cubic spinel structure.

The silica coated nanoparticles have a bit of a decrease in the width of the peaks and this could be attributed to the coating layer. The coating of the SiO_2 layer does not change the structure of Fe_3O_4 (Fig. 4.12b). However there are no relevant peaks of SiO_2 detected in the XRD patterns, which could indicate that SiO_2 form a very thin membrane on the surface of magnetite particles but doesn't show coalescence from larger crystals (Chen, *et al.*, 2001).

Fig 4.12(c) show a great shift in the diffraction peaks due to the titanium dioxide coating on the magnetite nanoparticles. The diffractogram still maintains the peaks due to the iron oxide but the intensity of the Fe_3O_4 peak dramatically diminishes compared with that of pure Fe_3O_4 , and shifted more to higher 2θ than that observed in (a). The peaks around 25.3° , 37.87° , 48.12° , 55.05° , 68.93° , 70.20° correspond to anatase TiO_2 as previously reported by Pang, *et al.*, (2012); Shi, *et al.*, (2012).

Figure 4.12(d) shows the silver doped magnetite titania nanoparticles, the peaks corresponding to anatase titanium dioxide are found in the material with additional peaks due to the silver doping. The peak at 32.42° was attributed to brookite phase titanium dioxide. The patterns displayed on figure 4.12(d) show Ag peak at 38° which corresponds to the 111 indices which overlaps with the 004 peak of anatase phase titanium dioxide (Liang, *et al.*, 2011). The overlapping of the diffraction peaks of silver with that of anatase titanium dioxide and the intensity of the peaks has decreased to a certain extent, and confirms that the silver particles have been doped successfully on the titanium dioxide shell, (Sobana, *et al.*, 2006). All the peaks are indexed with a face

centred cubic (fcc) single crystal, which indicates that the products were Ag, with good purity, which can be referenced to Ag powder from JCPDS 04-0783.

The diffractogram shows no other diffraction patterns characteristic of the silver nanoparticles because they are expected to be below the visibility limit of the X-ray diffraction instrument. The crystallite size was determined from the diffraction peak broadening using the following equation:

$$D = K\lambda / \beta \cos\theta$$

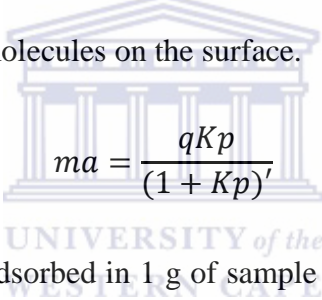
Where: λ is the wavelength, θ is the Bragg's angle, β is the full-width at half maximum

Table 4.6: XRD patterns of as-synthesized photocatalysts, indices and d- spacing values.

Sample	Peaks	Indices	d-spacing (nm)
Fe ₃ O ₄	30.4°	220	2.94
	35.6°	311	2.52
	43.2°	400	2.09
	53.8°	422	1.70
	57.2°	511	1.61
	62.9°	400	1.48
Fe ₃ O ₄ /SiO ₂	15-20°		5.91- 4.40
Fe ₃ O ₄ /SiO ₂ /TiO ₂	25.4 °	101	3.51
	37.8 °	004	2.38
	48.1 °	200	1.89
	54.1 °	105	1.69
	55.2 °	211	1.66
	68.8 °	116	1.36
	70.3 °	220	1.34
Ag-Fe ₃ O ₄ /SiO ₂ /TiO ₂	38.2°	111	2.37
	44.4°	200	2.04
	64.5°	220	1.45
	72.27°	311	1.31

Braunauer Emmett Teller Analysis

BET studies the adhesion of gas atoms and molecules on the surface of a material to measure its surface and porosity. This analysis is carried out by exposing the materials to gas and the amount adsorbed depends on the surface exposed, temperature, gas pressure and strength. The data obtained gives information about the pore size distribution, density, pore volume of the solids and their surface areas (Tan , *et al.*, 2012). Nitrogen gas is usually used for this analysis due to its strong interaction with most solids and its availability. The measurement is established from the gas physically adsorbed on the sample surface. The volume of gas is defined by Langmuir isotherms assuming a monolayer of gas molecules on the surface.


$$ma = \frac{qKp}{(1 + Kp)'}$$

where a is the amount of gas adsorbed in 1 g of sample (mol/g), p is partial pressure of the gas, q is the amount of active centres in 1 g of sample (mol/g), and K is equilibrium coefficient of adsorption.

However for samples where gas molecules are adsorbed in more than one layer, the BET isotherm is applicable:

$$\frac{p}{p_0} = \frac{1}{amC} + \frac{po(C - 1)}{amC'}$$

Where p_0 is tension of saturated vapour at particular temperature, C is the constant including adsorption and condensation heat and a_m is the amount of gas adsorbed in 1g of sample in a monolayer (mol/g).

The surface area of the solid is assessed from the capacity of the measured monolayer capacity and the cross-sectional area of the molecule being used as a probe. The surface area is determined by the following equation:

$$A_{sp} = N_A \cdot a_m \cdot \sigma,$$

Where A_{sp} is the specific surface area, N_A is the Avogadro constant, and σ is the area of the sample covered by one molecule of the adsorbing gas (Širc, *et al.*, 2012).

The determined values of the specific surface area are dependent on the adsorbing gas used; lower values are obtained with larger molecules. Adsorption studies use either nitrogen or argon gas (Thommes, 2010). The solid surface is usually cooled to maintain strong interaction between the gaseous and solid phases. A known amount of nitrogen gas is released slowly into the sample cell, while maintaining relative pressures less than atmospheric pressure by controlling conditions of the partial vacuum.

Sample Preparation

The sample preparation in BET is one of the important steps. All the samples must be degassed prior to analysis to obtain meaningful results. Degassing of solids is essential to reach a distinct intermediate state to remove volatile molecules physisorbed and also by alteration on the samples due to ageing and surface changes (Sing, 2001).

N₂ adsorption-desorption isotherms

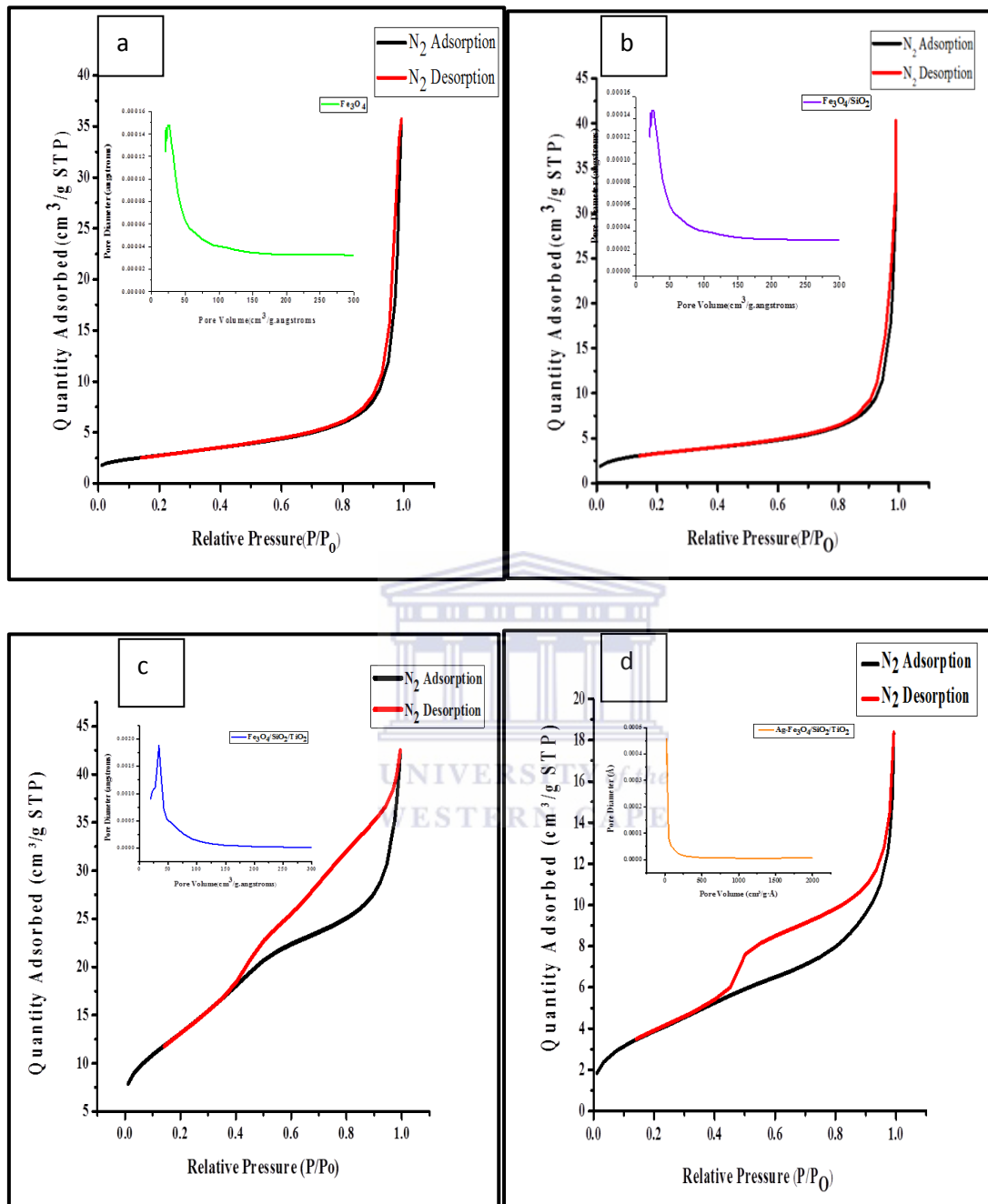


Figure 4.23: Nitrogen adsorption-desorption isotherms and corresponding pore size distributions of (a) Fe₃O₄ (b) Fe₃O₄/SiO₂ (c) Fe₃O₄/SiO₂/TiO₂ (d) Ag-Fe₃O₄/SiO₂/TiO₂

Figure 4.13 shows the adsorption–desorption isotherm of all synthesized photocatalysts. The isotherms of Fe₃O₄ and Fe₃O₄/SiO₂ nanoparticles were the type II patterns which correspond to a monolayer formation with distinct H3 hysteresis loops. The Fe₃O₄/SiO₂/TiO₂ sample and the silver doped titania photocatalyst gave type IV isotherms, which explains the formation of a monolayer followed by a multilayer with H2 and H4 hysteresis loops associated with the presence of micropores and mesopores according to the IUPAC classification. The bimodal pores allow for rapid diffusion of reactants and products during the photocatalytic process which will in turn increase the photocatalytic reaction (Liu, *et al.*, 2011). The pore size distributions were determined by the Barrett-Joyner-Halenda (BJH) method from the adsorption branch of the isotherm. The average pore width of Fe₃O₄ and Fe₃O₄/SiO₂ nanoparticles were found to be 2.54nm and 2.49 nm respectively. After the coating with titanium dioxide the average pore width increased to 2.72nm. The Ag-Fe₃O₄/SiO₂/TiO₂ particles have an average pore size of 2.249nm. The increase of pore size/ volume correspondingly enhances dye absorption quantity and ultraviolet absorption area, which can successfully improve the photocatalytic efficiency.

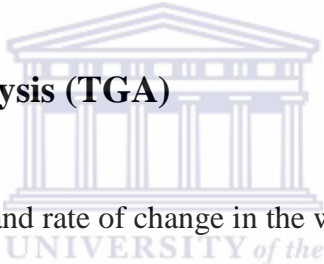
Table 4.7: BET surface area of the as-synthesized photocatalysts

Photocatalyst	Surface area (m ² /g)
Fe ₃ O ₄	9.82
Fe ₃ O ₄ /SiO ₂	11.92
Fe ₃ O ₄ /SiO ₂ /TiO ₂	48.02
Ag-Fe ₃ O ₄ /SiO ₂ /TiO ₂	14.54

The BET specific surface area of Fe_3O_4 and $\text{Fe}_3\text{O}_4/\text{SiO}_2$ nanoparticles were found to be $9.82\text{m}^2/\text{g}$ and $11.97\text{m}^2/\text{g}$ respectively. It is observed that the surface area decreased after the titanium dioxide catalyst was doped with silver. The decrease in the surface area of $\text{Ag-Fe}_3\text{O}_4/\text{SiO}_2/\text{TiO}_2$ particles may be due to the blocking of fine capillaries of the parent TiO_2 surface by metal film islands (Sakthivel, *et al.*, 2004).

Thermogravimetric Analysis and Differential Scanning Calorimetry

Thermogravimetric Analysis (TGA)



TGA measures the magnitude and rate of change in the weight of a sample as a function of time or temperature in a fixed atmosphere and heat rate usually under synthetic air or nitrogen.

Differential Scanning Calorimetry (DSC)

DSC is the measurement of the change in the heat flow rate to the sample and to a reference sample whilst subjected to a controlled temperature program (Höhne, *et al.*, 2013). The measurement of heat not only includes integral heat of reaction or transition but also the determination of partial heat developed at a selected temperature interval. These values are important for kinetic evaluations, determination of crystallinity and purity of the sample of study.

The samples were evaluated as powder and no further preparation was needed. Thermogravimetric analysis (TGA) and differential scanning calorimetry (DSC) of the samples was carried out using a Perkin Elmer Simultaneous Thermal Analyzer (STA 600) by heating the sample from 50 to 600 °C with the heating rate of 10 °C/min in the flow of compressed air (19.8 mL/min).

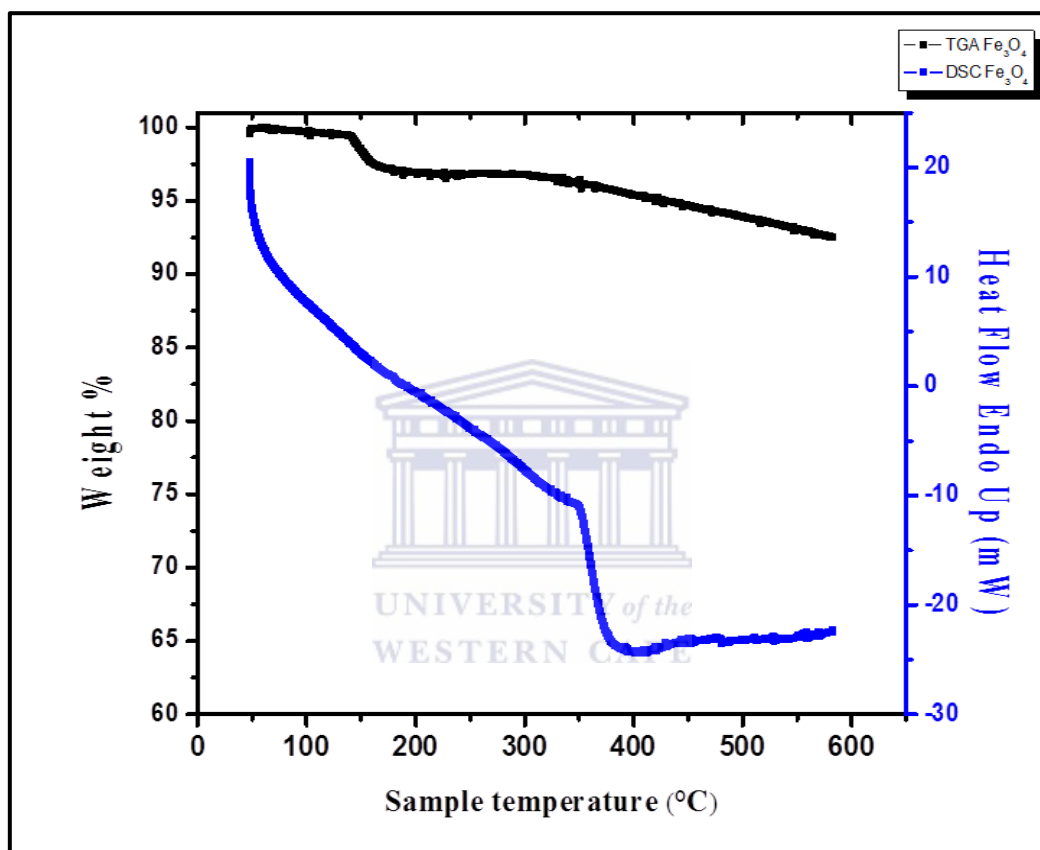


Figure 4.24: TGA and DSC graphs of Fe₃O₄

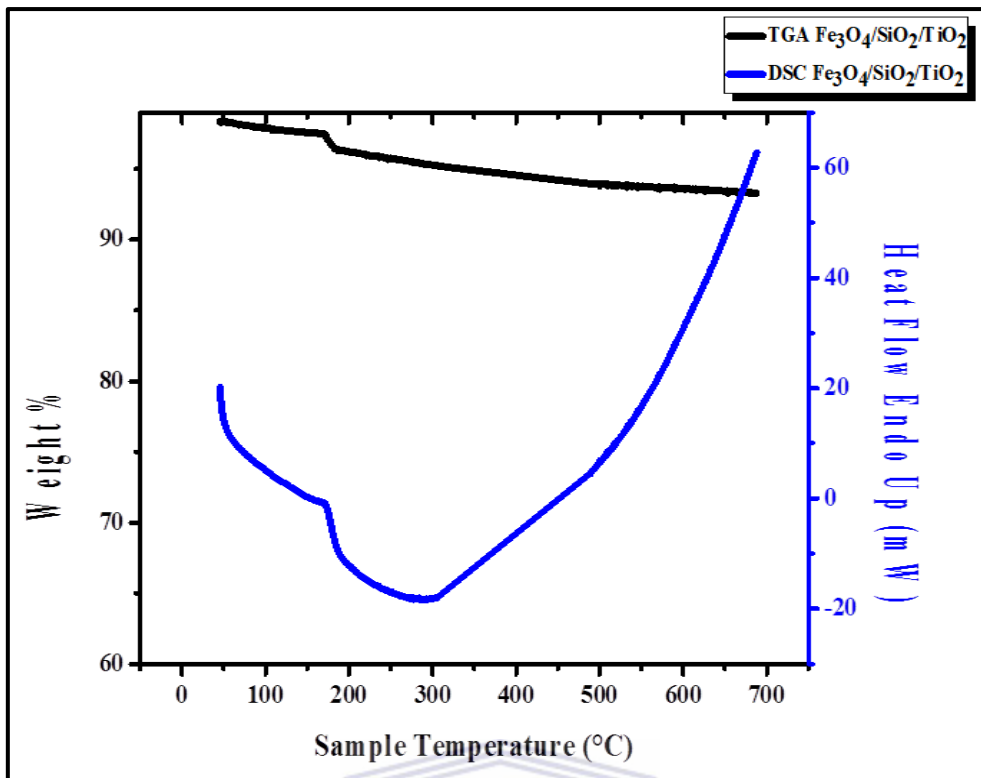


Figure 4.25: TGA and DSC graphs of Fe₃O₄/SiO₂/TiO₂

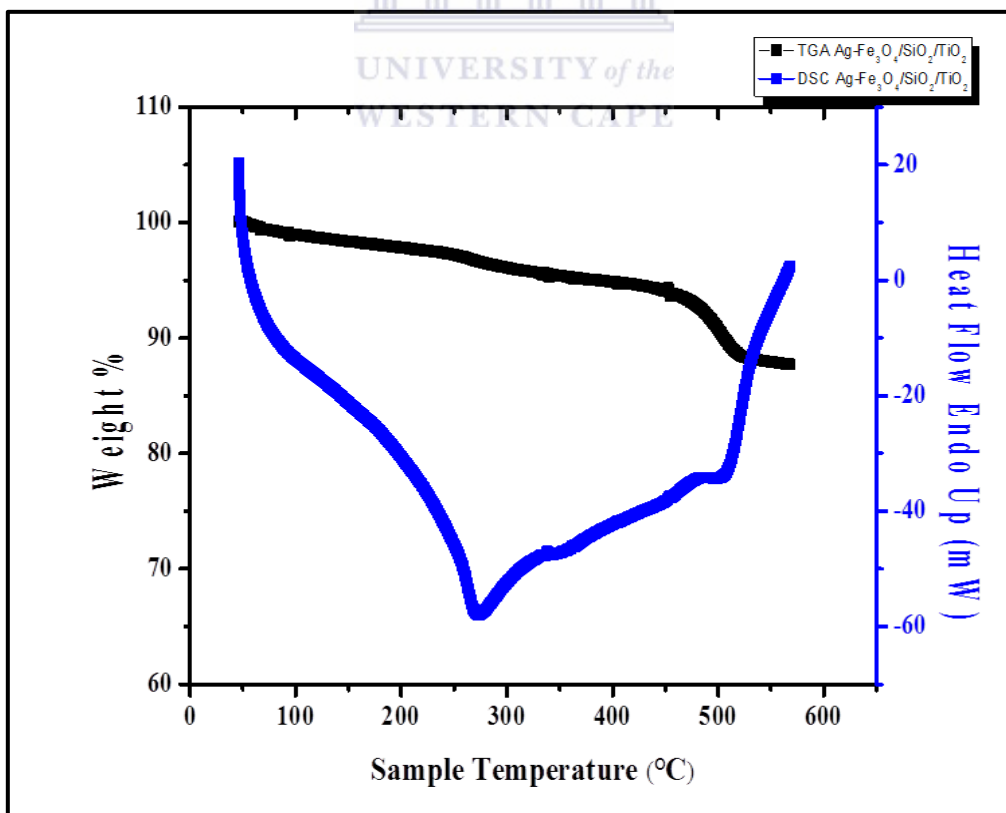


Figure 4.26: TGA and DSC graphs of Ag-Fe₃O₄/SiO₂/TiO₂

The total weight loss in the whole temperature range presented in figure 4.14 and 4.16 is 7.1%, 12.3 % for Fe_3O_4 and $\text{Ag-Fe}_3\text{O}_4/\text{SiO}_2/\text{TiO}_2$ respectively. There are three regions of weight loss; the first stage is from room temperature to 150 °C of weight loss upon heating which is due to the physisorbed water on the iron oxide. The second stage occurs approximately from 150 500 °C and is due to the removal of strongly bound water or surface hydroxyl groups from the catalyst. The third stage mass loss is less than 0.5% and is from 500 to 750 °C. Apart from the observed loss of water due to heating no other thermal degradation was observed, confirming phase and chemical purity of the obtained nanoparticles (Jadhav & Patil, 2014). Thus it is clear that amounts of adsorbed water or surface hydroxyl groups are much higher in Fe_3O_4 and $\text{Fe}_3\text{O}_4/\text{SiO}_2/\text{TiO}_2$ than $\text{Ag-Fe}_3\text{O}_4/\text{SiO}_2/\text{TiO}_2$ (Nagaveni, et al., 2004).

The DSC graphs for all three catalysts showed similar profiles; however the $\text{Ag-Fe}_3\text{O}_4/\text{SiO}_2/\text{TiO}_2$ nanocomposite showed very slow dehydroxylation and crystallization processes showing a broad peak at a slightly higher temperature. This is an indication that silver slows down the phase transformation and shifts phase transformation temperature to high temperature (Nagaveni, et al., 2004). Diffuse reflectance spectrum of the TiO_2 sample shows an absorption edge at approximately 403 nm, which is generally ascribed to charge-transfer from the valence band (mainly formed by 2p orbitals of the oxide anions) to the conduction band (mainly formed by 3d, t_{2g} orbitals of the Ti^{4+} cations).

Chapter 5: Results and Discussions

This chapter evaluates the catalytic performance of the as-synthesized nanocomposites' in comparison to that of commercial titanium dioxide powder for the degradation of MB under and in the absence of UV irradiation. It also represents and discusses the results obtained.

Photodegradation Studies

The prepared samples were weighed and added into 40 mL of methylene blue solutions (1×10^{-4} M standard solution). The mixed solutions were illuminated under a UV lamp in the photochemical reactor (with characteristic wavelength at 365 nm). During experiments 0.2ml samples were taken at different time intervals (5; 10; 15; 30; 60 and 120 min) and diluted with 1.8ml of water to make 2ml solutions. Then, the time-dependent absorbance changes of the solution were measured at the wavelength between 400 and 800 nm (using a Wirsam Scientific, GBC 920 UV-Vis Spectrometer).

The as-synthesized catalyst was tested for its photocatalytic activity on methylene blue dye. A standard solution of methylene blue (40ml of 1×10^{-4} M) and 0.01g catalyst was used for the photodegradation studies for evaluation using a ultra-violet spectrometer.

The concentration of dye was determined using the initial calibration curve which was recorded after spectrophotometric measurement of methylene blue solution absorbance for dye standard concentration (1×10^{-2} M, 5×10^{-3} M, 2.5×10^{-4} M, 1.25×10^{-4} M) at the specific wavelength corresponding to the maximum absorption of dye. The photodegradation process is illustrated below:

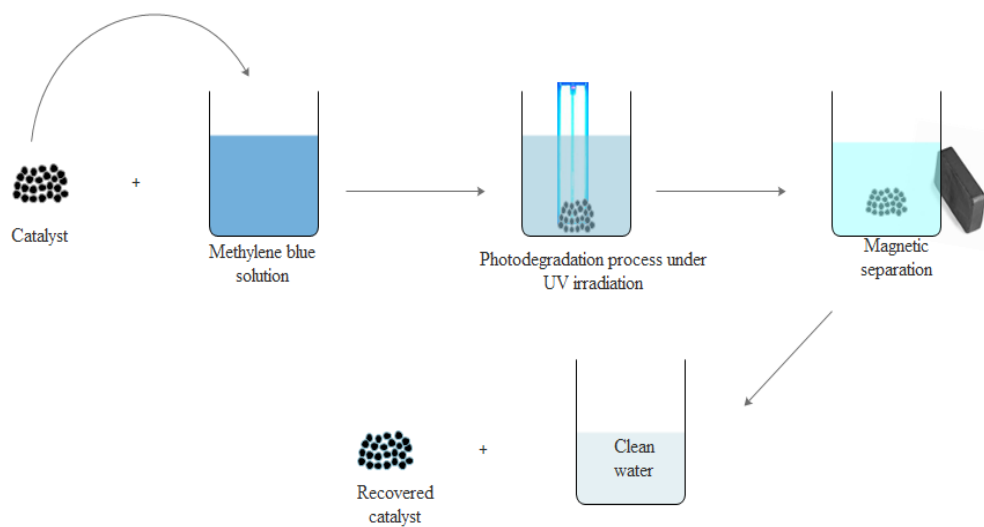


Figure 5.27: Photodegradation process of MB

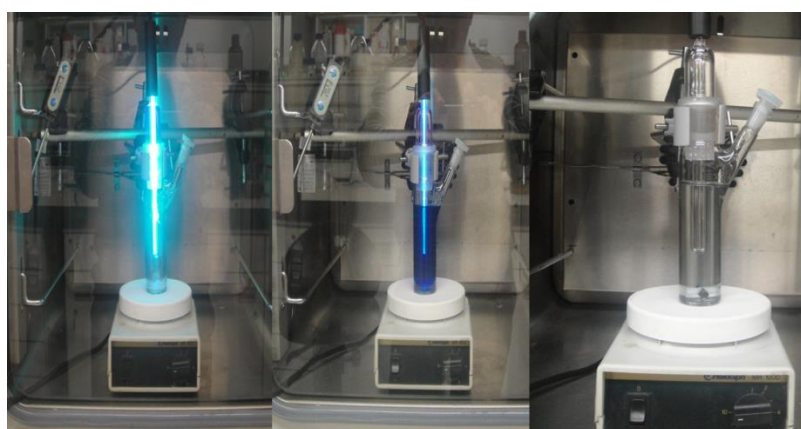
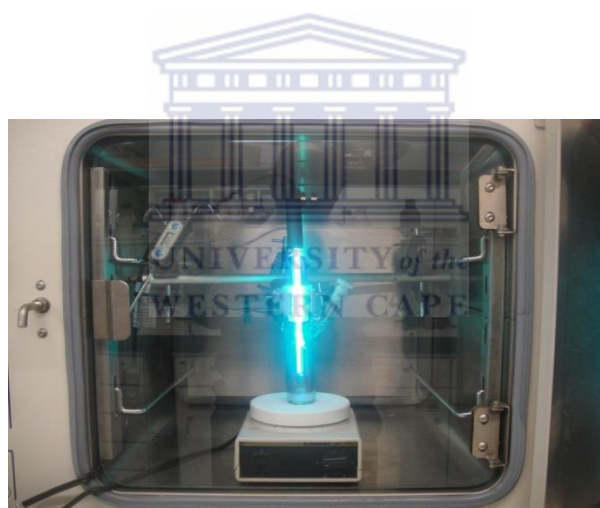


Figure 5.28: Reaction setup

The pictures presented in figure 5.1 and 5.2 show the setup used for the degradation of MB; where the solution was exposed to UV light and samples drawn at different time intervals.

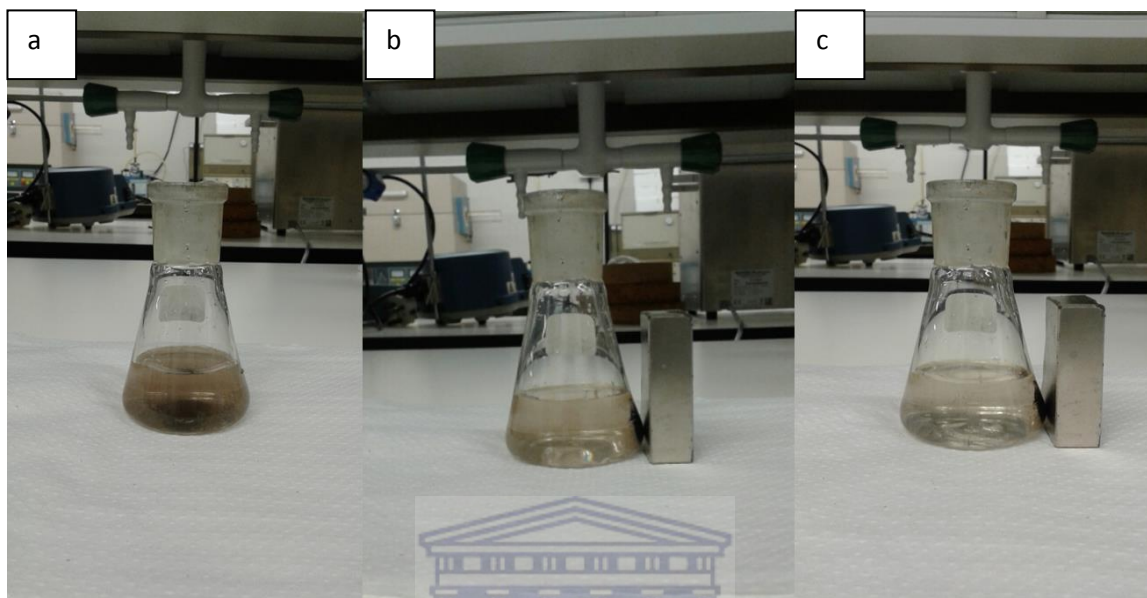


Figure 5.29: Separation method with external magnet

The picture presented above shows the separation method of the catalyst from water. The picture in a shows the catalyst suspended in water, b) shows 15s after a magnet was placed on the flask to recover the catalyst and c) 30seconds after the exposure to the external magnet. This confirms how easy the as-synthesized nanocomposite can be separated from a reaction.

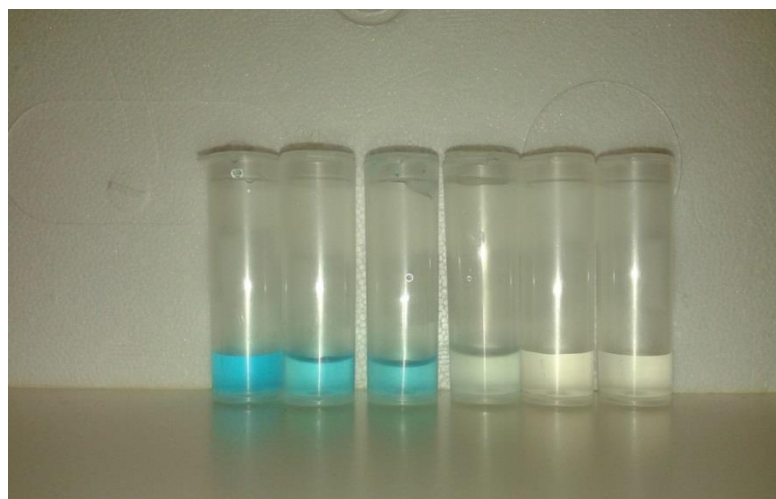
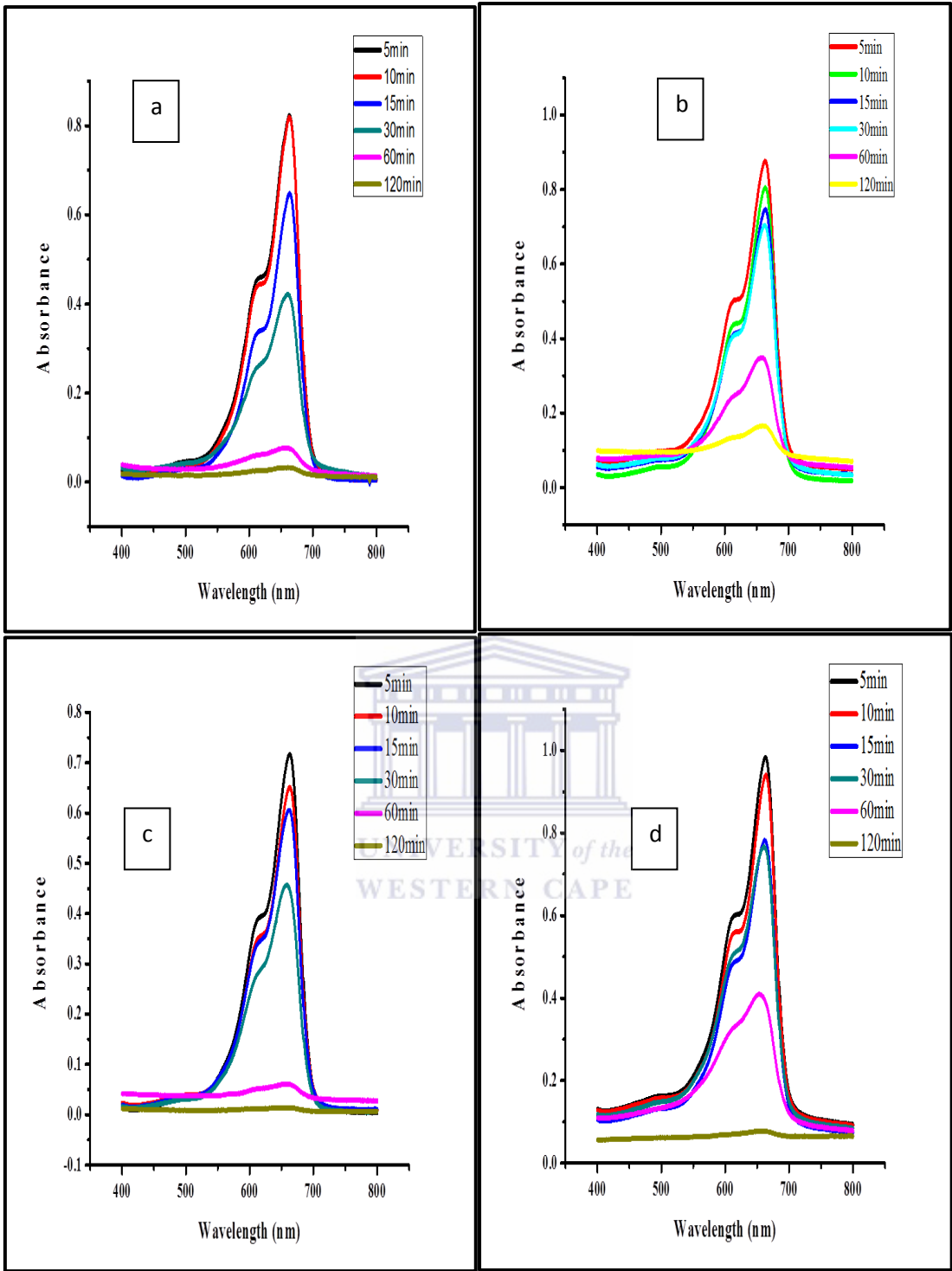


Figure 5.30: MB samples drawn after 5 min, 10 min, 15 min, 30 min, 60min and 120min from left to right respectively.

Ultraviolet spectra



The samples drawn from the reaction mixture were analysed using UV-Vis spectrometer in the range 400- 800nm. The absorbance of each sample solution was considered as a measure of the amount of MB concentration.



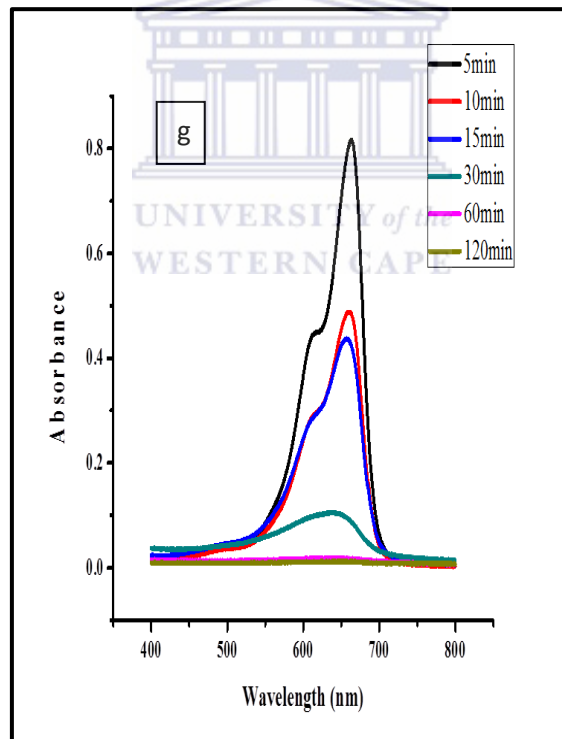
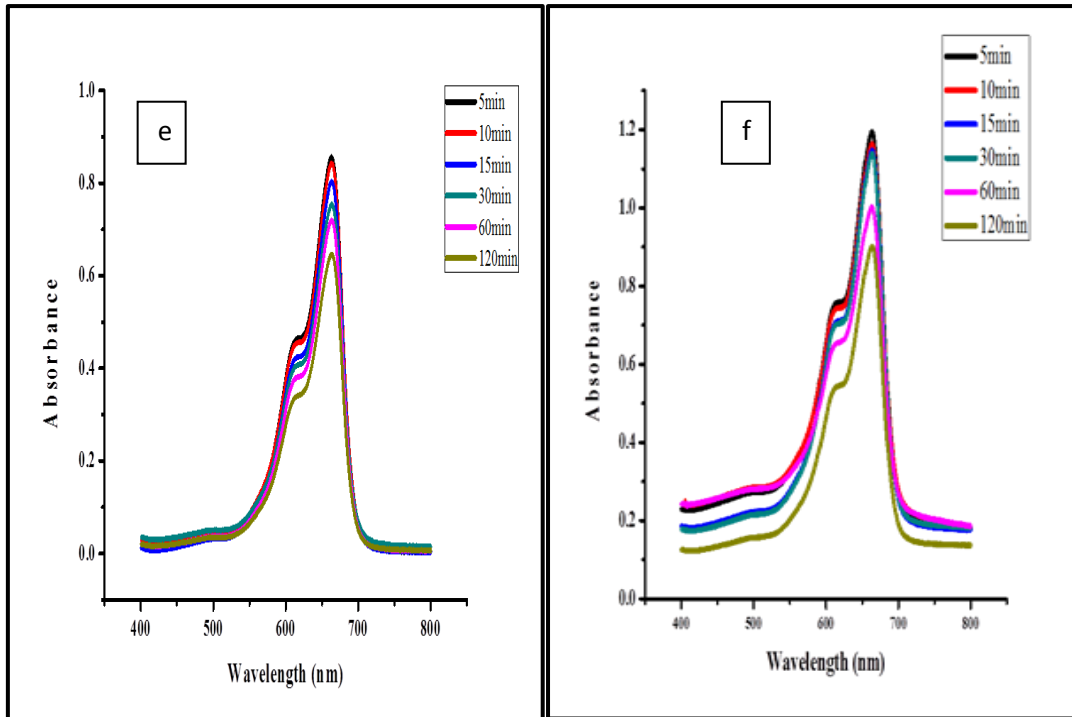


Figure 5.31: UV spectra of the photodegradation process over time using (a) blank, (b) Fe_3O_4 , (c) $\text{Fe}_3\text{O}_4/\text{SiO}_2/\text{TiO}_2$, (d) $\text{Ag-Fe}_3\text{O}_4/\text{SiO}_2/\text{TiO}_2$ (e), Commercial TiO_2 , (f) Com TiO_2 (no UV irradiation) and (g) $\text{Fe}_3\text{O}_4/\text{SiO}_2/\text{TiO}_2$ (no UV irradiation)

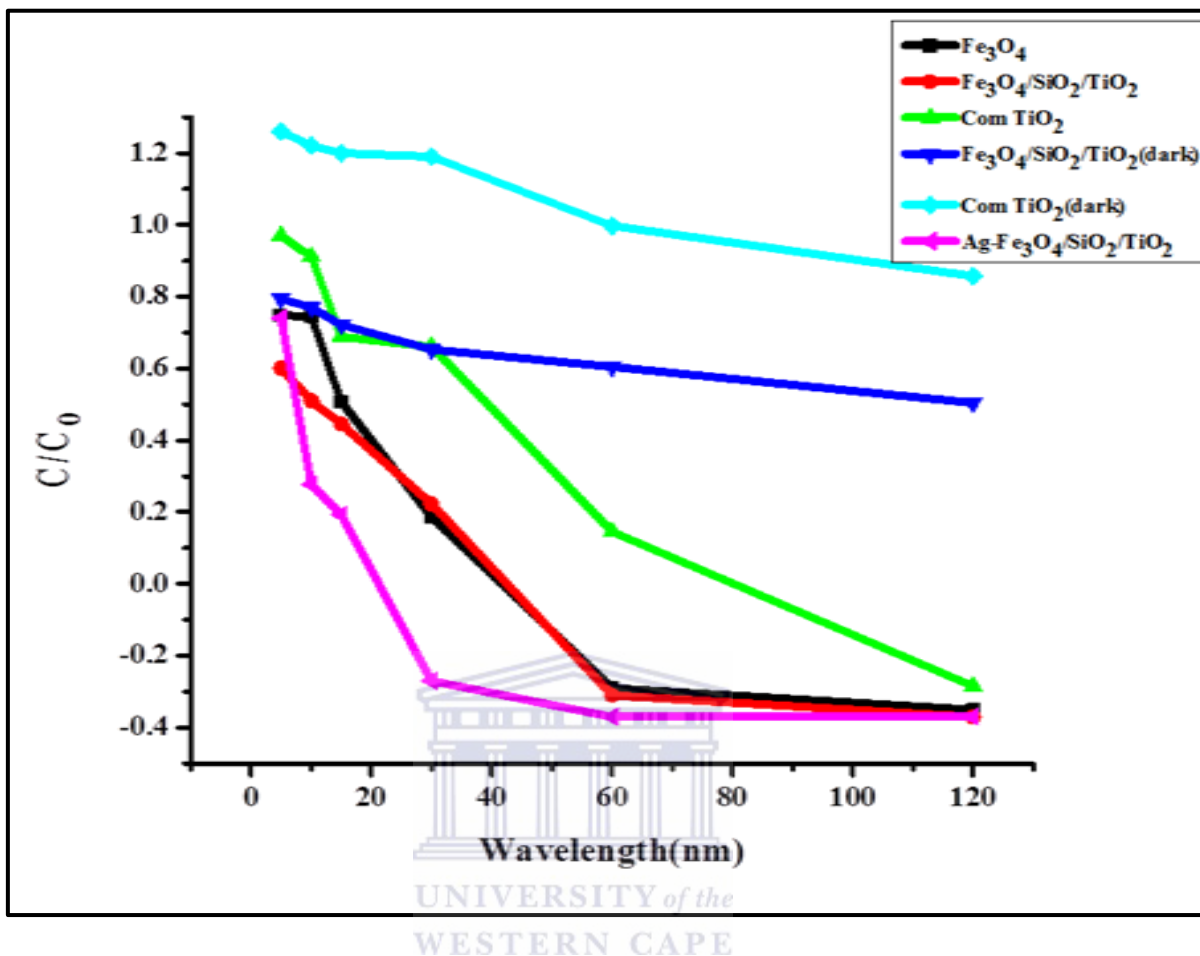


Figure 5.32: UV spectra of the photodegradation process over time using

Commercial TiO₂ (Degussa P25 titanium dioxide), which is known to be the best photocatalyst commercially available, was used as a reference to qualitatively assess the photocatalytic performance of the as-synthesized samples. Figure 5.5 shows the degradation of methylene under UV light in the presence of Fe₃O₄, Fe₃O₄/SiO₂/TiO₂, and Ag-Fe₃O₄/SiO₂/TiO₂ and in the absence of a catalyst. A rapid decrease in the absorption of methylene blue was observed at 664nm. The degradation rate is fast at the beginning of the reaction and then became slow. A sharp decrease of the major

absorption band within 30 min indicates that this sample exhibits excellent photocatalytic activity for the degradation of MB.

In the absence of a catalyst the degradation rate shows the same phenomenon however the degradation of the dye maintains the same rate even after 30min, suggesting the addition of catalysts increases the degradation of MB. The photocatalytic activity of Ag-coated $\text{Fe}_3\text{O}_4/\text{TiO}_2$ nanoparticles is much higher than that of Degussa P25 titania, Fe_3O_4 and the $\text{Fe}_3\text{O}_4/\text{TiO}_2$ nanoparticles. The deposition of metallic Ag nanoparticles on the surface of the $\text{Fe}_3\text{O}_4/\text{TiO}_2$ nanocomposites increases the photocatalytic activity, which indicates that the Ag-TiO₂ heterojunction can improve electron-charge separation efficiency.

In order to investigate the efficiencies of mineralization for MB in these three catalysts, photocatalytic performance was also measured during the reaction. The figures above show degradation efficiencies of dye waste water after 2hrs. From these results, it is noteworthy that the Ag-coated $\text{Fe}_3\text{O}_4/\text{SiO}_2/\text{TiO}_2$ microspheres are the strongest at mineralizing MB among the catalysts.

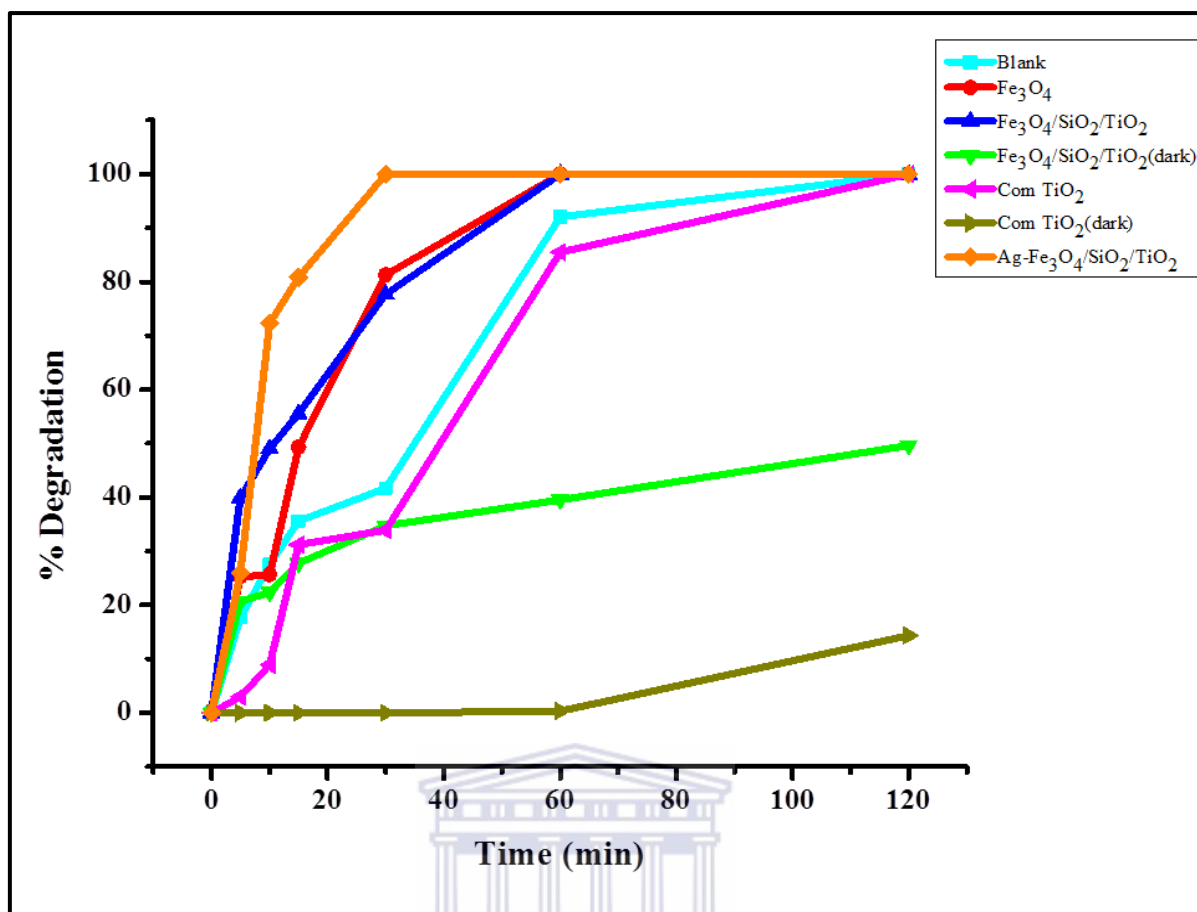


Figure 5.33: Degradation percentage of MB dye over time

The degradation was calculated using the formula

$$\% \text{degradation} = \frac{C_o - C_f}{C_o} \times 100$$

Where C_o is the initial concentration

C_f is the final concentration

The maximum MB degradation efficiency for the Ag coated Fe₃O₄/TiO₂ nanoparticles is about 81%, and complete disappearance of colour in 15min and good activity of silver doped titanium dioxide catalyst have been reported by (Sung-Suh, *et al.*, 2004; Sobana, *et al.*, 2006. The Fe₃O₄ and Fe₃O₄/SiO₂/TiO₂ reached 92% and 77.8% in 60 and 30 minutes respectively. This proved that the titanium dioxide shell improved the

photocatalytic performance of Fe_3O_4 nanoparticles. The commercial TiO_2 catalyst under UV irradiation showed 85.5% degradation of MB dye after 60min, which is less than that achieved by Fe_3O_4 . The $\text{Fe}_3\text{O}_4/\text{SiO}_2/\text{TiO}_2$ catalyst and commercial TiO_2 , in the absence of UV irradiation, only achieved 49.6 and 14.3% degradation of MB after two hours showing that the use of UV light also enhances the photodegradability of MB dye. It is also evident that the as-synthesized catalyst had better photocatalytic activity than commercial TiO_2 and this has also been reported (Gao, *et al.*, 2003; Shi, *et al.*, 2012).



Chapter 6: Conclusions, future work and recommendations

Conclusion

A silver doped magnetite titanium dioxide nanocomposite was successfully synthesized using sol-gel and hydrothermal techniques. The as-synthesized catalysts were characterized using FTIR, SEM, TEM, XRD, BET, TGA, and UV. The TEM measurements showed cubic shaped particles and spherical shaped Ag particles whose average size were 66 nm, 74nm and 61nm for Fe_3O_4 , $\text{Fe}_3\text{O}_4/\text{SiO}_2/\text{TiO}_2$ and $\text{Ag-Fe}_3\text{O}_4/\text{SiO}_2/\text{TiO}_2$. The synthetic techniques which were used were fast and give uniform distribution of crystallites of $\text{Fe}_3\text{O}_4/\text{SiO}_2/\text{TiO}_2$ confirmed by XRD studies.

The catalysts were evaluated for their photocatalytic performance for the degradation of a standard methylene blue solution. The as-synthesized catalysts showed good degradation activities compared to commercial P25 TiO_2 . Their performance showed degradation efficiency in the order $\text{Ag-Fe}_3\text{O}_4/\text{SiO}_2/\text{TiO}_2 > \text{Fe}_3\text{O}_4/\text{SiO}_2/\text{TiO}_2 > \text{Fe}_3\text{O}_4 > \text{Degussa P25 TiO}_2$. Silver nanoparticles on the TiO_2 surface behave as sites for electron accumulation; increasing the electron-hole separation (reducing recombination reactions). This promotes efficient channelling of charge carriers into useful reduction and oxidation reactions enhancing photocatalytic activity.

Furthermore the nanocomposite maintained good magnetic properties and could be separated easily from reaction mixture making use of an external magnet. The photocatalysts was recovered without any or negligible mass loss. The results of the present work and the referenced literature show that photocatalytic treatment of textile industry waste-wat

er is a promising tool for the decolourization and possible demineralisation of coloured wastewaters.

Future work and recommendations

The future work is to investigate the reusability and application of the catalyst for other dyes under varied reaction conditions such as MB solution concentration, catalyst loading. Silver deposition on the TiO₂ layer is suggested to decrease the bandgap of TiO₂ thus enhancing the photocatalytic performance of the nanocomposite. The bandgap studies of the nanocomposite and varying the Fe₃O₄/SiO₂/TiO₂ and Ag ratios. The catalysts synthesized in the study can also be evaluated for photocatalytic activity using visible light instead of ultra-violet irradiation.



Chapter 7: References

1. Akpan, U. G. & Hameed, B. H., 2009. Parameters affecting the photocatalytic degradation of dyes using TiO₂-based photocatalysts: A review. *Journal of Hazardous Materials*, 170(2-3), pp. 520-529.
2. Al-Bastaki, N. & Banat, F., 2004. Combining ultrafiltration and adsorption on bentonite in a one-step process for the treatment of colored waters. *Resources, Conservation and Recycling*, Volume 41, pp. 103-113.
3. Allhoff, F., Lin, P. & Moore, D., 2010. *What Is Nanotechnology and Why Does It Matter: from science to ethics*. s.l.:Wiley- Blackwell.
4. Andreozzi, R., Caprio, V., Insola, A. & Marotta, R., 1999. Advanced oxidation processes (AOP) for water purification and recovery. *Catalysis Today*, Volume 53, pp. 57- 59.
5. Arabatzis, I. M. et al., 2003. Silver-modified titanium dioxide thin films for efficient photodegradation of methyl orange. *Applied Catalysis B: Environmental*, Volume 42, pp. 187- 201.
6. Aziz, A. A. et al., 2012. Visible light improved, photocatalytic activity of magnetically separable titania. *Chemical Engineering Journal*, Volume 183, p. 349– 356.
7. Ba-Abbad, M. M. et al., 2012. Synthesis and Catalytic Activity of TiO₂ Nanoparticles for Photochemical Oxidation of Concentrated Chlorophenols under Direct Solar Radiation. *Int. J. Electrochem. Sci.*, Volume 7, pp. 4871 - 4888.
8. Bacardit, J., Stötzner, J., Chamarro, E. & Esplugas, S., 2007. Effect of Salinity on the Photo-Fenton Process. *Ind. Eng. Chem. Res.*, Volume 46, pp. 7615-7619.
9. Bafana, A., Devi, S. S. & Chakrabarti, T., 2011. Azo dyes: past, present and the future. *Environmental Reviews*, 19(1), pp. 350- 370.
10. Banat, F., Al-Asheh, S. & Qtaishat, M., 2005. Treatment of waters colored with methylene blue dye by vacuum membrane distillation. *Desalination*, Volume 174, pp. 87-96.
11. Banerjee, A. N., Joo, S. W. & Min, B. -K., 2012. Photocatalytic Degradation of Organic dyes by Sol-Gel-Derived Gallium-Doped Anatase Titanium Dioxide Nanoparticles for Environmental Remedation. *Journal of Nanomaterials*, Volume 2012, p. Article ID 201492 14 pages.

12. Barbusiński, K., 2009. Fenton reaction- controversy concerning the chemistry. *Ecological Chemistry and Engineering S*, 16(3), pp. 347- 358.
13. Behnajady, M. A. et al., 2008. The effect of particle size and crystal structure of titanium dioxide nanoparticles on the photocatalytic properties. *Journal of Environmental Science and Health, Part A: Toxic/Hazardous Substances & Environmental Engineering*, 43(5), pp. 460-467.
14. Beydoun, D. & Amal, R., 2002. Implications of heat treatment on the properties of a magnetic iron oxide/titanium dioxide photocatalyst. *Materials Science and Engineering*, Volume 94, pp. 71-81.
15. Beydoun, D. et al., 2002. Effect of copper (II) on the photocatalytic degradation of sucrose. *Journal of Molecular Catalysis A: Chemical*, Volume 177, pp. 265- 272.
16. Beydoun, D., Amal, R., Low, G. & McEvoy, S., 2002. Occurrence and prevention of photodissolution at the phase junction of magnetite and titanium dioxide. *Journal of Molecular Catalysis A: Chemical*, Volume 180, pp. 193-200.
17. Beydoun, D., Amal, R., Low, G. K.-C. & McEvoy, S., 2000. Novel Photocatalyst: Titania-Coated Magnetite. Activity and Photodissolution. *J. Phys. Chem. B*, Volume 104, pp. 4387-4396.
18. Binnie, C., Kimber, M. & Smethurst, G., 2002. *Basic water treatment*. 3rd ed. London: Thomas Telford Ltd.
19. Bokhimi, X. et al., 1999. Copper Precursor Effect on Reducibility and Titania Phases Concentration of Sol+Gel Cu/TiO₂ Catalyst. *Journal of Solid State Chemistry*, Volume 144, pp. 349-353.
20. Börjesson, J., 2006. *Scanning Electron Microscopy*. 01 02.
21. Carp, O., Huisman, C. L. & Reller, A., 2004. Photoinduced reactivity of titanium dioxide. *Progress in Solid State Chemistry*, Volume 32, pp. 33- 177.
22. Casbeer, E., Sharma, V. K. & Li, X.-Z., 2012. Synthesis and photocatalytic activity of ferrites under visible light: A review. *Separation and Purification Technology*, Volume 87, pp. 1-14.
23. Chakrabarti, S. & Dutta, B. k., 2004. Photocatalytic degradation of model textile dyes in wastewater using ZnO as semiconductor catalyst. *Journal of Hazardous Materials*, 112(3), pp. 269- 278.
24. Chakrabarti, S. & Dutta, B. K., 2004. Photocatalytic degradation of model textile dyes in wastewater using ZnO as semiconductor catalyst. *Journal of Hazardous Materials B*, Volume 112, pp. 269-278.

25. Chapline, M. G. & Wang, S. X., 2005. Observation of the Verwey transition in thin magnetite films. *Journal of Applied Physics*, 97(12), pp. 123091/1-123901/3.
26. Chen, F., Xie, Y., Zhao, J. & Lu, G., 2001. Photocatalytic degradation of dyes on a magnetically separated photocatalyst under visible and UV irradiation. *Chemosphere*, 44(5), pp. 1159- 1168.
27. Chen, Y.-H. et al., 2009. Platinum-Doped TiO₂/Magnetic Poly (methyl methacrylate) Microspheres as a Novel Photocatalyst. *Ind. Eng. Chem. Res.*, Volume 48, p. 7616–7623.
28. Cheng, F. Y. et al., 2005. Characterization of Aqueous Dispersions of Fe₃O₄ Nanoparticles and Their Biomedical Applications. *Biomaterials*, Volume 26, pp. 729- 738.
29. Cheng, J. et al., 2012. Anatase nanocrystals coating on silica-coated magnetite: Role of polyacrylic. *Chemical Engineering Journal*, Volume 210, p. 80–86.
30. Chequer, F. M. D. et al., 2013. Textile Dyes: Dyeing Process and Environmental Impact. In: M. Günay, ed. *Eco-Friendly Textile Dyeing and Finishing*. São Paulo: Intech, pp. 154- 176.
31. Chin, A. B. & Yaacob, I. I., 2007. Synthesis and characterization of magnetic iron oxide nanoparticles via w/o microemulsion and Massart's procedure. *Journal of Materials Processing Technology*, Volume 191, pp. 235-237.
32. Chin, S., Park, E., Kim, M. & Jung, J., 2010. Photocatalytic degradation of methylene blue with TiO₂ nanoparticles prepared by a. *Powder Technology*, Volume 201, p. 171–176.
33. Chirita, M. & Grozescu, I., 2009. Fe₂O₃ – Nanoparticles, Physical Properties and Their Photochemical and Photoelectrochemical Applications. *Chem. Bull. "POLITEHNICA" Univ. (Timișoara)*, 54(68), pp. 1-8.
34. Chong, M. N., Jin, B., Chow, C. W. & Saint, C., 2010. Recent developments in photocatalytic water treatment technology: A review. *Water research*, Volume 44, pp. 2997- 3027.
35. Colmenares, J. C. & Luque, R., 2014. Heterogeneous photocatalytic nanomaterials: prospects and challenges in selective transformations of biomass-derived compounds. *Chem. Soc. Rev.*, Volume 43, pp. 765-768.
36. Comparelli, R. et al., 2005. UV-induced photocatalytic degradation of azo dyes by organic-capped ZnO nanocrystals immobilized onto substrates. *Applied Catalysis B: Environmental*, 60(1-2), p. 1–11.

37. Coradin, T., Boissière, M. & Livage, J., 2006. Sol-gel chemistry in medicinal science. *Curr Med Chem.*, 13(1), pp. 99-108.
38. Cundy, A. B., Hopkinson, L. & Whitby, R. L., 2008. Use of iron-based technologies in contaminated: A review. *Sci Total Environ*, 400(1-3), pp. 42- 51.
39. Curri, M. L. et al., 2003. Colloidal oxide nanoparticles for the photocatalytic degradation of organic dye. *Materials Science and Engineering: C*, 23(1-2), p. 285–289.
40. Dalrymple, O. K., Yeh, D. H. & Trotz, M. A., 2007. Removing pharmaceuticals and endocrine-disrupting compounds from wastewater by photocatalysis. *Journal of Chemical Technology and Biotechnology*, Volume 82, p. 121–134.
41. Daneshvar, N., Salari, D., Niaei, A. & Khataee, A. R., 2006. Photocatalytic Degradation of the Herbicide Erioglaucine in the Presence of Nanosized Titanium Dioxide: Comparison and Modeling of Reaction Kinetics. *Journal of Environmental Science and Health, Part B: Pesticides, Food Contaminants, and Agricultural Wastes*, 41(8), pp. 1273-1290.
42. Darbandi, M., Thomann, R. & Nann, T., 2005. Single Quantum Dots in Silica Spheres by Microemulsion Synthesis. *Chem. Mater.*, Volume 17, pp. 5720-5725.
43. de Carvalho, H. P. et al., 2015. Removal of Acid Black 1 and Basic Red 2 from aqueous solutions by electrocoagulation/Moringa oleifera seed adsorption coupling in a batch system. *Water Sci Technol.*, 72(2), pp. 203-13.
44. De Gree, A., 2015. The History and Working Principle of the Scanning Electron Microscope (SEM). *Azo nano*, 19 March.
45. Deb, T. K. & Majumdar, S., 2013. Removal of Reactive Dyes from Textile Wastewater by Electrocoagulation Process: An Effective and Clean Approach. *International Journal of Environment and Bioenergy*, 6(2), pp. 96- 116.
46. Dong, X.-L. et al., 2013. Preparation of CdS–TiO₂/Fe₃O₄ photocatalyst and its photocatalyst properties. *J Sol-Gel Sci Technol*, Volume 66, p. 231–237.
47. Dronskowski, R., 2001. The little maghemite story. A classic functional material. *Advanced Functional Materials*, 11(1), pp. 27-29.
48. Dutta, T. et al., 2008. Toxicological investigation of surface engineered fifth generation poly (propyleneimine) dendrimers in vivo. *Nanotoxicology*, 2(2), pp. 62- 70.

49. Ehrampoush, M. H. et al., 2011. Removal of Methylene Blue dye from textile simulated sample using tubular reactor and $\text{TiO}_2/\text{UV-C}$ photocatalytic process. *Iran. J. Environ. Health. Sci. Eng.*, 8(1), pp. 35- 40.
50. Epling, G. A. & Lin, C., 2002. Photo assisted bleaching of dyes utilizing TiO_2 and visible light. *Chemosphere*, 46, 561-570 (2002), Volume 46, pp. 561-570.
51. Fan, H. et al., 2012. ZnO–graphene composite for photocatalytic degradation of methylene blue dye. *Catalysis Communications*, Volume 29, pp. 29-34.
52. Fang, Y.-f. et al., 2007. Photocatalytic degradation of the dye sulforhodamine-B: A comparative study. *Journal of Environmental Sciences*, Volume 19, pp. 97-102.
53. Feynman, R., 1960. There's plenty of room at the bottom (reprint from speech given at annual meeting of the American Physical Society). *Eng Sci*, Volume 23, pp. 22- 36.
54. Forgacs, E., Cserháti, T. & Oros, G., 2004. Removal of synthetic dyes from wastewaters: a review. *Environment International*, Volume 30, pp. 953-971.
55. Fu, Y. & Viraraghavan, T., 2001. Fungal decolourization of dye wastewater: a review. *Bioresource Technology*, Volume 79, pp. 251-262.
56. Fujishima, A. & Honda, K., 1972. Electrochemical photolysis of water at a semiconductor electrode. *Nature* 238, 238(5358), pp. 8-37.
57. Fujishima, A., Rao, T. N. & Tryk, D. A., 2000. Titanium dioxide photocatalysis. *Journal of Photochemistry and Photobiology C: Photochemistry Reviews*, 1(1), p. 1–21.
58. Gad-Allah, T. A. et al., 2008. *Journal of Hazardous Materials*, Volume 154, p. 572–577.
59. Gad-Allah, T. A., Kato, S., Satokawa, S. & Kojima, T., 2007. Role of core diameter and silica content in photocatalytic activity of $\text{TiO}_2/\text{SiO}_2/\text{Fe}_3\text{O}_4$ composite. *Solid State Sciences*, Volume 9, pp. 737- 743.
60. Gad-Allah, T. A., Kato, S., Satokawa, S. & Kojima, T., 2009. Treatment of synthetic dyes wastewater utilizing a magnetically separable photocatalyst ($\text{TiO}_2/\text{SiO}_2/\text{Fe}_3\text{O}_4$): Parametric and kinetic studies. *Desalination*, Volume 244, pp. 1- 11.
61. Gao, Y., Chen, B., Li, H. & Ma, Y., 2003. Preparation and Characterization of a magnetically separated photocatalyst and its catalytic properties. *Materials Chemistry and Physics*, Volume 80, pp. 348-355.

62. García-Morales, M. A. et al., 2013. Integrated Advanced Oxidation Process (Ozonation) and Electrocoagulation Treatments for Effluents. *Int. J. Electrochem. Sci.*, Volume 8, pp. 8752-8763.
63. Garg, V. K., Gupta, R., Yadav, A. B. & Kumar, R., 2003. Dye removal from aqueous solution by adsorption on treated sawdust. *Bioresource Technology*, Volume 89, pp. 121-124.
64. Ge, S. et al., 2009. Facile Hydrothermal Synthesis of Iron Oxide Nanoparticles with Tunable Magnetic Properties. *J. Phys. Chem. C*, Volume 113, p. 13593–13599.
65. Girginova, P. I. et al., 2010. Silica coated magnetite particles for magnetic removal of Hg^{2+} from water. *Journal of Colloid and Interface Science*, 345(2), pp. 234-240.
66. Gogate, P. R. & Pandit, A. B., 2004. A review of imperative technologies for wastewater treatment I: oxidation technologies at ambient conditions. *Advances in Environmental Research*, 8(3-4), pp. 501-551.
67. Golder, A. K., Hridaya, N., Samanta, A. N. & Ray, S., 2005. Electrocoagulation of methylene blue and eosin yellowish using mild steel electrodes. *Journal of Hazardous Materials*, 127(1- 3), pp. 134- 140.
68. Gribb, A. A. & Banfield, J. F., 1997. Particle size effects on transformation kinetics and phase stability in nanocrystalline TiO_2 . *American Mineralogist*, Volume 82, pp. 717-728.
69. Gruber, D. D., 2013. EM Sample Preparation Coating Technology. Leica Microsystems, April.
70. Gu, H. W., Xu, K. M., Xu, C. J. & Xu, B., 2006. Biofunctional Magnetic Nanoparticles for Protein Separation and Pathogen Detection. *Chem. Commun.*, Volume 9, pp. 941- 949.
71. Gubin, S. P., Koksharov, Y. A., Khomutov, G. B. & Yurkov, G. Y., 2005. Magnetic nanoparticles: preparation, structure and properties. *Russian Chemical Reviews*, 74(6), pp. 489-520.
72. Gupta, S. M. & Tripathi, M., 2011. A review of TiO_2 nanoparticles. *Chinese Science Bulletin*, 56(16), p. 1639–1657.
73. Hakuta, Y., Hayashi, H. & Arai, K., 2003. Fine particle formation using supercritical fluids. *Curr. Opin. Solid State Mat. Sci.*, Volume 7, p. 341–351.

74. Hanaor, D. & Sorrell, C., 2011. Review of the anatase to rutile phase transformation. *Journal of Material Science*, 46(4), pp. 1-20.
75. Hariani, P. L. et al., 2013. Synthesis and Properties of Fe₃O₄ Nanoparticles by Co-precipitation Method to Removal Procion Dye. *International Journal of Environmental Science and Development*, 4(3), pp. 336-340.
76. Harraz, F. A. et al., 2014. Magnetic nanocomposite based on titania– silica/cobalt ferrite for photocatalytic degradation of methylene blue dye. *Ceramics International*, Volume 40, p. 375–384.
77. Hayashi, H. & Hakuta, Y., 2010. Hydrothermal Synthesis of Metal Oxide Nanoparticles in Supercritical Water. *Materials*, Volume 3, pp. 3794-3817.
78. Height, M. J., Pratsinis, S. E., Mekasuwandumrong, O. & Prasertdam, P., 2006. Ag-ZnO catalysts for UV-photodegradation of methylene blue. *Applied Catalysis B: Environmental*, 63(3- 4), pp. 305- 312.
79. Hench, L. L. & West, J. K., 1990. The Sol-Gel Process. *Chem. Rev.*, Volume 90, pp. 33-72.
80. Henderson, M. A., 2011. A surface science perspective on TiO₂ photocatalysis. *Surf. Sci. Rep.*, Volume 66, pp. 185-297.
81. Hermann, J. M., Disdier, J. & Pichat, P., 1988. Photocatalytic deposition of silver on powder titania. The consequences for the recovery of silver. *J.Catal.* Volume 113, pp. 72- 81.
82. Hermann, J.-M., 1999. Heterogeneous photocatalysis: fundamentals and applications to the removal of various types of aqueous pollutants. *Catalysis Today*, 53(1), pp. 115-129.
83. Hernández-Rodríguez, M. J. et al., 2014. Treatment of effluents from wool dyeing process by photo-Fenton at solar pilot plant. *Journal of Environmental Chemical Engineering*, Volume 2, p. 163–171.
84. Herney-Ramirez, J., Vicente, M. A. & Madeira, L. M., 2010. Heterogeneous photo-Fenton oxidation with pillared clay-based catalysts for wastewater treatment: A review. *Applied Catalysis B: Environmental*, Volume 98, pp. 10-26.
85. Hintsho, N. et al., 2014. Photo-catalytic activity of titanium dioxide carbon nanotubeno-composites modified with silver and palladium nanoparticles. *Applied Catalysis B: Environmental*, Volume 156–157, p. 273–283.
86. Höhne, G., Hemminger, W. F. & Flammersheim, H. -J., 2013. *Differential Scanning Calorimetry. 2*, illustrated ed. s.l.: Springer Science & Business Media.

87. Houas , A. et al., 2001. Photocatalytic degradation pathway of methylene blue in water. *Applied Catalysis B: Environmental*, Volume 31, pp. 145-157.
88. Hu, X., Yang, J. & Zhang, J., 2011. Magnetic loading of $\text{TiO}_2/\text{SiO}_2/\text{Fe}_3\text{O}_4$ nanoparticles on electrode surface for photoelectrocatalytic degradation of diclofenac. *Journal of Hazardous Materials*, Volume 196, pp. 220-227.
89. Huang, W.-J., Fang, G.-C. & Wang, C.-C., 2005. A nanometer-ZnO catalyst to enhance the ozonation of 2, 4, 6-trichlorophenol in water. *Colloids and Surfaces A: Physicochemical and Engineering Aspects*, 260(1-3), pp. 45-51.
90. Huang, X. et al., 2011. Synthesis of polyaniline-modified $\text{Fe}_3\text{O}_4/\text{SiO}_2/\text{TiO}_2$ composite microspheres and their photocatalytic application. *Materials Letters*, Volume 65, p. 2887–2890.
91. Hussein, F. H., 2011. Photochemical Treatments of Textile Industries Wastewater. In: P. P. Hauser, ed. *Advances in Treating Textile Effluent*. Iraq: Intech, pp. 117-144.
92. Inan, H., Dimoglo, A., Şimşek, H. & Karpuzcu, M., 2004. Olive oil mill wastewater treatment by means of electro-coagulation. *Separation and Purification Technology*, 36(1), pp. 23-31.
93. Islam, M. S. et al., 2012. Hydrothermal Novel Synthesis of Neck-structured Hyperthermia-suitable Magnetic (Fe_3O_4 , $\gamma\text{-Fe}_2\text{O}_3$ and $\alpha\text{-Fe}_2\text{O}_3$) Nanoparticles. *Journal of Scientific Research*, 4(1), pp. 99-107.
94. Jadhav, S. A. & Patil, S. V., 2014. Facile synthesis of magnetic iron oxide nanoparticles and their characterization. *Front. Mater. Sci.*, 8(2), p. 193–198.
95. Jafari , N. et al., 2012. Degradation of a textile reactive azo dye by a combined biological-photocatalytic process: *Candida tropicalis* Jks2 - TiO_2/Uv . *Iranian J Environ Health Sci Eng.*, 9(1), p.33.
96. Jana, N. R., Chen, Y. & Peng, X., 2004. Size -and Shape-Controlled Magnetic (Cr, Mn, Fe, Co, Ni) Oxide Nanoocrystals via a Simple and General Approach. *Chemistry of Materials*, 16(20), pp. 3931-3935.
97. Jang , Y. . J., Simer, C. & Ohm, . T., 2006. Comparison of zinc oxide nanoparticles and its nano-crystalline particles on the photocatalytic degradation of methylene blue. *Materials Research Bulletin*, Volume 41, pp. 67-77.

98. Kahn, O., 1988. Magnetic Ordering of Mn^{II} Cu^{II} Bimetallic Systems: Design of Molecular Ferromagnets. *Organic and Inorganic Low-Dimensional Crystalline Materials*, Volume 168, pp. 93-108.
99. Khataee, A. R., Vatanpour, V. & Amani Ghadim, A. R., 2009. Decolorization of CI Acid Blue 9 solution by UV/Nano-TiO₂, Fenton, Fenton-like, electro-Fenton and electrocoagulation processes: a comparative study. *Journal of Hazardous Materials*, 161(2-3), p. 1225–1233.
100. Kim, D. K. et al., 2001. Synthesis and characterization of surfactant-coated superparamagnetic monodispersed iron oxide nanoparticles. *Journal of Magnetism and Magnetic Materials*, 225(1-2), pp. 30-36.
101. Kim, D.-W., Enomoto, N., Nakagawa, Z.-e. & Kawamura, K., 1996. Molecular Dynamic Simulation in Titanium Dioxide Polymorphs: Rutile, Brookite, and Anatase. *Journal of the American Ceramic Society*, 79(4), p. 1095–1099.
102. Kim, Y., Lee, B. & Yi, J., 2003. Preparation of Functionalized Mesostructured Silica Containing Magnetite (MSM) for the Removal of Copper Ions in Aqueous Solutions and Its Magnetic Separation. *Separation Science and Technology*, 38(11), p. 2533–2548.
103. Kiss, A. A., 2014. Distillation technology: still young and full of breakthrough opportunities. *J Chem Technol Biotechnol*, Volume 89, pp. 479-498.
104. Klavarioti, M., Mantzavinos, D. & Kassinos, D., 2009. Removal of residual pharmaceuticals from aqueous systems by advanced oxidation processes. *Environ Int.*, 35(2), pp. 402-17.
105. Kobya, M., Can, O. T. & Bayram, M., 2003. Treatment of textile wastewaters by electrocoagulation using iron and aluminium electrodes. *Journal of Hazardous Materials*, 100(1-3), pp. 163-178.
106. Kronick, P., Gilpin, R. W. & Biochem, J., 1986. Use of Superparamagnetic Particles for Isolation of Cells. *J. Biochem. Biophys. Methods*, 12(1- 2), pp. 73-80.
107. Kulkarni, M. & Thakur, P., 2014. Photocatalytic Degradation and Mineralization of Reactive Textile Azo Dye Using Semiconductor Metal Oxide Nano Particles. *International Journal of Engineering Research and General Science*, 2(2), pp. 245-254.

108. Kumar, J. & Bansal, A., 2013. Photocatalysis by Nanoparticles of Titanium Dioxide for Drinking Water Purification: A Conceptual and State-of-Art Review. *Materials Science Forum*, Volume 764, pp. 130- 150.
109. Kurinobu, S. et al., 2007. Decomposition of pollutants in wastewater using magnetic photocatalyst particles. *Journal of Magnetism and Magnetic Materials*, 310(2), pp. 1025-1027.
110. Lachheb, H. et al., 2002. Photocatalytic degradation of various types of dyes (Alizarin S, Crocein Orange G, Methyl Red, Congo red, and Methylene Blue) in water by UV-irradiated titania. *Applied Catalysis B: Environmental*, Volume 39, p. 75–90.
111. Lam, U. V., Mammucari, R., Suzuki, K. & Foster, N. R., 2008. Processing of Iron Oxide Nanoparticles by Supercritical Fluids. *Ind. Eng. Chem. Res.*, Volume 47, pp. 599-614.
112. Landmann, M., Rauls, E. & Schmidt, W. G., 2012. The electronic structure and optical response of rutile, anatase and brookite TiO₂. *J. Phys.: Condens. Matter*, Volume 24, p. 195503 (6pp).
113. Laurent, S. et al., 2008. Magnetic Iron Oxide Nanoparticles: Synthesis, Stabilization, Vectorization, Physicochemical Characterizations, and Biological Applications. *Chem. Rev.*, Volume 108, pp. 2064-2010.
114. Lee, B.-. N., Liaw, W.-. D. & Lou, J.-. C., 1999. Photocatalytic Decolorization of Méthylène Blue in Aqueous TiO₂ Suspension. *Environmental Engineering Science*, 16(3), pp. 165- 175.
115. Legube, B. & Leitner, N. K. V., 1999. Catalytic ozonation: a promising advanced oxidation technology for water treatment. *Catalysis Today*, Volume 53, pp. 61- 72.
116. Li, Y., Zhang, M., Guo, M. & Wang, X., 2009. Preparation and properties of a nano TiO₂/Fe₃O₄ composite superparamagnetic photocatalyst. *Rare Metals*, 28(5), pp. 423-427.
117. Liang, Y.-C. et al., 2011. Photocatalysis of Ag-Loaded TiO₂ Nanotube Arrays Formed by Atomic Layer Deposition. *The Journal of Physical Chemistry C*, Volume 115, p. 9498–9502.
118. Lin, C.-L., Lee, C.-F. & Chiu, W.-Y., 2005. Preparation and properties of poly (acrylic acid) oligomer stabilized superparamagnetic ferrofluid. *Journal of Colloid and Interface Science*, 291(2), pp. 411-420.

119. Linley, S., Leshuk, T. & Gu, F. X., 2013. Synthesis of Magnetic Rattle-Type Nanostructures for Use in Water. *ACS Appl. Mater. Interfaces*, Volume 5, p. 2540–2548.
120. Liu, H. et al., 2011. Synthesis of $\text{TiO}_2/\text{SiO}_2@\text{Fe}_3\text{O}_4$ magnetic microspheres and their properties of photocatalytic degradation dyestuff. *Catalysis Today*, Volume 175, pp. 293- 298.
121. Liu, S., Sun, H., Liu, S. & Wang, S., 2013. Graphene facilitated visible light photodegradation of methylene blue over titanium dioxide photocatalysts. *Chemical Engineering Journal*, Volume 214, p. 298–303.
122. Liu, S.-Q., 2012. Magnetic semiconductor nano-photocatalysts for the degradation. *Environ Chem Lett*, 10(3), pp. 209-216.
123. Liu, S.-Q. et al., 2013. Graphene oxide enhances the Fenton-like photocatalytic activity of nickel ferrite for degradation of dyes under visible light irradiation. *Carbon*, Volume 64, pp. 197- 206.
124. Liu, X. et al., 2014. Heterogeneous Fenton oxidation of Direct Black G in dye effluent using functional kaolin-supported nanoscale zero iron. *Environ Sci Pollut Res*, Volume 21, p. 1936–1943.
125. Lodha, S., Jain, A. & Punjabi, P. B., 2011. A novel route for waste water treatment: Photocatalytic degradation of rhodamine B. *Arabian Journal of Chemistry*, Volume 4, p. 383–387.
126. Lu, A. -H., Salabas, E. L. & Schueth, F., 2007. Magnetic nanoparticles: synthesis, protection, functionalization, and application. *Angewandte Chemie, International Edition*, 46(8), pp. 1222-1244.
127. Luntraru, V. I. et al., 2011. Synthesis and characterization of magnetite - titanium dioxide - 4-Benzene-azo- α -naphthylamine and methylene blue composites. *Optoelectronics and Advanced Materials- Rapid Communications*, 5(11), pp. 1229-1232.
128. Luttrell, T. et al., 2014. Why is anatase a better photocatalyst than rutile? - Model studies on epitaxial TiO_2 films. *Sci Rep.*, Volume 4, p. 4043.
129. Ma, H., Zhuo, Q. & Wangx, B., 2009. Electro-catalytic degradation of methylene blue wastewater assisted by Fe_2O_3 -modified kaolin. *Chemical Engineering Journal*, 155(1- 2), pp. 248- 253.

130. Madaeni, S. S., 1999. The application of membrane technology for water disinfection. *Water Research*, 33(2), pp. 301-308.
131. Madhu, G. H., Raj, M. A. L. A. & Pai, K. V. K., 2009. Titanium oxide (TiO₂) assisted photocatalytic degradation of methylene blue. *Journal of environmental biology / Academy of Environmental Biology*, 30(2), pp. 259-264.
132. Majewski, P. & Thierry, B., 2007. Functionalized magnetite nanoparticles - Synthesis, properties, and bio-applications. *Critical Reviews in Solid State and Materials Sciences*, 32(3-4), pp. 203-215.
133. Margulies, D. T. et al., 1997. Origin of the Anomalous Magnetic Behaviour in Single Crystal Fe₃O₄ Films. *Review Letters*, 79(25), pp. 5162-5165.
134. Margulis-Goshen, K. & Magdassi, S., 2012. Organic nanoparticles from microemulsions: Formation and applications. *Current Opinion in Colloid & Interface Science*, Volume 17, pp. 290-296.
135. Mascolo, M. C., Pei, Y. & Ring, T. A., 2013. Room Temperature Co-Precipitation Synthesis of Magnetite Nanoparticles in a large pH Window with Different Bases. *Materials*, Volume 6, pp. 5549-5567.
136. McBain, S. C., Yiu, H. H. & Dobson, J., 2008. Magnetic nanoparticles for gene and drug delivery. *Int. J. Nanomedicine*, 3(2), pp. 169-180.
137. Mills, A., Morris, S. & Davies, R., 1993. Photomineralisation of 4-chlorophenol sensitised by titanium dioxide: a study of the intermediates. *Journal of Photochemistry and Photobiology, A: Chemistry*, 70(2), pp. 183-191.
138. Mohabansi, N. P., Tekade, P. V. & Bawankar, S. V., 2011. Physico-chemical Parameters of Textile Mill Effluent, Hinganghat, Dist. Wardha (M.S.). *Current World Environment*, 6(1), pp. 165-168.
139. Mollah, M. Y., Schennach, R., Parga, J. & Cocke, D. L., 2001. Electrocoagulation (EC) - science and applications. *Journal of Hazardous Materials B*, Volume 84, pp. 29-41.
140. Mulder, M., 1997. *Basic principles in membrane technology*. Holland: Kluwer Academic Publishers.
141. Muruganandham, M., Sobana, S. & Swaminathan, M., 2006. Solar assisted photocatalytic and photochemical degradation of Reactive Black 5. *Journal of Hazardous Materials*, 137(3), pp. 1371-1376.
142. Muscat, J., Swamy, V. & Harrison, N. M., 2002. First-principles calculations of the phase stability of TiO₂. *Physical Review B*, Volume 65, p. 224112.

143. Nagaveni, K., Hegde, M. S. & Madras, G., 2004. Structure and Photocatalytic Activity of $Ti_{1-x}M_xO_2$ ($M = W, V, Ce, Zr, Fe, \text{ and } Cu$) Synthesized by Solution Combustion Method. *J. Phys. Chem. B*, Volume 108, pp. 20204-20212.
144. Nagaveni, K., Sivalingam, G., Hegde, M. S. & Madras, G., 2004. Solar photocatalytic degradation of dyes. High activity of combustion synthesized nano TiO_2 . *Applied Catalysis B: Environ.* Volume 48, pp. 83- 93.
145. Nahar, L. & Arachchige, I. U., 2013. Sol-Gel Methods for the Assembly of Metal and Semiconductor Nanoparticles. *JSM Nanotechnol Nanomed*, 1(1), p. 1003.
146. Naje, A. N., Norry, A. S. & Suhail, A. M., 2013. Preparation and Characterization of SnO_2 Nanoparticles. *International Journal of Innovative Research in Science, Engineering and Technology*, Volume 2, pp. 7068-7072.
147. Nandhini, R., Vaishnavi, K. V., Vadasundari, V. & Rangabhashiyam, S., 2012. Decolourization studies of synthetic textile dye using aspergillus species. *Asian Journal of Science and Technology* Vol. 4, Issue 11, pp. 080- 082.
148. Neyens, E. & Baeyens, J., 2003. A review of classic Fenton's peroxidation as an advanced oxidation technique. *Journal of Hazardous Materials*, 98(1-3), pp. 33-50.
149. Ohtani, B., Ogawa, Y. & Nishimoto, S.-i., 1997. Photocatalytic Activity of Amorphous-Anatase Mixture of Titanium (IV) Oxide Particles Suspended in Aqueous Solutions. *J. Phys. Chem. B*, 101(19), p. 3746-3752.
150. Ollis, D. F., 1993. Comparative Aspects of Advanced Oxidation Processes. *Acs Symposium Series*, Volume 518, pp. 18- 34.
151. Pang, S. C., Kho, S. Y. & Chin, S. F., 2012. Fabrication of Magnetite/Silica/Titania Core-Shell Nanoparticles. *Journal of Nanomaterials*.
152. Pastoriza-Santos, I. et al., 2000. One-Pot Synthesis of $Ag@TiO_2$ Core-Shell Nanoparticles and Their Layer-by-Layer Assembly. *Langmuir*, Volume 16, pp. 2731-2735.
153. Peralta-Zamora, P. et al., 1999. Degradation of reactive dyes I. a comparative study of ozonation, enzymatic and photochemical processes. *Chemosphere*, 38(4), pp. 835- 852.
154. Pignatello, J. J., Oliveros, E. & MacKay, A., 2006. Advanced Oxidation Processes for Organic Contaminant Destruction Based on the Fenton Reaction and Related Chemistry. *Critical Reviews in Environmental Science and Technology*, 36(1), pp. 1-84.

155. Piscopo, A., Robert, D. & Weber, J. V., 2001. Influence of pH and chloride anion on the photocatalytic degradation of organic compounds. Part I. Effect on the benzamide and para-hydroxybenzoic acid in TiO₂ aqueous solution. *Applied Catalysis, B: Environmental*, 35(2), pp. 117-124.
156. Polshettiwar, V. et al., 2011. Magnetically Recoverable Nanocatalysts. *Chemical Reviews*, Volume 111, pp. 3036-3075.
157. Poole Jr, C. P. & Owens, F. J., 2003. *Introduction to Nanotechnology*. Illustrated ed. Hoboken, New Jersey: John Wiley & Sons.
158. Pouran, S. R., Abdul Aziz, A. R. & Daud, W. M. M. A. W., 2015. Review on the main advances in photo-Fenton oxidation system for recalcitrant wastewaters. *Journal of Industrial and Engineering Chemistry*, Volume 21, pp. 53- 69.
159. Radetic, T., 2011. *Fundamentals of Scanning Electron Microscopy and Energy Dispersive X-ray Analysis in SEM and TEM*. NFMC Spring School on Electron Microscopy, April.
160. Rafatullaha, M., Sulaiman, O., Hashima, R. & Ahmad, A., 2010. Adsorption of methylene blue on low-cost adsorbents: A review. *Journal of Hazardous Materials*, Volume 177, pp. 70- 80.
161. Rahman, I. A. & Padavettan, V., 2012. Synthesis of Silica Nanoparticles by Sol-Gel: Size-Dependent Properties, Surface Modification, and Applications in Silica-Polymer Nanocomposites—A Review. *Journal of Nanomaterials*, Volume 2012, pp. Article ID 132424, 15 pages.
162. Raileanu, M. et al., 2005. Sol-gel Fe₃O₄ - SiO₂ nanocomposites. *Romanian Journal of Physics*, 50(5-6), pp. 595-606.
163. Raming, T. P., Winnubst, A. J. A., van Kats, C. M. & Philipse, A. P., 2002. The Synthesis and Magnetic Properties of Nanosized Hematite (α -Fe₂O₃) Particles. *Journal of Colloid and Interface Science*, 249(2), pp. 346-350.
164. Rao, K. S. et al., 2005. A novel method for synthesis of silica nanoparticles. *Journal of Colloid and Interface Science*, 289(1), pp. 125- 131.
165. Rashid, J., Barakat, M. A., Ruzmanova, Y. & Chianese, A., 2015. Fe₃O₄/SiO₂/TiO₂ nanoparticles for photocatalytic degradation of 2-chlorophenol in simulated wastewater. *Environ Sci Pollut Res.*, Volume 22, p. 3149–3157.
166. Robinson, T., McMullan, G., Marchant, R. & Nigam, P., 2001. Remediation of dyes in textile effluent: a critical review on current treatment technologies with a proposed alternative. *Bioresource Technology*, 77(3), p. 247–255.

167. Roy, R., 1994. Accelerating the kinetics of low-temperature inorganic syntheses. *Journal of Solid State Chemistry*, Volume 111, pp. 11-17.
168. Ruzmanova, Y., Stoller, M. & Chianese, A., 2013. Photocatalytic Treatment of Olive Mill Wastewater by Magnetic Core Titanium Dioxide Nanoparticles. *Chemical Engineering Transactions*, Volume 23, pp. 2269- 2274.
169. Saggiaro, E. M. et al., 2011. Use of Titanium Dioxide Photocatalysis on the Remediation of Model Textile Wastewaters Containing Azo Dyes. *Molecules*, Volume 16, pp. 10370-10386.
170. Saien, J., Delavari, H. & Solymani, A. R., 2010. Sono-assisted photocatalytic degradation of styrene-acrylic acid copolymer in aqueous media with nano titania particles and kinetic studies. *Journal of Hazardous Materials*, 177(1-3), pp. 1031-1038.
171. Sakthivel, S. et al., 2003. Solar photocatalytic degradation of azo dye: comparison of photocatalytic efficiency of ZnO and TiO₂. *Solar Energy Materials and Solar Cells*, 77(1), pp. 65-82.
172. Sakthivel, S. et al., 2004. Enhancement of photocatalytic activity by metal deposition: characterisation and photonic efficiency of Pt, Au and Pd deposited on TiO₂ catalyst. *Water Research*, Volume 38, p. 3001–3008.
173. Sakthivel, S. et al., 2004. Enhancement of photocatalytic activity by metal deposition: Characterization and photonic efficiency of Pt, Au and Pd deposited on TiO₂ catalyst. *Water Research*, 38(13), p. 3001–8.
174. Sampathkumar, K., Arjunan, T. V., Pitchandia, P. & Senthilkumar, P., 2010. Active solar distillation—A detailed review. *Renewable and Sustainable Energy Reviews*, 14(6), pp. 1503-1526.
175. Sannino, D., Vaiano, V., Sacco, O. & Ciambelli, P., 2013. Mathematical modelling of photocatalytic degradation of methylene blue under visible light irradiation. *Journal of Environmental Chemical Engineering*, 1(1- 2), pp. 56- 60.
176. Santra, S. et al., 2001. Synthesis and Characterization of Silica-Coated Iron Oxide Nanoparticles in Microemulsion: The Effect of Nonionic Surfactants. *Langmuir* 2001, 17, 2900-2906, Volume 17, pp. 2900-2906.
177. Sato, S., Kadowaki, T. & Yamaguti, K., 1984. Photocatalytic oxygen isotopic exchange between oxygen molecule and the lattice oxygen of titanium dioxide prepared from titanium hydroxide. *Journal of Physical Chemistry*, 88(14), pp. 2930- 2931.

178. Sclafani, A. & Herrmann, J.-M., 1998. Influence of metallic silver and of platinum-silver bimetallic deposits on the photocatalytic activity of titania (anatase and rutile) in organic and aqueous media. *Journal of Photochemistry and Photobiology A: Chemistry*, 113(2), pp. 181- 188.
179. Sclafani, A., Palmisano, L. & Schiavello, M., 1990. Influence of the preparation methods of titanium dioxide on the photocatalytic degradation of phenol in aqueous dispersion. *J. Phys. Chem.*, 94(2), p. 829–832.
180. Seery, M. K., George, R., Floris, P. & Pillai, S. C., 2007. Silver doped titanium dioxide nanomaterials for enhanced visible light photocatalysis. *Journal of Photochemistry and Photobiology A: Chemistry*, Volume 189, pp. 258- 263.
181. Shen , W. et al., 2008. Photocatalytic degradation for methylene blue using zinc oxide prepared by codeposition and sol–gel methods. *Journal of Hazardous Materials*, Volume 152, pp. 172-175.
182. Shi, F., Li, Y., Zhang, Q. & Wang, H., 2012. Synthesis of Fe₃O₄/C/TiO₂ Magnetic Photocatalyst via Vapor Phase Hydrolysis. *International Journal of Photoenergy*.
183. Shi, Z., Fan, Y., Xu, N. & Shi, J., 2000. Kinetics of Photocatalytic Degradation of Methylene Blue over TiO₂ Particles in Aqueous Suspensions. *Chinese J. Chem. Eng*, 8(1), pp. 15-19.
184. Shimizu, N., Ogino, C., Dadjour, M. F. & Murata, T., 2007. Sonocatalytic degradation of methylene blue with TiO₂ pellets in water. *Ultrasonics Sonochemistry*, 14(2), pp. 184- 190.
185. Siddiquey, I. A. et al., 2008. Control of the photocatalytic activity of TiO₂ nanoparticles by silica coating with polydiethoxysiloxane. *Dyes Pigm.*, Volume 76, pp. 754- 759.
186. Sing, K., 2001. The use of nitrogen adsorption for the characterisation of porous materials. *Colloids and Surfaces A: Physicochemical and Engineering Aspects* 187–188 (2001) 3–9, Volume 187-188, pp. 3-9.
187. Širc, J. et al., 2012. Morphological Characterization of Nanofibers: Methods and Application in Practice. *Journal of Nanomaterials*, Volume 2012, pp. Article ID 327369, 14 pages.
188. Sobana, N., Muruganadham, M. & Swaminathan, M., 2006. Nano-Ag particles doped TiO₂ for efficient photodegradation of direct azo dyes. *Journal of Molecular Catalysis A: Chemical*, Volume 258, pp. 124- 132.

189. Soltani, T. & Entezari, M. H., 2013. Soplar photocatalytic degradation of RB5 by ferrite bismuth nanoparticles synthsized via ultrasound. *Ultrason. Sonochem.*, Volume 20, pp. 1245-1253.
190. Somiya, S. & Roy, R., 2000. Hydrothermal synthesis of fine oxide powders. *Bull. Mater. Sci.*, 23(6), pp. 453-460.
191. Song, X. & Gao, L., 2007. Fabrication of Bifunctional Titania/Silica-Coated Magnetic Spheres and their Photocatalytic Activities. *J. Am. Ceram. Soc.*, 90(12), pp. 4015- 4019.
192. Soon, A. N. & Hameed, B. H., 2011. Heterogeneous catalytic treatment of synthetic dyes in aqueous media using Fenton and photo-assisted Fenton process. *Desalination*, 269(1-3), p. 1–16.
193. Soriano, J. J. et al., 2014. Toxicity of the azo dyes Acid Red 97 and Bismarck Brown Y to Western clawed frog (*Silurana tropicalis*). *Environ Sci Pollut Res*, Volume 21, p. 3582–3591.
194. Stefanita, C. -G., 2008. From Bulk to Nano: The Many Sides of Magnetism. Illustrated ed. Berlin Heidelberg: Springer Science & Business Media.
195. Stolz, A., 2001. Basic and applied aspects in the microbial degradation of azo dyes. *Appl. Microbiol. Biotechnol*, Volume 56, pp. 69-80.
196. Styliidi, M., Kondarides, D. I. & Verykios, X. E., 2003. Pathways of solar light-induced photocatalytic degradation of azo dyes in aqueous TiO₂ suspensions. *Applied Catalysis, B: Environmental*, 40(4), pp. 271-286.
197. Su, Y. L., Deng, Y. R., Zhao, L. & Du, Y. X., 2013. Photocatalytic degradation of microcystin-LR using TiO₂ nanotubes under irradiation with UV and natural sunlight. *Chinese Science Bulletin*, 58(10), pp. 1156-1161.
198. Subramanian, V., Pangarkar, G. & Beenackers, A. A., 2000. Photocatalytic degradation of PHBA: relationship between substrate adsorption and photocatalytic degradation. *Clean Prod. Process*, 2 (2000), p. 149, Volume 2, p. 149.
199. Suchanek, W. L. & Riman, R. E., 2006. Hydrothermal Synthesis of Advanced Ceramic Powders. *Advances in Science and Technology*, Volume 45, pp. 184-193.
200. Sudha, M., Saranya, A., Selvakumar, G. & Sivakumar, N., 2014. Microbial degradation of Azo Dyes: A review. *Int.J.Curr.Microbiol.App.Sci*, 3(2), pp. 670-690.

201. Sum, O. S. N., Feng, J., Hub, X. & Yue, P. L., 2005. Photo-assisted Fenton mineralization of an azo-dye Acid Black 1 using a modified laponite clay-based Fe nanocomposite as a heterogeneous catalyst. *Topics in Catalysis*, 33(1-4), pp. 233-242.
202. Sun, J. et al., 2012. Degradation of the antibiotic sulfamonomethoxine sodium in aqueous solution by photo-Fenton oxidation. *Chinese Science Bulletin*, 57(5), pp. 558-564.
203. Sung-Suh, H. M. et al., 2004. Comparison of Ag deposition effects on the photocatalytic activity of nanoparticulate TiO₂ under visible and UV light irradiation. *Journal of Photochemistry and Photobiology A: Chemistry*, Volume 163, pp. 37- 44.
204. Swaminathan, M., Muruganandham, M. & Sillanpaa, M., 2013. Advanced Oxidation Processes for Wastewater Treatment. *International Journal of Photoenergy*, p. Article ID 683682 3.
205. Tan, Y. H. et al., 2012. Surface area and pore size characteristics of nanoporous gold subjected to thermal, mechanical, or surface modification studied using gas adsorption isotherms, cyclic voltammetry, thermogravimetric analysis, and scanning electron microscopy. *J Mater Chem.*, 22(14), pp. 733-6745.
206. Tang, J., Wang, W., Zhao, G. L. & Li, Q., 2009. Colossal and Seebeck Coefficient and low thermal conductivity in reduced TiO₂. *J. Physics Condens. Matter*, 21(20), p. 20573 4 pages.
207. Tartaj, P. et al., 2003. The preparation of magnetic nanoparticles for applications in biomedicine. *Journal of Physics D: Applied Physics*, Volume 36, pp. 182–197.
208. Tartaj, P. et al., 2005. Advances in magnetic nanoparticles for biotechnology applications. *Journal of Magnetism and Magnetic Materials*, Volume 290, pp. 28-34.
209. Tayade, R. J., Kulkarni, R. G. & Jasra, R. V., 2007. Enhanced Photocatalytic Activity of TiO₂-Coated NaY and HY Zeolites for the Degradation of Methylene Blue in Water. *Ind. Eng. Chem. Res.*, 2007, 46 (2), pp 369–376, 46(2), pp. 369-376.
210. Teja, A. S. & Koh, P.-Y., 2009. Synthesis, properties, and applications of magnetic iron oxide nanoparticles. *Progress in Crystal Growth and Characterization of Materials*, Volume 55, pp. 22-45.

211. Thommes, M., 2010. Physical Adsorption Characterization of Nanoporous Materials. *Chemie Ingenieur Technik* 2010, 82, No. 7, 82(7), pp. 1059-1073.
212. Thompson, T. L. & Yates Jr., J. T., 2006. Surface science studies of the photoactivation of TiO₂--new photochemical processes. *Chem Rev.*, 106(10), pp. 4428-53.
213. Tia, G. et al., 2011. 3D hierarchical flower-like TiO₂ nanostructure: morphology control and its photocatalytic property. *CrystEngComm*, 13(8), pp. 2994-3000.
214. Toor, A. P. et al., 2005. Photocatalytic degradation of direct yellow 12 dye using UV/TiO₂ in a shallow pond slurry reactor. *Dyes and Pigments*, 68(1), pp. 53-60.
215. Turhan, K. & Ozturkcan, S. A., 2013. Decolorization and Degradation of Reactive Dye in Aqueous Solution in a Semi-batch Bubble Column Reactor. *Water Air Soil Pollut*, Volume 224, pp. 1353-1365.
216. Umoren, S. A., Etim, U. J. & Israel, A. U., 2013. Adsorption of methylene blue from industrial effluent using poly (vinyl alcohol). *J. Mater. Environ. Sci.*, 4(1), pp. 75- 86.
217. Valencia, S., Juan, M. M. & Gloria, R., 2010. Study of the bandgap of synthesized titanium dioxide nanoparticles using the sol-gel method and a hydrothermal treatment. *Open Materials Science Journal*, 4(1), pp. 9- 14.
218. Vamathevan, V. et al., 2002. Photocatalytic oxidation of organics in water using pure and silver-modified titanium dioxide particles. *Journal of Photochemistry and Photobiology A: Chemistry*, Volume 148, pp. 233-245.
219. Vigneswaran, S., Vigneswaran, B. & Ben-Aïm, R., 1991. Application of microfiltration for water and wastewater treatment. 31 ed. Bangkok, Thailand: Environmental Sanitation Information Center, ENSIC.
220. Wang, C. et al., 2009. Magnetic (γ-Fe₂O₃@SiO₂)_n@TiO₂ Functional Hybrid Nanoparticles with Activated Photocatalytic Ability. *J. Phys. Chem. C*, Volume 113, p. 4008–4011.
221. Wang, J., Sun, J., Sun, Q. & Chen, Q., 2003. One-step hydrothermal process to prepare highly crystalline Fe₃O₄ nanoparticles with improved magnetic properties. *Materials Research Bulletin*, 38(7), pp. 1113-1118.
222. Wang, L. et al., 2010. Nanoparticle-based environmental sensors. *Materials Science and Engineering: R: Reports*, 70(3- 6), p. 265–274.
223. Wang, R. et al., 2011. Photocatalytic Activity of Heterostructures Based on TiO₂ and Halloysite Nanotubes. *Appl. Mater. Interfaces*, Volume 3, p. 4154–4158.

224. Watson, S., Beydoun, D. & Amal, R., 2002. Synthesis of a novel magnetic photocatalyst by direct deposition of nanosized TiO₂ crystals onto a magnetic core. *Journal of Photochemistry and Photobiology A: Chemistry*, Volume 148, pp. 303-313.
225. Wodka, D. et al., 2010. Photocatalytic Activity of Titanium Dioxide Modified by Silver Nanoparticles. *Applied Materials and Interfaces*, 2(7), pp. 1945-1953.
226. Wongwailikhit, K. & Horwongsakul, S., 2011. The preparation of iron (III) oxide nanoparticles using W/O microemulsion. *Materials Letters*, Volume 65, p. 2820–2822.
227. Wu, C.-H. & Chern, J.-M., 2006. Kinetics of Photocatalytic Decomposition of Methylene Blue. *Ind. Eng. Chem. Res.*, 45(19), pp. 6450- 6457.
228. Wu, W., He, Q. & Jiang, C., 2008. Magnetic Iron Oxide Nanoparticles: Synthesis and Surface Functionalization Strategies. *Nanoscale Res. Lett.* 3(11), p. 397–415.
229. Xia, Q. -H. et al., 2005. Advances in Homogeneous and Heterogeneous Catalytic Asymmetric Epoxidation. *Chem. Rev.*, Volume 105, pp. 1603-1662.
230. Xia, X. H. et al., 2008. Synthesis and photocatalytic properties of TiO₂ nanostructures. *Materials Research Bulletin*, 43(8-9), pp. 2187-2195.
231. Xie, Y. B. & Li, X. Z., 2006. Interactive oxidation of photoelectrocatalysis and electro Fenton for azo dye degradation using TiO₂-Ti mesh and reticulated vitreous carbon electrodes. *Materials Chemistry and Physics*, 95(1), pp. 39-50.
232. Xu, C., Rangaiah, G. P. & Zhao, X. S., 2014. Photocatalytic Degradation of Methylene Blue by Titanium Dioxide: Experimental and Modeling Study. *Industrial & Engineering Chemistry Research*, Volume 53, p. 14641–14649.
233. Xu, J., Ao, Y., Fu, D. & Yuan, C., 2008. Low-temperature preparation of anatase titania-coated magnetite. *Journal of Physics and Chemistry of Solids*, Volume 69, pp. 1980- 1984.
234. Xu, N. et al., 1999. Effects of Particle Size of TiO₂ on Photocatalytic Degradation of Methylene Blue in Aqueous Suspensions. *Ind. Eng. Chem. Res.*, Volume 38, pp. 373-379.
235. Xu, P. et al., 2012. Use of iron oxide nanomaterials in wastewater treatment: A review. *Science of the Total Environment*, Volume 424, pp. 1- 10.
236. Xuan, S. et al., 2009. Magnetically Separable Fe₃O₄/TiO₂ Hollow Spheres: Fabrication and Photocatalytic Activity. *J. Phys. Chem. C*, Volume 113, pp. 553-558.

237. Yu, J. C., Lin, J., Lo, D. & Lam, S. K., 2000. Influence of Thermal Treatment on the Adsorption of Oxygen and Photocatalytic Activity of TiO₂. *Langmuir*, 16(18), pp. 7304-7308.
238. Yu, J. et al., 2006. Enhanced photocatalytic activity of TiO₂ powder (P25) by hydrothermal treatment. *Journal of Molecular Catalysis A: Chemical*, 253(1-2), pp. 112-118.
239. Zhang, Q. & Gao, L., 2009. Preparation of nanocrystalline TiO₂ powders for the photocatalytic oxidation of phenol. *Res. Chem. Intermed.*, Volume 35, pp. 281-286.
240. Zhang, X. & Chan, K.-Y., 2003. Water-in-Oil Microemulsion Synthesis of Platinum-Ruthenium Nanoparticles, Their Characterization and Electrocatalytic Properties. *Chem. Mater.*, Volume 15, pp. 451-459.
241. Zheng, C. et al., 2013. Treatment Technologies for Organic Wastewater. In: W. E. a. R. K. Chowdhury, ed. *Water Treatment*. Xi'an Jiaotong: Intech, pp. 250- 285.
242. Zheng, Y.-h., Cheng, Y., Bao, F. & Wang, Y., 2006. Synthesis and magnetic properties of Fe₃O₄ nanoparticles. *Materials Research Bulletin*, 41(3), pp. 525-529.
243. Zhou, G. et al., 2015. Fenton-like degradation of Methylene Blue using paper mill sludge- derived magnetically separable heterogeneous catalyst: Characterization and mechanism. *Journal of Environmental Sciences*, Volume 35, p. 20 – 26.
244. Zille, A., G órnacka, B., Rehorek, A. & Cavaco-Paulo, A., 2005. Degradation of Azo Dyes by *Trametes villosa* Laccase over Long Periods of Oxidative Conditions. *Applied Environmental Microbiology*, pp. 6711-6718.